Dynamical Systems in Beyond Standard Theory Cosmology

Stephanie Buttigieg

Supervised by Dr Jackson Levi Said

Co-supervised by Prof. Joseph Sultana

Department of Physics

Faculty of Science

University of Malta

May, 2022

A dissertation submitted in partial fulfilment of the requirements for the degree of B.Sc. (Hons) in Mathematics and Physics.

WWW.UM.EDU.MT

First edition, Monday 2nd May, 2022

To my friends and family,

the centre of my universe.

Acknowledgements

I would firstly like to thank my supervisor, Dr Jackson Levi Said, who was always there to guide me through this project and beyond. Your optimism and support was very much appreciated, especially when stress started to kick in. I would also like to thank my co-supervisor Prof. Joseph Sultana. Your attention to detail pushed me to make sure I can defend every sentence and equation I wrote in this work with confidence. My gratitude also goes out to all the lecturers within the departments of mathematics and physics, who not only prepared me for exams and assessments, but also gave me invaluable advice for my career. I would not be where I am today without the full support of my parents; my mum who sacrificed so much to make sure I can follow my dreams, and my dad, who instilled in me the passion for anything related to mathematics and science. I would also like to thank my friends, especially Rebekah, Paolo, Lexy and Julia, who endured me talking passionately about my research topic and my masters applications, and who were always there to listen to me complain about all the work I have to do. Your company will be missed greatly next year.

Finally, I have to express my gratitude to all the women in science who came before me and broke the glass ceiling. I would not be submitting a dissertation in cosmology if they had not paved the way.

Abstract

The standard ΛCDM cosmological model, based on Einstein's theory of General Relativity, explains the late-time acceleration of the Universe by introducing a cosmological constant to represent dark energy. The observed tension between the value of the Hubble constant obtained using late-time and early-time measurements, alongside other problems with ΛCDM, has emphasized the need to understand the true nature of this dark energy. In this work, the gravitational theory itself is modified to explain the observed acceleration of the Universe. In particular, the $f(T, T_G)$ modification of the Teleparallel Equivalent of General Relativity, based on the torsion scalar T and the invariant T_G which is the teleparallel equivalent to the Gauss-Bonnet term, is studied through the use of dynamical systems. By analysing the phase portraits of differential equations encompassing the dynamics of the four chosen models, or forms of $f(T, T_G)$, their predicted cosmological evolution is investigated and compared to observations to study the viability of this modification. We find that all the models can result in a dark-energy-dominated universe, in line with observations. The dynamics of a cosmological constant can be reproduced with phantom-like and quintessence-like solutions also possible. Finally, by studying the behaviour at infinity, we see that the models can also result in past/future singularities.

Contents

1 Introduction **1**

2 GR and TEGR **7**
2.1 Einstein's Theory of General Relativity 7
2.1.1 An Introduction to Tensors and Manifolds 7
2.1.2 The Levi Civita Connection 9
2.1.3 The Riemann and Einstein Tensors 10
2.1.4 Gravitation and the Einstein Field Equations 12
2.1.5 Modifications of GR 15
2.2 Teleparallel Gravity 17
2.2.1 Tetrads and the Spin Connection 17
2.2.2 Local Lorentz Transformations and the Weitzenböck Gauge 18
2.2.3 Teleparallel Equivalent of General Relativity 19
2.2.4 Modifications of TEGR 21

3 Cosmology & Dynamical Systems **23**
3.1 The Standard Model of Cosmology 23
3.1.1 The Expansion of the Universe 24
3.1.2 The FLRW Metric 26
3.1.3 Cosmic Dynamics 27
3.1.4 Observational Parameters 31
3.1.5 The Accelerating Universe 33
3.1.6 Challenges for the Standard Model 34
3.2 $f(T, T_G)$ Cosmology 35
3.3 Dynamical Systems Applied to Cosmology 39

3.3.1 Introduction to Dynamical Systems . . . 40
3.3.2 Linear Stability Theory . . . 41
3.3.3 Behaviour at Infinity . . . 44
3.3.4 Dynamical Systems to Probe Novel Cosmologies . . . 45

4 Dynamical Analysis **47**

4.1 Model 1: Power Law Model . . . 48
4.1.1 Finite Phase Space Analysis . . . 51
4.1.2 Analysis at Infinity . . . 52
4.1.3 Cosmological Implications . . . 55
4.1.4 Model 1 Variation . . . 61
4.2 Model 2: Exponential Model . . . 65
4.2.1 Finite Phase Space Analysis . . . 68
4.2.2 Analysis at Infinity . . . 69
4.2.3 Cosmological Implications . . . 71
4.3 Model 3: Mixed Power Law Model . . . 74
4.3.1 Finite Phase Space Analysis . . . 78
4.3.2 Analysis at Infinity . . . 79
4.3.3 Cosmological Implications . . . 80
4.3.4 Model 3 Variation . . . 84
4.4 Model 4: Logarithmic model . . . 85
4.4.1 Finite Phase Space Analysis . . . 87
4.4.2 Analysis at Infinity . . . 88
4.4.3 Cosmological Implications . . . 90
4.5 Summary . . . 93

5 Conclusions **95**

References **99**

List of Figures

1.1 The original graph from Hubble's paper depicting Hubble's Law. 2
1.2 Temperature map of the CMB obtained by *Planck*. 3

2.1 Parallel transport of a vector on a sphere. Figure adapted from Carroll (2004). 10
2.2 A visual representation of matter causing the spacetime manifold to curve. . 13
2.3 Geometrical difference between the curvature and torsion tensors. 20

3.1 The Hubble tension's evolution over the past two decades. 25
3.2 Evolution of radiation, matter and dark energy with redshift. 30
3.3 Graphs showing the magnitude of SNIa against redshift and constraints on the matter and dark energy density parameters. 34
3.4 Phase space portrait for the system defined in Eqs. (3.58) & (3.59). 43

4.1 Trajectories in the phase space for the $f_1(T, T_G)$ cosmological scenario defined by Eqs. (4.14)-(4.10) with parameters $\alpha_1 = -1, P_1 = \frac{1}{3}$. 57
4.2 Global phase portrait for $f_1(T, T_G)$ with parameters $\alpha_1 = -1, P_1 = \frac{1}{3}$ in the (R, Θ, Φ) coordinates. 58
4.3 Trajectories in the phase space for the $f_1(T, T_G)$ cosmological scenario defined by Eqs. (4.14)-(4.10) with parameters $\alpha_1 = -1, P_1 = \frac{1}{8}$. 59
4.4 Global phase portrait for $f_1(T, T_G)$ with parameters $\alpha_1 = -1, P_1 = \frac{1}{8}$ in the (R, Θ, Φ) coordinates. 60
4.5 Trajectories in the phase space for the $f_1(T, T_G)$ cosmological scenario defined by Eqs. (4.14)-(4.10) with parameters $\alpha_1 = \frac{1}{2}, P_1 = 2$. 61
4.6 Global phase portrait for $f_1(T, T_G)$ with parameters $\alpha_1 = \frac{1}{2}, P_1 = 2$ in the (R, Θ, Φ) coordinates. 62

4.7 Trajectories in the phase space for the $f_1(T, T_G)$ cosmological scenario defined by Eqs. (4.44)-(4.45) with $\alpha_1 = -\sqrt{6}$. 65

4.8 Trajectories in the phase space for the $f_2(T, T_G)$ cosmological scenario defined by Eqs. (4.74), (4.75) and (4.70) with parameters $\alpha_2 = -1, P_2 = 1$. 72

4.9 Global phase portrait for $f_2(T, T_G)$ with parameters $\alpha_1 = -1, P_2 = 1$ in the (R, Θ, Φ) coordinates. 74

4.10 Trajectories in the phase space for the $f_2(T, T_G)$ cosmological scenario defined by Eqs. (4.74), (4.75) and (4.70) with parameters $\alpha_2 = -1, P_2 = -\frac{1}{10}$. . . . 75

4.11 Global phase portrait for $f_2(T, T_G)$ with parameters $\alpha_2 = -1, P_2 = -\frac{1}{10}$ in the (R, Θ, Φ) coordinates. 75

4.12 Trajectories in the phase space for the $f_3(T, T_G)$ cosmological scenario defined by Eqs. (4.104), (4.105) and (4.101) with parameters $\alpha_3 = -1, P_3 = 1, \beta_3 = \frac{1}{3}$. 81

4.13 Global phase portrait for $f_3(T, T_G)$ with parameters $\alpha_3 = -1, P_3 = 1, \beta_3 = \frac{1}{3}$ in the (R, Θ, Φ) coordinates. 82

4.14 Trajectories in the phase space for the $f_3(T, T_G)$ cosmological scenario defined by Eqs. (4.104), (4.105) and (4.101) with parameters $\alpha_3 = 1, P_3 = 2, \beta_3 = \frac{2}{3}$. 83

4.15 Trajectories in the phase space for the $f_4(T, T_G)$ cosmological scenario defined by Eqs. (4.137), (4.138) and (4.134) with parameters $\alpha_4 = -1, P_4 = 10$. . . 91

4.16 Global phase portrait for $f_4(T, T_G)$ with parameters $\alpha_4 = -1, P_4 = 10$ in the (R, Θ, Φ) coordinates. 91

4.17 Trajectories in the phase space for the $f_4(T, T_G)$ cosmological scenario defined by Eqs. (4.137), (4.138) and (4.134) with parameters $\alpha_4 = 2, P_4 = \frac{1}{2}$. 92

4.18 Global phase portrait for $f_4(T, T_G)$ with parameters $\alpha_4 = 2, P_4 = \frac{1}{2}$ in the (R, Θ, Φ) coordinates. 93

List of Tables

3.1 Fixed points of the system defined in Eqs. (3.58) & (3.59). 43

4.1 The critical points at infinity alongside their existence and stability conditions for $f_1(T, T_G)$. 55
4.2 Values of the dark energy density parameter, deceleration parameter, dark energy equation-of-state parameter and the Hubble parameter at the infinite fixed points of $f_1(T, T_G)$. 56

List of Abbreviations

GR general relativity 1
LIGO Laser Interferometer Gravitational-Wave Observatory 1
EHT Event Horizon Telescope 1
FIRAS Far InfraRed Absolute Spectrophotometer 3
COBE Cosmic Background Explorer 3
CMB cosmic microwave background 3
CDM cold dark matter 4
TEGR Teleparallel Equivalent of General Relativity 5
SR Special Relativity 8
WEP Weak Equivalence Principle 12
EEP Einstein Equivalence Principle 12
wrt with respect to 13
EM electromagnetism 17
STEGR symmetric teleparallel equivalent of general relativity 19
DOF degrees of freedom 20
SDSS Sloan Digital Sky Survey 23
SNIa type Ia Supernovae 24
FLRW Friedmann–Lemaître–Robertson–Walker 26
EoS equation of state 29
LST linear stability theory 41

1

Introduction

Einstein's theory of general relativity (GR), first published in 1915 (Einstein, 1915), revolutionised the way we understand gravity, which underpins our understanding of the Universe. Until then, gravity was understood in the simple Newtonian way, an action-at-a-distance attractive force between two massive objects, inversely proportional to the square of their distance apart. Einstein not only improved upon Newton's theory, but completely reinvented it. He explained gravity through the curvature of spacetime; matter curves spacetime and this curvature dictates how matter moves. Since its publication, GR has passed every experimental test it was subjected to, the first of which was explaining the anomalous perihelion precession of Mercury's orbit (Turyshev, 2008). Up until the present day, more and more predictions of this theory are being confirmed by observations as our experimental tools are getting even more refined. One of these latest major results was the first image of a black hole obtained by the Event Horizon Telescope (EHT) collaboration (Akiyama et al., 2019). These astronomical objects were predicted by Einstein in places where the curvature of spacetime becomes so large that not even light can escape. In 2016, another of Einstein's predictions was confirmed by observations. The Laser Interferometer Gravitational-Wave Observatory (LIGO) detected gravitational waves, which are ripples in the fabric of spacetime itself, originating from the merger of two black holes (Abbott et al., 2016). This was not only a triumph for the LIGO experiment, whose mirrors can detect a change in distance 10,000 times smaller than a proton, but also for GR. All these successes have cemented this theory as our best description of gravity. But the theory is not without its flaws, and the search for a modified theory of gravity has been gathering steady momentum in the past few years for good reasons (Clifton et al., 2012).

The first crack in the theory appeared with the cosmological constant Λ. When Einstein was deriving his gravitational theory, the Universe was assumed to be static,

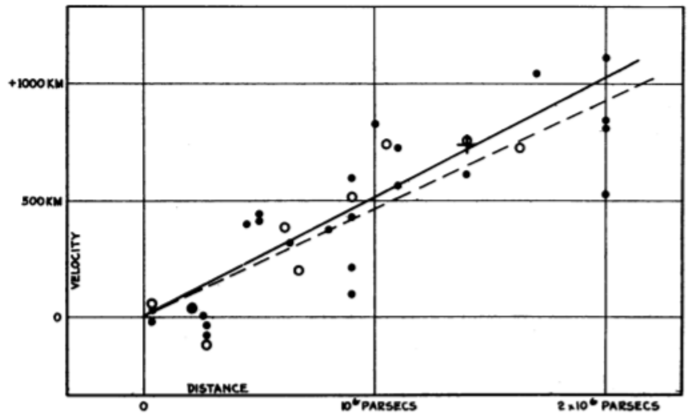

Figure 1.1: The original graph from Hubble's paper (Hubble, 1929) depicting Hubble's Law. The graph shows radial velocities of extra-galactic nebulae, corrected for solar motion, against estimated distance.

there was no contraction or expansion. However, Einstein realised that his field equations could not describe such a static universe with a non-zero matter content without the introduction of a cosmological constant term, something which he later referred to as his "biggest blunder" (O'Raifeartaigh, 2018), a comment which took on an even greater meaning with the discovery of the expansion of the Universe. In 1922, Friedmann was the first to show that Einstein's theory could describe such an expanding universe (Friedmann, 1922). In 1927, Lemaître subsequently proposed an expanding universe to explain the observed redshift of spiral nebulae and proposed a law relating redshift with the velocity of recession (Lemaitre, 1927). This relation was then confirmed observationally by Hubble in 1929 and thus became known as **Hubble's Law** (Hubble, 1929). Hubble's original graph showing the linear relation between recession velocity and distance can be seen in Fig. 1.1.

The discovery that matter in the Universe seems to be expanding away from other matter led to the idea that in the past, everything was contained in a much smaller volume than it is now. If we trace this evolution back enough, we arrive to what is now known as the **Hot Big Bang**, the initial explosion that created all the content of the Universe. The theory of the Universe as a system that evolves over time is what is known as the **Big Bang theory** (Liddle, 2003) and in the 1940s was developed mainly by Gamow (Alpher et al., 1948).

On the other hand, physicists like Hoyle, Bondi and Gold did not agree with this emerging theory of the Universe and formulated the **Steady-State Theory**. This suggests that matter is constantly being created in order to fill the gaps in an expanding universe and thus the Universe remains unchanged (Bondi and Gold, 1948).

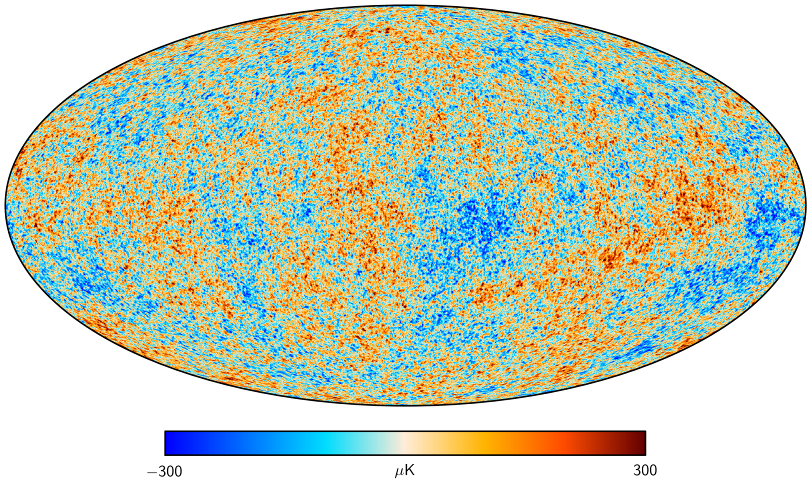

Figure 1.2: Temperature map of the CMB obtained by *Planck* (Planck Collaboration et al., 2016)

The debate about which of the two theories, the steady-state theory or the Big Bang theory, correctly describes the Universe, was by and large decided in favour of the latter through the discovery of the cosmic microwave background (CMB) by Penzias and Wilson in the mid-1960s (Penzias and Wilson, 1965). The CMB is radiation that can be detected in whatever direction we point our telescopes to from Earth and which originated from what is known as the last-scattering surface. This is the point in the Universe's history at redshift $z \approx 1100$ when the temperature was low enough so that photons and atoms could decouple and consequently photons undergo last scattering (Dodelson, 2003). Thus, the CMB can offer a snapshot of what this hot, dense early Universe looked like (Jones and Lasenby, 1998). The Far InfraRed Absolute Spectrophotometer (FIRAS) experiment of the Cosmic Background Explorer (COBE) mission determined the temperature of the CMB to be 2.72548 ± 0.00057 K (Fixsen, 2009). Although the temperature spectrum of the CMB is remarkably smooth, small fluctuations of a few tens of microKelvin, have been detected (Liddle, 2003). These anisotropies can be seen in Fig. 1.2 which shows a temperature map of the CMB obtained by the *Planck* space telescope (Planck Collaboration et al., 2016). The anisotropy spectrum can reveal a great amount of information about the Universe, including strong indications of a spatially flat geometry and values of various cosmological parameters (Jackson, 2007).

Einstein was quick to accept the Big Bang theory and its implications of an expanding Universe, even before the discovery of the CMB. He published a model of the expanding Universe in 1931 in which he omitted the cosmological constant term (Einstein, 1931; O'Raifeartaigh and McCann, 2014), claiming that had the expansion of the Universe been discovered before the publication of his theory, no such term would have been included in the first place. This is in contrast with other physicists, such as Friedmann and Lemaître, who still included Λ in the field equations (O'Raifeartaigh, 2018).

Einstein's determination to eliminate Λ from his theory was thwarted by the discovery of the acceleration of the Universe (Riess et al., 1998) in the late 1990s. This acceleration was inferred from the observation that certain astronomical objects appear dimmer than expected at large redshift. The details of this discovery are discussed in Sec. 3.1.5. Observational evidence also indicates that although the Universe seems to be flat, the total matter density of the Universe is much less than that required for such a flat universe (Ostriker and Steinhardt, 1995) and so the existence of dark energy needs to be inferred in order to explain both of these phenomena. Dark energy makes up $67.9 \pm 1.3\%$ of the energy content of the Universe (Aghanim et al., 2020) and is theoretically described by Λ in the context of GR in the standard model of cosmology.

Another major cosmological discovery was that of the existence of cold dark matter (CDM). The existence of low-luminosity matter was first inferred by Zwicky in his 1933 paper in which he found that the dynamical mass of a galaxy cluster was at least a hundred times greater than its luminosity mass (Arun et al., 2017; Zwicky, 1933). One of the most compelling pieces of evidence in favour of dark matter was first discovered by Rubin (1983) and involves the rotation curve of spiral galaxies. Newtonian mechanics predicts that the rotational velocity v of a galaxy should vary with the distance r from the centre as $v \propto r^{-1/2}$. What is observed however is that the rotational velocity remains constant at large distances. Rubin noticed that this rotation curve is best described by a dark matter halo extending to a large distance beyond the visible matter radius of the galaxy. Other evidence in favour of dark matter includes the velocity of galaxies in clusters (Rasia et al., 2004), and gravitational lensing (Kaiser and Squires, 1993). Dark matter makes up $25.8 \pm 0.8\%$ of the energy content of the Universe, which is the majority of all the matter content (Tanabashi et al., 2018). Together, Λ and CDM are a vital part of the standard cosmological model, ΛCDM, which is based on Einstein's theory of GR. The other major principles of the ΛCDM model are discussed in Sec. 3.1.

The ΛCDM model seems to explain the dynamics of our Universe quite accurately. However, in the context of this model, dark matter and dark energy make up more than 95% of the energy content of the Universe. Although we have started to make some progress in our theoretical understanding of dark matter (Feng, 2010), it has not yet been directly detected and both of these dark components remain a mystery. This suggests that there might be a different theory of gravity which can explain all the observed phenomena without the need to infer the existence of dark energy and dark matter (Clifton et al., 2012).

Despite our lack of understanding of dark energy and dark matter, the ΛCDM model is widely accepted by the scientific community. However, the model is not without its flaws. One of the most significant tensions that has become even more evident through recent measurements is known as the **Hubble tension** (Bernal et al., 2016). The Hubble constant H_0 measures the current rate at which the Universe is expanding. There are two main methods by which this constant is measured. One uses local measurements from astronomical objects of known brightness called standard candles (Riess et al., 2016). This method gives a value of H_0 that is independent of any cosmological model. The other method uses the fluctuation spectrum of the CMB together with the ΛCDM model to obtain a model-dependant value of H_0 (Jackson, 2007). More details about these two methods and the precise values obtained are given in Sec. 3.1.1. It has become clear in recent years that the values obtained using these late-time and early-time measurements of H_0 are diverging. As measurement techniques become more accurate, this divergence can no longer be attributed to systematic errors and the statistical difference between the two values has reached a 5σ level (Riess et al., 2021). This could mean that the ΛCDM model is incomplete, i.e. another component must be added for this tension to be resolved. An example of this approach is the work by Poulin et al. (2019), in which early dark energy is used to resolve the Hubble tension. The disadvantage of this method is that even more unknown components are added in order to make the model fit observations. The alternative explanation is that the ΛCDM model, and the theory of gravity it is based upon, GR, are not the right description of Nature and need to be modified.

There are further motivations for finding modified theories of gravity including other problems with ΛCDM; see Sec. 3.1.6. Another motivation comes from the attempt at finding a unified theory that explains all the fundamental forces in a single theoretical framework. Attempts at unifying GR and quantum mechanics, the two main theories in modern physics, have so far been unsuccessful, and so modified theories of gravity might allow for different approaches through which this problem is tackled (Clifton et al., 2012).

There have been numerous proposals of modified theories of gravity. A review of these theories is given by Clifton et al. (2012). One of such modified gravity theories is the **Teleparallel Equivalent of General Relativity (TEGR)**, which explains gravity through torsion rather than curvature (Bahamonde et al., 2021). TEGR itself produces the same dynamics as GR, however, modifications of these two theories produce distinct dynamics.

In this work the $f(T, T_G)$ (Kofinas and Saridakis, 2014) extension of TEGR will be considered to uncover new behaviour. This modification is based on the torsion scalar

T and the invariant T_G, the teleparallel equivalent of the Gauss-Bonnet term in GR. The cosmological dynamics that this theory can produce will be investigated to determine whether the $f(T, T_G)$ modification can describe the late-time behaviour of the Universe. This will be done via a dynamical systems approach. This method has the power of uncovering the general dynamics of a gravitational model without the need to impose any constraints or initial conditions (Bahamonde et al., 2018). Thus, this provides the perfect approach at an initial investigation of this modification.

The structure of the dissertation is as follows. In Chapter 2 the theories of GR and TEGR are introduced. Modifications of the two theories are also discussed, with an emphasis made on the $f(T, T_G)$ modification. In Chapter 3, the standard cosmological model is discussed together with the dynamics of the Universe and problems with ΛCDM. This is then compared to the cosmological dynamics resulting from the $f(T, T_G)$ modification. This chapter concludes with an introduction to the dynamical systems approach applied to cosmological models. Chapter 4 discusses in detail the dynamical analysis performed on the four chosen $f(T, T_G)$ models, and the cosmological implications of the results. Finally, Chapter 5 summarises the findings of this work and draws some conclusions.

Note that the convention $c = 1$ will be used throughout this study unless otherwise stated.

2

General Relativity and its Teleparallel Equivalent

Even though, in recent years, growing problems with Einstein's theory of GR have started to surface, mainly when incorporated into the ΛCDM cosmological model as seen in Chapter 1, it still remains an extremely successful theory. So much so that most of the alternative gravitational theories build upon the geometric foundations of GR and its teleparallel equivalent, rather than taking a non-geometric approach. Thus, in this chapter, the mathematical formulation of GR will be explicitly developed and then compared to TEGR, which explains gravity through torsion rather than curvature.

Although TEGR and GR are dynamically equivalent theories, TEGR offers new possibilities when it comes to modifications of the theory. This is in part due to the possibility of constructing second order theories which are distinct from the original theory itself, something which is not possible using curvature-based GR. Thus, TEGR and its modifications warrant in-depth investigations, as indeed are being carried out in the literature. For a review of such modifications see (Bahamonde et al., 2021). The main modification that will be introduced in this chapter is the $f(T, T_G)$ modification, which will be the focus of most of this work.

2.1 | Einstein's Theory of General Relativity

2.1.1 | An Introduction to Tensors and Manifolds

Tensors are algebraic objects on which GR is based upon. Carroll (2004), defines a tensor as 'a multilinear map from a collection of dual vectors and vectors to $\mathbb{R}$.' We say that a tensor has rank (k, l), where k is the number of covariant indices, and l is the number of contravariant indices. Tensors are invariant under a change of coordinate systems, however tensor components change as,

$$T'^{\mu_1...\mu_k}{}_{\nu_1...\nu_l} = \frac{\partial x'^{\mu_1}}{\partial x^{\mu_1}} ... \frac{\partial x'^{\mu_k}}{\partial x^{\mu_k}} \frac{\partial x^{\nu_1}}{\partial x'^{\nu_1}} ... \frac{\partial x^{\nu_l}}{\partial x'^{\nu_l}} T^{\mu_1...\mu_k}{}_{\nu_1...\nu_l} \,, \tag{2.1}$$

where we are transforming from a coordinate system x^i to another coordinate system x'^i.

The physical importance of tensors is rooted in their property of being invariant under diffeomorphism transformations. This means that the form of any physical law is preserved under an arbitrary differentiable coordinate transformation. This is an important condition for physical laws as coordinate maps do not exist a priori in nature but are rather a mathematical construct to help express physical laws and so should not affect the predictions of a theory. The same concept is seen in the theory of Special Relativity (SR) in which the laws of mechanics have the same form in any inertial frame (Blagojević, 2002).

Another mathematical object of importance is a manifold. An n-dimensional manifold is a topological space which locally looks like $\mathbb{R}^n$. Two illustrative examples of a two-dimensional manifold are the surfaces of a two-sphere and that of a torus. In GR, spacetime is represented by a four-dimensional manifold. The local properties of $\mathbb{R}^n$ reflect the laws of SR holding locally about each point in spacetime, which is known as local Lorentz invariance (Bahamonde et al., 2021).

With every manifold we can associate a metric tensor $g_{\mu\nu}$ which generalises the idea of an inner product of two vectors in flat space. $g_{\mu\nu}$ is a symmetric tensor of rank (0,2) which is usually taken to be non-degenerate, i.e. it has non-zero determinant, in order to define the inverse metric tensor $g^{\mu\nu}$. A metric which has one time-like dimension is called Lorentzian. These are the type of metrics that are dealt with in GR.

The metric also generalizes the concept of Pythagoras' theorem in flat space since we can use it to define the line element (Carroll, 2004),

$$ds^2 = g_{\mu\nu} dx^\mu dx^\nu \,, \tag{2.2}$$

with x^μ representing a coordinate system. This idea can then be extended to define the path length for spacelike paths, i.e. paths with $ds^2 > 0$,

$$\Delta s = \int \sqrt{g_{\mu\nu} \frac{dx^\mu}{d\lambda} \frac{dx^\nu}{d\lambda}} d\lambda \,, \tag{2.3}$$

and the proper time for timelike paths, i.e. those with $ds^2 < 0$,

$$\Delta \tau = \int \sqrt{-g_{\mu\nu} \frac{dx^\mu}{d\lambda} \frac{dx^\nu}{d\lambda}} d\lambda \,. \tag{2.4}$$

In GR the metric tensor is not known a priori like in SR but is rather the solution of Einstein's field equations (see Sec. 2.1.4). The metric tensor in GR is referred to as the fundamental object of study as its uses are far-reaching. In addition to the generalisation of the line element, these also include the determination of causality by defining the speed of light, and the definition of a notion of past and future.

The metric tensor and its inverse can also be used to raise and lower indices of tensor objects through the following relations (Carroll, 2004),

$$g^{\mu\nu}V_\nu = V^\mu\,, \tag{2.5}$$

$$g_{\mu\nu}\omega^\nu = \omega_\mu\,. \tag{2.6}$$

This gives us a way to change covariant components into contraviariant ones and vice versa.

A special example of a metric tensor is the Minkowski metric $\eta_{\mu\nu}$ on flat space whose matrix representation is given by $\text{diag}(-1,1,1,1)$. Since the metric tensor is not unique for a given manifold, there are other metrics that can be used on flat space such as $ds^2 = -dt^2 + dr^2 + r^2 d\theta^2 + r^2 \sin^2\theta d\phi^2$ arising from spherical polar coordinates (t, r, θ, ϕ) (Camilleri, 1999).

2.1.2 | The Levi Civita Connection

When dealing with a curved manifold, the concept of a partial derivative is no longer sufficient and needs to be generalised to the covariant derivative ∇, an operator which gives the partial derivative in the case of flat space but transforms as a tensor in the case of an arbitrary manifold. For a vector field V^μ, we can do this by writing ∇ as the sum of the partial derivative and some correction in the form of a matrix,

$$\nabla_\mu V^\nu = \partial_\mu V^\nu + \mathring{\Gamma}^\nu_{\mu\lambda} V^\lambda\,. \tag{2.7}$$

The matrices $\mathring{\Gamma}^\nu_{\mu\lambda}$ are called the connection coefficients.

To understand the need for these corrections, consider the parallel transport of a vector. This is the concept of moving a vector along a path while keeping it constant at all times. This is done unknowingly when dealing with vectors in flat space. In order to compare two vectors, for example by subtracting them, we shift both to the same starting point. Now consider a vector on a curved surface such as a sphere. When parallel transporting this vector along a curve with the same start and end points, the resulting vector will not necessarily align with the original vector even though the vector was not transformed in any way. This is illustrated in Fig. 2.1. The difference arises due to the curvature of the surface and in order to compare vectors, the covariant derivative

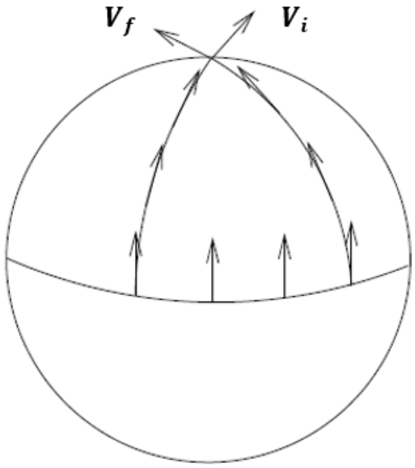

Figure 2.1: Parallel transport of a vector on a sphere. Figure adapted from Carroll (2004).

is used so as to account for such differences. The idea of the covariant derivative of a vector can then be extended to tensors.

We can define the torsion tensor using these connection coefficients,

$$\mathring{T}_{\mu\nu}{}^{\lambda} = \mathring{\Gamma}^{\lambda}_{\mu\nu} - \mathring{\Gamma}^{\lambda}_{\nu\mu} = 2\mathring{\Gamma}^{\lambda}_{[\mu\nu]} \,. \tag{2.8}$$

This torsion tensor will be of specific importance when dealing with TEGR.

In GR, a unique connection arising from the metric of a manifold $g_{\mu\nu}$ is used. This is referred to as the Levi-Civita connection, with the connection coefficients called the Christoffel symbols, and is defined as (Carroll, 2004),

$$\mathring{\Gamma}^{\sigma}_{\mu\nu} = \frac{1}{2} g^{\sigma\rho} \left(\partial_\mu g_{\nu\rho} + \partial_\nu g_{\rho\mu} - \partial_\rho g_{\mu\nu} \right) . \tag{2.9}$$

This connection is metric compatible and so satisfies $\nabla_\rho g_{\mu\nu} = 0$. It also has the property of being torsion-free, meaning that the Christoffel symbols are symmetric in the lower two indices. A direct consequence of this is that $\mathring{T}_{\mu\nu}{}^{\lambda} = 0$ leaving only one way to describe gravity, through curvature.

2.1.3 | The Riemann and Einstein Tensors

The connection defined above sets the geometrical framework to describe gravity. However, certain specific tensors need to be constructed in order to describe a theory which is diffeomorphism invariant as discussed in Sec. 2.1.1. These will be required to characterize gravitational fields and construct a Lagrangian which will eventually lead to the Einstein field equations.

The most fundamental of such tensors is the **Riemann tensor**, or the curvature tensor (Wald, 1984),

$$\mathring{R}^{\rho}{}_{\sigma\mu\nu} = \partial_{\mu}\mathring{\Gamma}^{\rho}_{\mu\sigma} - \partial_{\nu}\mathring{\Gamma}^{\rho}_{\mu\sigma} + \mathring{\Gamma}^{\rho}_{\mu\lambda}\mathring{\Gamma}^{\lambda}_{\nu\sigma} - \mathring{\Gamma}^{\rho}_{\mu\lambda}\mathring{\Gamma}^{\lambda}_{\mu\sigma}\,, \tag{2.10}$$

which characterises the curvature of a manifold at every point in the following way. If all the components of this tensor vanish, then we can always find a coordinate system in which the metric $g_{\mu\nu}$ is constant everywhere and thus the manifold can be considered to be flat. Having a constant metric is also a sufficient condition for having $\mathring{R}^{\rho}{}_{\sigma\mu\nu} = 0$. Thus, having a non-zero Riemann tensor necessarily implies that the manifold has curvature (Camilleri, 1999).

In order to describe the symmetries of the Riemann tensor it is useful to use the Riemann tensor with all lower indices, using the metric tensor as defined in Eq. (2.6),

$$\mathring{R}_{\rho\sigma\mu\nu} = g_{\rho\lambda}\mathring{R}^{\lambda}{}_{\sigma\mu\nu}\,. \tag{2.11}$$

The Riemann tensor has the following properties:

- It is antisymmetric in the last two indices: $\mathring{R}_{\rho\sigma\mu\nu} = -\mathring{R}_{\rho\sigma\nu\mu}$
- It is also antisymmetric in its first two indices: $\mathring{R}_{\rho\sigma\mu\nu} = -\mathring{R}_{\sigma\rho\mu\nu}$
- It is symmetric in the first pair of indices with the second pair: $\mathring{R}_{\rho\sigma\mu\nu} = \mathring{R}_{\mu\nu\rho\sigma}$
- It satisfies the first (algebraic) Bianchi identity: $\mathring{R}_{\rho[\sigma\mu\nu]} = 0$
- It satisfies the second (differential) Bianchi identity: $\nabla_{[\lambda}\mathring{R}_{\rho\sigma]\mu\nu} = 0$.

These symmetries reduce the number of degrees of freedom of the tensor from n^4 to $\frac{1}{12}n^2(n^2-1)$, with n being the dimension of the manifold. In GR, $n = 4$ and so the Riemann tensor has 20 independent components (Carroll, 2004).

When defining the Riemann tensor as in Eq. (2.10) using the Levi-Civita connection, the only independent contraction that one can perform is,

$$\mathring{R}_{\mu\nu} = \mathring{R}^{\lambda}{}_{\mu\lambda\nu}\,. \tag{2.12}$$

Other contractions either vanish or reduce to $\pm\mathring{R}_{\mu\nu}$ (Schutz, 2009). This is known as the **Ricci tensor** and is a symmetric tensor.

We can take a further contraction using the metric, to obtain the **Ricci scalar**,

$$\mathring{R} = \mathring{R}^{\mu}{}_{\mu} = g^{\mu\nu}\mathring{R}_{\mu\nu}\,. \tag{2.13}$$

This scalar will turn out to be extremely useful when defining the Einstein-Hilbert action in Sec. 2.1.4.

Taking two contractions of the second Bianchi identity gives a relation between the covariant derivatives of the Ricci tensor and scalar (Carroll, 2004),

$$\nabla^{\mu}\mathring{R}_{\rho\mu} - \frac{1}{2}\nabla_{\rho}\mathring{R} = 0\,. \tag{2.14}$$

If we define the **Einstein tensor** as,

$$\mathring{G}_{\mu\nu} = \mathring{R}_{\mu\nu} - \frac{1}{2}\mathring{R}g_{\mu\nu}\,, \tag{2.15}$$

then Eq. (2.14) reduces to,

$$\nabla^{\mu}\mathring{G}_{\mu\nu} = 0\,. \tag{2.16}$$

The Einsten tensor in Eq. (2.15) will appear in the Einstein field equations and Eq. (2.16) is essential to ensure consistency of these field equations (Wald, 1984).

2.1.4 | Gravitation and the Einstein Field Equations

A physical law of gravity should mathematically describe two things; how the gravitational field affects the motion of matter, and how matter determines the gravitational field. Newton's classical theory of gravity does this through the equations,

$$\mathbf{a} = -\nabla\Phi \tag{2.17}$$

$$\nabla^2\Phi = 4\pi G\rho\,, \tag{2.18}$$

where $\mathbf{a}$ is the acceleration of a body, Φ is the gravitational potential, G is Newton's gravitational constant, and ρ is the matter density (Carroll, 2004).

Einstein formulated his theory of gravitation based on the Weak Equivalence Principle (WEP):

> 'The motion of freely-falling particles are the same in a gravitational field and a uniformly accelerated frame, in small enough regions of spacetime.' (Carroll, 2004)

and the Einstein Equivalence Principle (EEP):

> 'Any local physical experiment not involving gravity will have the same result if performed in a freely falling inertial frame as if it were performed in the flat spacetime of special relativity.' (Schutz, 2009)

The WEP implies that gravity and inertia should be seen as related phenomena, while the EEP means that gravity does not change any physical laws locally. The WEP leads to the idea that the motion of a test particle in a gravitational field can equivalently be

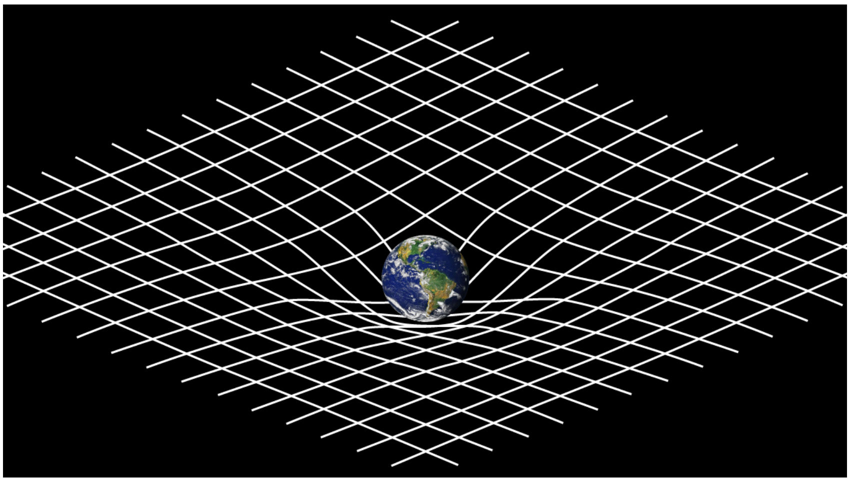

Figure 2.2: A visual representation of matter causing the spacetime manifold to curve. Figure credit: NASA (Mattson, 2015).

viewed as the motion along a geodesic in curved space. A geodesic is the generalisation of a straight line to curved space; it is the path of least resistance that a particle will travel along when not experiencing any external, non-gravitational forces. It is also a curve of extremal length between two points, meaning that it is stationary with respect to (wrt) variations. A particle's position x is thus determined by the geodesic equation (Schutz, 2009),

$$\frac{d^2x^\alpha}{d\tau^2} + \mathring{\Gamma}^\alpha_{\mu\nu}\frac{dx^\mu}{d\tau}\frac{dx^\nu}{d\tau} = 0\,. \tag{2.19}$$

If we use the Levi-Civita connection in flat space, Eq. (2.19) reduces to $d^2x^\mu/d\lambda^2 = 0$ which is simply the equation of a straight line (Carroll, 2004).

The source of the curvature of spacetime is the matter in spacetime itself. In simple terms as John Wheeler puts it in Misner et al. (1973),

'Spacetime tells matter how to move and matter tells spacetime how to curve.'

A visual representation of this can be seen in Fig. 2.2. In GR, the Newtonian potential is replaced by the metric while the mass density is generalised to the energy-momentum tensor $\Theta^{\mu\nu}$ which encompasses all the information about the energy-like aspects of the Universe including energy density, pressure and stress. These originate from matter, radiation and non-gravitational fields.

By generalising Eq. (2.18) to a relativistic setting and ensuring that in the weak field limit, the Newtonian theory is recovered, the **Einstein field equations of general relativity** can be obtained (Carroll, 2004),

$$\mathring{R}_{\mu\nu} - \frac{1}{2}\mathring{R}g_{\mu\nu} = 8\pi G\Theta_{\mu\nu}\,. \tag{2.20}$$

The left hand side of the equation can be recognised as Einstein's tensor $\mathring{G}_{\mu\nu}$ defined in Eq. (2.15), while the right hand side represents the matter content of the Universe.

Equation (2.20) comprises of a total of sixteen equations, however since both sides are symmetric tensors with two indices, these are reduced to ten independent equations. Furthermore, the Bianchi identity in Eq. (2.16) represents four constraints on the Ricci tensor and so the number of independent equations is reduced to six. Since the metric, which is the dynamical variable, has ten unknown components, this implies that by solving the field equations we cannot fully determine the metric. This ambiguity is desired as it implies that the Einstein field equations only determine $g_{\mu\nu}$ up to a general coordinate transformation (Ohanian and Ruffini, 2013).

A more modern approach to derive the field equations uses the principle of least action and was first proposed by Hilbert in 1915. This principle states that the trajectory of a particle is that along which the action is locally stationary. This action should be the integral over the spacetime manifold M of a Lagrange density $\mathcal{L}$ (Carroll, 2004),

$$S_H = \int_M \mathcal{L}_H d^4x \,. \tag{2.21}$$

$\mathcal{L}$ can be written as $\sqrt{-g}$ multiplied by a scalar, where g is the determinant of the metric tensor. Since the gravitational potential in Newton's theory satisfies a second order differential equation, we require an action that depends on the derivatives of the metric of at most second order. The Ricci scalar $\mathring{R}$, defined in Sec. 2.1.3, is the only independent scalar constructed from the metric which depends on at most its second order derivatives. Thus, Hilbert proposed the action (Hilbert, 1915),

$$S_H = \frac{1}{2\kappa^2} \int_M \mathring{R} \sqrt{-g}\, d^4x \,, \tag{2.22}$$

where $\kappa^2 = 8\pi G$. The coefficient of the integral is chosen so that in the weak-field limit, Newton's theory is recovered.

Varying this action wrt the metric, one finds that the condition for $g_{\mu\nu}$ to be a critical point is,

$$\mathring{R}_{\mu\nu} - \frac{1}{2}\mathring{R} g_{\mu\nu} = 0 \,. \tag{2.23}$$

These are the Einstein field equations in vacuum i.e. in the absence of any matter content. The variation is taken wrt the metric as this is the only fundamental degree of freedom of the theory. In Sec. 2.2.3, when dealing with TEGR, we will see that this theory has more than one degree of freedom and so the minimisation will need to be performed more than once.

To factor in the contribution of matter, an action of the form,

$$S = S_H + S_M \,, \tag{2.24}$$

is considered. Varying wrt the metric once again we obtain,

$$\mathring{R}_{\mu\nu} - \frac{1}{2}\mathring{R}g_{\mu\nu} = 8\pi G\Theta_{\mu\nu}\,, \tag{2.25}$$

where the stress-energy-momentum tensor is given by,

$$\Theta_{\mu\nu} = -\frac{1}{\sqrt{-g}}\frac{\delta S_M}{\delta g^{\mu\nu}}\,. \tag{2.26}$$

In order to fit the astronomical observations of the time which implied a static universe, as seen in Chapter 1, it was necessary to modify the Einstein-Hilbert action to,

$$S = \frac{1}{2\kappa^2}\int_M (\mathring{R} - 2\Lambda)\sqrt{-g}\, d^4x + S_M\,, \tag{2.27}$$

where Λ is a constant known as the **cosmological constant**. Varying this action wrt the metric gives the following field equations,

$$\mathring{R}_{\mu\nu} - \frac{1}{2}\mathring{R}g_{\mu\nu} + \Lambda g_{\mu\nu} = 8\pi G\Theta_{\mu\nu}\,. \tag{2.28}$$

By fine tuning Λ, Einstein managed to obtain a static universe solution.

The term in Λ in Eq. (2.28) is usually taken on the right hand side of the equation and can be thought of as contributing to the energy-momentum tensor. Hence, adding the cosmological constant is equivalent to introducing a vacuum energy density (Carroll, 2004) given by,

$$\rho\text{vac} = \frac{\Lambda}{8\pi G}\,. \tag{2.29}$$

Λ represents what is known as **dark energy** and makes up 68% of all the matter and energy content in the universe (Ade et al., 2014) (see Chapter 3 for a further discussion).

2.1.5 | Modifications of GR

As discussed before, GR has proven to be a very successful theory. However, problems with the theory remain. Some of these relate to inflation, late-times acceleration, the tension in the value of the Hubble constant and the failure in unifying GR with quantum theory in order to obtain a unified theory (Debono and Smoot, 2016). Details of some of these problems will be further discussed in Sec. 3.1.6. These cosmological problems challenge the position of GR as the accepted theory of gravitation and motivate the need to look for modifications of it.

Another major problem is our inability to explain the nature of dark, or non-baryonic, matter and dark energy. Some progress is being made especially when it comes to explaining the nature of dark matter, see for example Arkani-Hamed et al. (2009), however, an alternative is to modify the theory of gravity itself rather than modify the matter content of the theory. In this way the observed effects of dark matter and dark energy can be explained without having to assume their existence. There are a number of ways how this can be done, one of which is modifying the Einstein-Hilbert action, and thus consequently the field equations.

An example of this is $f(\mathring{R})$ gravity, a family of modifications in which the action is modified to (De Felice and Tsujikawa, 2010),

$$S = \int_M f(\mathring{R})\sqrt{-g}\, d^4x \,. \tag{2.30}$$

Here $f(\mathring{R})$ is some differentiable function of the Ricci scalar $\mathring{R}$. The simplest function is $f(\mathring{R}) = \mathring{R}$ which would recover the original field equations in Eq. (2.20). The correct choice of the function f can lead to a theory in which late-times acceleration is explained without the need for a cosmological constant (de la Cruz-Dombriz and Dobado, 2006). The drawback of such a modification is that in order to accurately produce a theory consistent with observations, an action with a complicated structure is required and so other types of modifications should be examined.

Another family of modified theories involves the Gauss-Bonnet term (de la Cruz-Dombriz and Sáez-Gómez, 2012)given by,

$$\mathring{G} = \mathring{R}^2 - 4\mathring{R}_{\mu\nu}\mathring{R}^{\mu\nu} + \mathring{R}_{\mu\nu\kappa\lambda}\mathring{R}^{\mu\nu\kappa\lambda} \,. \tag{2.31}$$

As a result of Gauss' theorem, $\mathring{G}$ is a topological surface term and so an action of the form,

$$S = \int_M \mathring{G}\sqrt{-g}\, d^4x \,, \tag{2.32}$$

does not affect the equations of motion. However, by considering the action,

$$S = \int_M f(\mathring{R}, \mathring{G})\sqrt{-g}\, d^4x \,, \tag{2.33}$$

new dynamics can be obtained (Quiros, 2021).

Both of the modifications in Eqs. (2.30) and (2.33) lead to theories which are of fourth-order in the derivative of the metric. Additionally, all other modifications of GR are also restricted to at least fourth order due to Lovelock's theorem. This states that if a gravitational action in four dimensions contains only up to the second derivative of the metric, then the only equations of motion resulting from such an action are the Einstein field equations (Lovelock, 1972). This puts a lower limit on the complexity of the modified theories we can obtain from curvature-based GR and motivates the investigation of TEGR.

2.2 | Teleparallel Gravity

An alternate theory of gravity that Einstein himself investigated is TEGR. In this theory, the gravitational interaction is a result of the torsion of a connection with zero curvature rather than due to the curvature of a zero-torsion connection (Krššák et al., 2019). TEGR can be dynamically equivalent to GR, however it can also produce novel theories through modifications of the teleparallel action. One of the main differences between TEGR and GR is that TEGR meets the requirements of a gauge theory, like electromagnetism (EM). Although Einstein's own attempts to unify EM and TEGR have failed, modifications of TEGR are proving to be a good candidate for explaining what GR, and other curvature-based gravity theories, fail to, such as the accelerated expansion of the Universe (Bengochea and Ferraro, 2009) and inflation (Ferraro and Fiorini, 2007).

2.2.1 | Tetrads and the Spin Connection

As in the theory of GR, spacetime is a 4-dimensional manifold with a metric $g_{\mu\nu}$ whose tangent space at each point is Minkowski Space with a metric η_{AB}. Note that capital letters denote Lorentz indices whereas small Greek letters denote spacetime indices. In teleparallel gravity, the dynamical variables are the tetrad (or vierbein) field $e^A{}_\mu$ and the spin connection $\hat{\omega}^A{}_{B\mu}$. This means that in TEGR, the fundamental dynamical variable in GR which is the metric, is split into two, the tetrad field and the spin connection.

The tetrads form a basis, independent of any coordinate system, for the tangent space. They can be related to the basis formed from a coordinate system x^μ through,

$$\partial_\mu = e^A{}_\mu e_A \,. \tag{2.34}$$

Similarly to how we cannot, in general, define a coordinate chart that covers the whole manifold, we cannot find a tetrad field which exists globally and so we define such tetrads only locally (Bahamonde et al., 2021). For the metric to be non-degenerate, the tetrad is required to have an inverse/dual $E_A{}^\mu$ which satisfies,

$$E_A{}^\mu e^A{}_\nu = \delta^\mu_\nu \quad \text{and} \quad E_A{}^\mu e^B{}_\mu = \delta^B_A \,. \tag{2.35}$$

If we choose these basis vectors to be orthonormal, i.e.,

$$g_{\mu\nu} E_A{}^\mu E_B{}^\nu = \eta_{AB} \,, \tag{2.36}$$

then we obtain the following equations for the metric and inverse metric respectively,

$$g_{\mu\nu} = \eta_{AB} e^A{}_\mu e^B{}_\nu \,, \tag{2.37}$$

$$g^{\mu\nu} = \eta^{AB} E_A{}^{\mu} E_B{}^{\nu} \,. \tag{2.38}$$

Thus, the tetrad can be seen as the transformation between the spacetime metric $g_{\mu\nu}$ and the local Minkowski metric η_{AB}. They can also be thought of as a set of orthonormal vector fields which diagonalise the metric tensor.

We can use the tetrads and their inverse to switch between Latin to Greek indices and back. For a vector V whose representation in a coordinate basis is $V^{\mu}\partial_{\mu}$, we can obtain the tetrad representation $V^A e_A$ using,

$$V^A = e^A{}_{\mu} V^{\mu} \,. \tag{2.39}$$

This idea can then be extended to multi-index tensors (Carroll, 2004).

In the coordinate bases formulation, the covariant derivative was defined as the partial derivative in addition to some correction term given by the connection coefficients. In order to extend this concept to non-coordinate bases we need to define the **spin connection**, $\omega^A{}_{B\mu}$, which gives the covariant derivative,

$$\nabla_{\mu} X^A{}_B = \partial_{\mu} X^A{}_B + \omega^A{}_{C\mu} X^C{}_B - \omega^C{}_{B\mu} X^A{}_C \,. \tag{2.40}$$

Using the property that tensors transform independently of the basis, we can obtain a relationship between the affine teleparallel connection $\Gamma^{\rho}{}_{\mu\nu}$ and the spin connection $\omega^A{}_{B\mu}$,

$$\Gamma^{\rho}{}_{\mu\nu} = E_A{}^{\rho} (\partial_{\nu} e^A{}_{\mu} + \omega^A{}_{B\nu} e^B{}_{\mu}) \,. \tag{2.41}$$

This is the unique affine connection satisfying the **tetrad postulate**,

$$\partial_{\mu} e^A{}_{\nu} + \omega^A{}_{B\mu} e^B{}_{\nu} - \Gamma^{\rho}{}_{\nu\mu} e^A{}_{\rho} = 0 \,. \tag{2.42}$$

This postulate is a result of the requirement that the covariant derivative of the tetrad field vanishes, i.e. $\nabla_{\mu} e^A{}_{\mu} = 0$. This condition is satisfied by any affine connection, irrespective of assumptions made when deriving it, such as the connection being torsion free or metric compatible (Bahamonde et al., 2021).

2.2.2 | Local Lorentz Transformations and the Weitzenböck Gauge

The tetrad field and spin connection that give a metric $g_{\mu\nu}$ and an affine connection $\hat{\Gamma}^{\rho}{}_{\mu\nu}$ are not unique but are rather uniquely determined up to local Lorentz transformations. This means that if one changes the tetrad to,

$$e^A{}_{\mu} \to e'^A{}_{\mu} = \Lambda^A{}_B e^B{}_{\mu} \,, \tag{2.43}$$

the metric resulting from Eq. (2.37) is unchanged. We also have the usual freedom to choose a different basis and so Eq. (2.37) is also invariant under general coordinate transformations.

Similarly, the affine connection remains unchanged if we replace the spin connection by,

$$\omega^{A}{}_{B\mu} \to \omega'^{A}{}_{B\mu} = \Lambda^{A}{}_{C}(\Lambda^{-1})^{D}{}_{B}\omega^{C}{}_{D\mu} + \Lambda^{A}{}_{C}\partial_{\mu}(\Lambda^{-1})^{C}{}_{B}\,. \tag{2.44}$$

This means that we are free to choose a gauge through the spin connection. In teleparallel gravity the gauge that is chosen is known as the **Weitzenböck gauge** and is the one in which the spin connection vanishes, i.e. $\omega^{A}{}_{B\mu} = 0$ (Bahamonde et al., 2021). Equation (2.41) then gives the **Weitzenböck connection**,

$$\Gamma^{\rho}_{\mu\nu} = E_{A}{}^{\rho}\partial_{\nu}e^{A}{}_{\mu}\,. \tag{2.45}$$

This is a metric compatible connection, i.e. $\nabla_{\rho}g_{\mu\nu} = 0$, with a vanishing curvature but non-vanishing torsion.

2.2.3 | Teleparallel Equivalent of General Relativity

We can define the curvature and torsion tensors in the same way as in Eqs. (2.10) and (2.8), respectively, using the teleparallel connection to get (Krššák et al., 2019),

$$R^{A}{}_{B\mu\nu} = \partial_{\mu}\omega^{A}{}_{B\nu} - \partial_{\nu}\omega^{A}{}_{B\mu} + \omega^{A}{}_{C\mu}\omega^{C}{}_{B\nu} - \omega^{A}{}_{C\nu}\omega^{C}{}_{B\mu}\,, \tag{2.46}$$

and,

$$T^{A}{}_{\mu\nu} = \partial_{\mu}e^{A}{}_{\nu} - \partial_{\nu}e^{A}{}_{\mu} + \omega^{A}{}_{B\mu}e^{B}{}_{\nu} - \omega^{A}{}_{B\nu}e^{B}{}_{\mu}\,. \tag{2.47}$$

Since in the Weitzenböck gauge, the spin connection is zero, it follows from Eq. (2.46) that the Riemann tensor vanishes. On the other hand the torsion tensor is non-zero and simplifies to,

$$T^{A}{}_{\mu\nu} = \partial_{\mu}e^{A}{}_{\nu} - \partial_{\nu}e^{A}{}_{\mu}\,. \tag{2.48}$$

The geometrical difference between the curvature and torsion tensors is highlighted in Fig. 2.3. Whereas curvature quantifies the rotation of a vector which has been parallel transported along a closed curve on a manifold, torsion quantifies the non-closure of a parallelogram formed when two vectors are transported along each other.

Although it will not be discussed in detail in this work, it is interesting to note that the non-metricity of spacetime can also be used to describe gravity. This gives rise to what is known as the symmetric teleparallel equivalent of general relativity (STEGR). Together with GR and TEGR it forms part of 'the geometrical trinity of gravity' which is

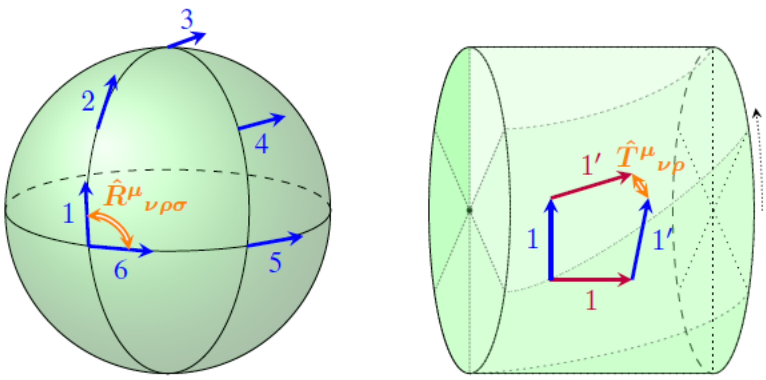

Figure 2.3: Geometrical difference between the curvature and torsion tensors. Figure taken from (Bahamonde et al., 2021).

a consequence of the universality implied by the equivalence principle (Jimenez et al., 2019). Each connection in these three theories of gravity should have $4^3 = 64$ independent components, however due to symmetries some of these freedoms are removed. Adding the degrees of freedom (DOF) of all three theories together recovers the original number of 64 DOF.

One can also define the contorsion tensor as the difference between the Weitzenböck and Levi-Civita connections (Combi and Romero, 2018),

$$K^{\rho}{}_{\mu\nu} = \mathring{\Gamma}^{\rho}_{\mu\nu} - \Gamma^{\rho}_{\mu\nu}\,. \tag{2.49}$$

Despite $K^{\rho}{}_{\mu\nu}$ being defined as the difference between two non-tensorial quantities, the contorsion tensor does indeed transform as a tensor. Expressing the torsion tensor as $T_{\mu\nu}{}^{\lambda} = \Gamma^{\lambda}_{\mu\nu} - \Gamma^{\lambda}_{\nu\mu}$, allows us to write this contorsion tensor purely in terms of the torsion tensor,

$$K^{\rho}{}_{\mu\nu} = \frac{1}{2} g^{\rho\sigma} \left(T_{\nu\sigma\mu} + T_{\mu\sigma\nu} - T_{\sigma\mu\nu} \right). \tag{2.50}$$

Since, in TEGR, all the information about the gravitational field is contained in the torsion tensor, we can use this to construct invariants which will be useful when formulating the Lagrangian of the theory. Of particular importance is the invariant T known as the torsion scalar which is quadratic in the torsion tensor and is given by,

$$T = \frac{1}{4} T^{\mu\nu\lambda} T_{\mu\nu\lambda} + \frac{1}{2} T^{\mu\nu\lambda} T_{\lambda\nu\mu} - T_{\nu}{}^{\nu\mu} T^{\lambda}{}_{\lambda\mu}\,. \tag{2.51}$$

This scalar can be seen as the teleparallel equivalent to the Ricci scalar $\mathring{R}$ in GR in the sense that we can use T to construct an action that gives rise to the field equations. This action is given by,

$$S_{\mathrm{TEGR}} = -\frac{1}{2\kappa^2} \int_M T e \, d^4 x\,, \tag{2.52}$$

where $e = \det(e^{A}{}_{\mu}) = \sqrt{-g}$ (Bahamonde et al., 2021) and we are identifying the Lagrangian of the theory as $\mathcal{L} = -Te$. Since the torsion tensor, and thus the torsion scalar, only contain up to the first-derivative of the metric, so does this Lagrangian. This is in contrast with GR whose Lagrangian $\mathcal{L}_H$ is constructed from the Ricci scalar. This results in the Einstein-Hilbert action containing up to second order derivatives of the metric.

Varying the action in Eq. (2.52) wrt the tetrad field results in the same field equations derived from the Einstein-Hilbert action as given in Eq. (2.25). This is because the Ricci scalar $\mathring{R}$ and the torsion scalar T are related via a boundary term B,

$$T + \mathring{R} = B\,, \tag{2.53}$$

and consequently GR and TEGR are necessarily dynamically equivalent theories. The boundary term B is related to the Lovelock theorem discussed in Sec. 2.1.5 and is what forces all second-order curvature-based theories to be equivalent to GR. When using the tetrad field as the fundamental variable of the theory rather than the metric, we can consider modifications of the four-dimensional action in Eq. (2.52) which produce second order theories that are distinct from TEGR, without violating the Lovelock theorem (Bahamonde et al., 2021). This is one of the main advantages that the teleparallel formulation has over traditional GR.

Apart from varying the action S_{TEGR} wrt the tetrad field, we can also vary this action wrt the spin connection. This is because the spin connection represents an independent degree of freedom and thus extra equations are required for it to be determined. In TEGR, these spin connection equations coincide with the antisymmetric form of the tetrad field equations and are automatically satisfied. This is in line with the idea that the spin connection represents degrees of freedom associated with the Lorentz group and so cannot contribute more independent dynamical equations to describe the gravitational system (Golovnev et al., 2017).

2.2.4 | Modifications of TEGR

As was done in Sec. 2.1.5 for the theory of GR, we can also consider modifications of TEGR to explain phenomena such as late-time acceleration as well as to produce competing theories of cosmology more generally. The simplest modification that one can perform is to extend the TEGR action to (Cai et al., 2016),

$$S = \frac{1}{2\kappa^2}\int_M ef(T)d^4x\,. \tag{2.54}$$

Although the Einstein-Hilbert action and the TEGR action, Eqs. (2.22) and (2.52), result in the same dynamics, $f(\mathring{R})$ and $f(T)$ theories give rise to different field equations. One of the main differences is that the $f(T)$ field equations are of second order, meaning that they contain up to second time derivatives of the scale factor $a(t)$, while those resulting from the $f(\mathring{R})$ modification are of fourth order. This has wide-ranging cosmological implications and this theory has been studied extensively (Cai et al., 2016).

Although the torsion scalar T is the simplest, it is not the only invariant constructed from the torsion tensor. One can define the invariant T_G as,

$$\begin{aligned} T_G = (&K^{\kappa}{}_{\varphi\pi}K^{\varphi\lambda}{}_{\rho}K^{\mu}{}_{\chi\sigma}K^{\chi\nu}{}_{\tau} - 2K^{\kappa\lambda}{}_{\pi}K^{\mu}{}_{\varphi\rho}K^{\varphi}{}_{\chi\sigma}K^{\chi\nu}{}_{\tau} \\ &+ 2K^{\kappa\lambda}{}_{\pi}K^{\mu}{}_{\varphi\rho}K^{\varphi\nu}{}_{\chi}K^{\chi}{}_{\sigma\tau} + 2K^{\kappa\lambda}{}_{\pi}K^{\mu}{}_{\varphi\rho}K^{\varphi\nu}{}_{\sigma,\tau})\delta^{\pi\rho\sigma\tau}_{\kappa\lambda\mu\nu}. \end{aligned} \tag{2.55}$$

Here $K^{\rho}{}_{\mu\nu}$ is the contorsion tensor defined in Eq. (2.50) and $\delta^{\pi\rho\sigma\tau}_{\kappa\lambda\mu\nu}$ is the generalised Kronecker delta defined as,

$$\delta^{\mu_1 \dots \mu_p}_{\nu_1 \dots \nu_p} = \begin{cases} +1 & \text{if } \nu_1 \dots \nu_p \text{ are distinct integers and are an even permutation of } \mu_1 \dots \mu_p \\ -1 & \text{if } \nu_1 \dots \nu_p \text{ are distinct integers and are an odd permutation of } \mu_1 \dots \mu_p \\ 0 & \text{otherwise.} \end{cases} \tag{2.56}$$

We can thus consider another class of modified theories of gravity resulting from the action,

$$S = \frac{1}{2\kappa^2}\int_M e f(T, T_G) d^4x\,. \tag{2.57}$$

$f(T, T_G)$ gravity is the teleparallel equivalent to $f(\mathring{R}, \mathring{G})$ gravity resulting from the action in Eq. (2.33). However, these two modifications result in different dynamics, as in the case of $f(\mathring{R})$ and $f(T)$ gravity. T_G is quartic in the torsion tensor and so this class of modifications is more general than the $f(T)$ class (Kofinas et al., 2014). The $f(T, T_G)$ modification will be the main focus of this work and the cosmology resulting from the action in Eq. (2.57) is described in Sec. 3.2.

3

Cosmology & Dynamical Systems

3.1 | The Standard Model of Cosmology

Our current best model for understanding the dynamics of the Universe is the ΛCDM model as introduced in Chapter 1. ΛCDM has been successful in explaining multiple properties of the observed Universe including the power spectrum of the CMB anisotropies (Page et al., 2003), the abundance of the light elements hydrogen, helium and lithium (Cyburt et al., 2016), the spectrum and statistical properties of large-scale structure (Bernardeau et al., 2002), and the accelerated expansion of the Universe (Perlmutter et al., 1999; Riess et al., 1998).

The central assumptions of the ΛCDM model are the following (Perivolaropoulos and Skara, 2021).

- The main components of the Universe are radiation (photons and neutrinos), ordinary matter (baryons and leptons), CDM, which is responsible for structure formation (Hu, 1998), and vacuum energy, which is driving the late-time acceleration.
- GR is the correct theory that describes gravity on cosmological scales.
- The cosmological principle holds at sufficiently large scales. This means that the Universe is considered to be homogeneous and isotropic on large scales. Homogeneity means the Universe looks the same at each point i.e. it has the same density throughout, while isotropy means that the Universe looks the same, in terms of polarisation, in every direction. This isotropy is confirmed by observations of the CMB (Readhead and Lawrence, 1992) and large-scale smoothness has been observed in galaxy surveys such as the Sloan Digital Sky Survey (SDSS) (Blanton et al., 2017).

- The spatial geometry of the Universe is considered to be flat, in line with observations (Ade et al., 2014).

In this section the main features of the ΛCDM model and the need to look beyond it to obtain a better cosmological model which describes Nature will be discussed.

3.1.1 | The Expansion of the Universe

A fundamental piece of observational evidence in cosmology is that everything in the Universe is receding away from us. This is inferred from observing the spectra of galaxies. By comparing the observed emission spectra to the expected ones, their red shift z can be calculated using,

$$z = \frac{\lambda_{obs} - \lambda_{em}}{\lambda_{em}}, \tag{3.1}$$

where λ_{obs} is the observed wavelength and λ_{em} is the emitted one. For a nearby object, we can relate this redshift to the velocity, v, of the galaxy through the equation,

$$z = \frac{v}{c} \tag{3.2}$$

with c being the speed of light.

When observing a large number of galaxies, the general trend is found to be that galaxies are receding away from us as their light as detected on Earth is red-shifted. Some nearby galaxies are an exception to this rule as they have peculiar velocities caused by random motion. This is because the principle of homogeneity only holds for galaxies outside of the Local Group (Liddle, 2003).

In his 1929 paper (Hubble, 1929), Edwin Hubble proposes a linear relationship between the velocity v of a galaxy and its distance from Earth d given by,

$$v = H_0 d\,. \tag{3.3}$$

The constant of proportionality H_0 is what is known as **Hubble's constant**. This linear relationship can be seen in Fig. 1.1. To measure the recessional velocity v of an object along our line of sight we make use of the redshift and relate it to the velocity via Eq. (3.2). The distance d represents the proper distance to an object which can be estimated by making use of what are known as standard candles. These are astronomical objects whose intrinsic luminosity can be inferred from their other properties, such as type Ia Supernovae (SNIa) and Cepheid variables.

Recent measurements using these standard candles give a Hubble constant value of $H_0 = 73.30 \pm 1.04$ km/sec/Mpc (Riess et al., 2021) while data from *Planck*, gives

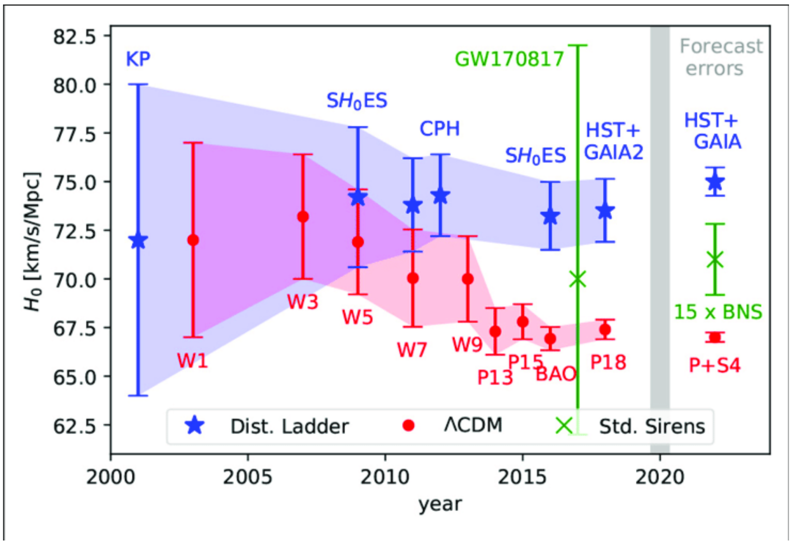

Figure 3.1: The Hubble tension's evolution over the past two decades. Figure taken from (Ezquiaga and Zumalacarregui, 2018). The blue stars correspond to measurements of H_0 made from the local Universe, calibrated using Cepheids. Red dots show measurements from the CMB based on ΛCDM, and green crosses show measurements using gravitational waves as standard sirens. Data sources include (Abbott et al., 2017), (Aghanim et al., 2020) and (Riess et al., 2018).

$H_0 = 67.4 \pm 0.5$ km/sec/Mpc (Aghanim et al., 2020). The latter uses measurements of the CMB anisotropies to give a ΛCDM-dependant value for H_0. This statistically significant 5σ difference between the two values has been confirmed repeatedly and there is sufficient evidence to conclude that it does not arise from systematic measurement errors. This difference is known as the Hubble tension and is an indication that the ΛCDM model is not an accurate description of the Universe, thus motivating the need to investigate modified theories of gravity resulting in different cosmological predictions (Di Valentino et al., 2021). Figure 3.1 shows values of H_0 obtained using different standard candles and CMB measurements over the years and clearly reflects the growing Hubble tension. Note that in this figure, measurements using gravitational waves as standard sirens are also included. This measurement compares the predicted energy of the gravitational wave with the actual energy detected. This comparison can then be used to calculate the distance to the galaxy in which the event creating these gravitational waves took place. Significant improvement of this method is expected within the next two decades which will surely improve our understanding of the nature of dark energy (Holz and Hughes, 2005).

Note that although the expansion of the Universe might make it seem that homogeneity is violated as galaxies are observed to be receding away from us, this is not the case as everything in the Universe is experiencing the same phenomenon. This concept is best understood by comparing the Universe to a balloon covered in dots, which is being blown up. In order to express this mathematically we make use of comoving coordinates which are coordinates that are carried through with the expansion. The real distance $\vec{r}$ and the comoving distance $\vec{x}$ are related via,

$$\vec{r} = a(t)\vec{x}\,, \tag{3.4}$$

where $a(t)$ is known as the **scale factor** and characterises the expansion. At the present time t_0, the scale factor is set to be equal to one.

In accordance with Hubble's Law, we can define the **Hubble parameter** as,

$$H(t) \equiv \frac{\dot{a}}{a}\,. \tag{3.5}$$

This measures how rapidly the scale factor changes (Dodelson, 2003). Through this equation it is clear that the term 'Hubble constant' is misleading as although the cosmological principle forces H to be a constant in space, it is not necessarily a constant in time. What is known as the Hubble constant H_0 is rather the value of the Hubble parameter at the present time i.e. $H_0 = H(t_0)$ (Liddle, 2003).

3.1.2 | The FLRW Metric

In order to incorporate the cosmological principle in the mathematical description of the Universe, we consider the spacetime manifold to be $\mathbb{R} \times \Sigma$, with $\mathbb{R}$ representing the time direction and Σ being a maximally symmetric three-manifold. The spacetime metric thus takes the form,

$$ds^2 = -dt^2 + a^2(t)d\sigma^2\,, \tag{3.6}$$

with $d\sigma$ representing the metric on Σ (Carroll, 2004). This metric allows the spatial component to be time-dependant.

The specific form of the metric in Eq. 3.6 which represents a maximally symmetric space is known as the **Friedmann–Lemaître–Robertson–Walker (FLRW) metric** and is given by,

$$ds^2 = -dt^2 + a^2(t)\left[\frac{dr^2}{1-\kappa r^2} + r^2(d\theta^2 + \sin^2\theta\, d\Phi^2)\right]\,, \tag{3.7}$$

in spherical polar coordinates. Here the parameter $\kappa = k/R_0^2$, with R_0 being the current radius of curvature, quantifies the geometry of the universe. $k = -1$ corresponds to constant negative curvature and leads to an open universe, $k = 1$ represents constant positive curvature and gives a closed universe, while $k = 0$ corresponds to a flat universe. The Planck collaboration in 2015 (Ade et al., 2016) constrained the value of the curvature density parameter Ω_K, which can be thought of as the curvature density of the Universe, to,

$$\Omega_K = 0.000 \pm 0.005\,. \tag{3.8}$$

This strongly indicates a spatially flat universe and so we can simplify the FLRW metric, in Cartesian coordinates, to (Kofinas et al., 2014),

$$ds^2 = -dt^2 + a^2(t)(dx^2 + dy^2 + dz^2)\,. \tag{3.9}$$

Note that in the rest of this work, a flat universe will be considered so as to reflect observational evidence. In addition, Cartesian coordinates will be used since they satisfy the Weitzenböck gauge conditions. This is because since these coordinates respect cosmological symmetries, the antisymmetric part of the field equations will vanish in any teleparallel gravity theory (Bahamonde et al., 2021).

Using Eq. (2.9), we can obtain the Christoffel symbols for the flat FLRW metric in Cartesian coordinates,

$$\mathring{\Gamma}^{0}{}_{00} = 0\,, \tag{3.10}$$
$$\mathring{\Gamma}^{0}{}_{0\mu} = \mathring{\Gamma}^{0}{}_{\mu 0} = 0\,, \tag{3.11}$$
$$\mathring{\Gamma}^{0}{}_{\mu\nu} = \delta_{\mu\nu}\dot{a}a\,, \tag{3.12}$$
$$\mathring{\Gamma}^{\mu}{}_{0\nu} = \mathring{\Gamma}^{\mu}{}_{\nu 0} = \delta_{\mu\nu}\frac{\dot{a}}{a}\,, \tag{3.13}$$

with all the other components $\mathring{\Gamma}^{\rho}{}_{\mu\nu}$ equal to zero (Dodelson, 2003). Using these values to explicitly calculate the Ricci tensor $\mathring{R}_{\mu\nu}$ and the Ricci scalar $\mathring{R}$ gives,

$$\mathring{R}_{00} = -3\frac{\ddot{a}}{a}\,, \tag{3.14}$$
$$\mathring{R}_{ij} = \delta_{ij}(2\dot{a}^2 + a\ddot{a})\,, \tag{3.15}$$
$$\mathring{R} = 6\left[\frac{\ddot{a}}{a} + \left(\frac{\dot{a}}{a}\right)^2\right]\,, \tag{3.16}$$

for $i, j = 1, 2, 3$. These will be used to obtain the specific form of Einstein's field equations in the case of a flat FLRW universe.

3.1.3 | Cosmic Dynamics

Since the Universe is dynamic, the scale factor evolves with time and this evolution depends on the matter and energy content. Mathematically, this evolution is described through what are known as the **Friedmann equations**, obtained by substituting the FLRW metric in Einstein's field equations as given in Eq. (2.28).

To obtain these equations we first need to specify the exact form of the energy-momentum tensor which appears in the field equations. The simplest way to do this is to model the contents of the Universe as a perfect isotropic fluid with density ρ and pressure p. This gives the energy-momentum tensor with one index raised as,

$$T^{\mu}{}_{\nu} = \mathrm{diag}(-\rho, p, p, p)\,. \tag{3.17}$$

Thus, using the expressions in Eqs. (3.10) - (3.16), the time-time component of Einstein's field equations becomes (Liddle, 2003),

$$H(t)^2 = \left(\frac{\dot{a}}{a}\right)^2 = \frac{8\pi G\rho}{3} + \frac{\Lambda}{3}\,. \tag{3.18}$$

This is known as the **the first Friedmann equation**, or simply as the Friedmann equation.

Due to isotropy, there is only one independent equation for the spatial part of the Einstein field equations given by (Carroll, 2004),

$$\frac{\ddot{a}}{a} + 2\left(\frac{\dot{a}}{a}\right)^2 = 4\pi G(\rho - p)\,. \tag{3.19}$$

Substituting for $(\dot{a}/a)^2$ from (3.18) we obtain,

$$\frac{\ddot{a}}{a} = -\frac{4\pi G}{3}(\rho + 3p)\,, \tag{3.20}$$

which is known as the **second Friedmann equation** or the **acceleration equation**. This equation implies that if the content of the universe has a positive pressure, which is what we are used to in the classical picture, then $\ddot{a}$ is negative, meaning that the Universe undergoes a decelerated expansion.

We can apply the usual law of conservation of energy to the stress-energy tensor in Eq. (3.17), by making use of the covariant derivative. Considering specifically the zeroth component (Carroll, 2004),

$$\begin{aligned} 0 &= \nabla_{\mu} T^{\mu}{}_{0} \\ &= \partial_{\mu} T^{\mu}{}_{0} + \mathring{\Gamma}^{\mu}_{\mu\lambda} T^{\lambda}{}_{0} - \mathring{\Gamma}^{\lambda}_{\mu 0} T^{\mu}{}_{\lambda}\,, \end{aligned} \tag{3.21}$$

we obtain,

$$\dot{\rho} + 3\frac{\dot{a}}{a}(\rho + p) = 0\,. \tag{3.22}$$

This is known as the **fluid equation** and describes how the energy density in the Universe changes because of two effects. The first term in Eq. (3.22) represents the dilation of energy because of the expansion of the Universe, while the second term shows that energy has gone into work during expansion. Note that pressure does not contribute a force that helps the Universe expand. This is because in a homogeneous universe, pressure is the same everywhere while a pressure gradient is needed in order to generate a force (Liddle, 2003). Note that we can use this fluid equation to give an alternate derivation of Eq. (3.20). This is done by differentiating Eq. (3.18) wrt time, and then substituting for $\dot{\rho}$ using Eq. (3.22) (Liddle, 2003).

The final equation that is required in order to solve for the evolution of the unknown quantities $a(t)$, $\rho(t)$ and $p(t)$ is what is known as the **equation of state (EoS)** which relates the pressure and density. In the context of cosmology, the EoS of the relevant sources takes on the simple linear form,

$$p = w\rho \,, \tag{3.23}$$

where w is called the equation-of-state parameter. There are specific values of w that are of interest. The first is $w = 0$ which holds in the case of non-relativistic matter, simply referred to as matter or dust. This is any material which exerts negligible pressure. Solving the fluid equation in this case gives $\rho \propto a^{-3}$. The second significant value of w is $1/3$ which corresponds to radiation. This follows from the fact that radiation, for example in the form of photons and neutrinos, satisfies the equation $p = \rho c^2/3$. In this case, the fluid equation gives $\rho \propto a^{-4}$. It follows that since radiation density drops off at a faster rate than matter density, in a universe containing just these two components, matter will eventually always dominate.

The final class of physically interesting values of w is motivated by the discovery of the late-times acceleration of the Universe (see Sec. 3.1.5). From Eq. (3.20) we notice that in order to achieve a positive acceleration we require $\rho + 3p < 0$. This inequality is true for $w < -1/3$, with these EoS parameters corresponding to dark energy. For the density of this component to remain constant, we require $w = -1$ and so this is the EoS parameter of a cosmological constant (Melchiorri et al., 2003).

Constraints on the equation of state of dark energy support the cosmological constant model however, some variation in w is not ruled out (Bean and Melchiorri, 2002). As such, other values of w for dark energy, and their implications on the fate of the Universe, have been investigated in the literature. These are split into two classes, the first of which is quintenssence-like dark energy with $w > -1$. This characterises a scalar field that evolves over time, which is currently displaced from, but is slowly approaching, the minimum of its potential (Caldwell et al., 1998; Ratra and Peebles, 1988). The second class has $w < -1$, known as phantom energy, and is similarly represented by a scalar field, this time with a negative kinetic energy term. Such a phantom energy density would become infinite over time, overcoming all other density components in the

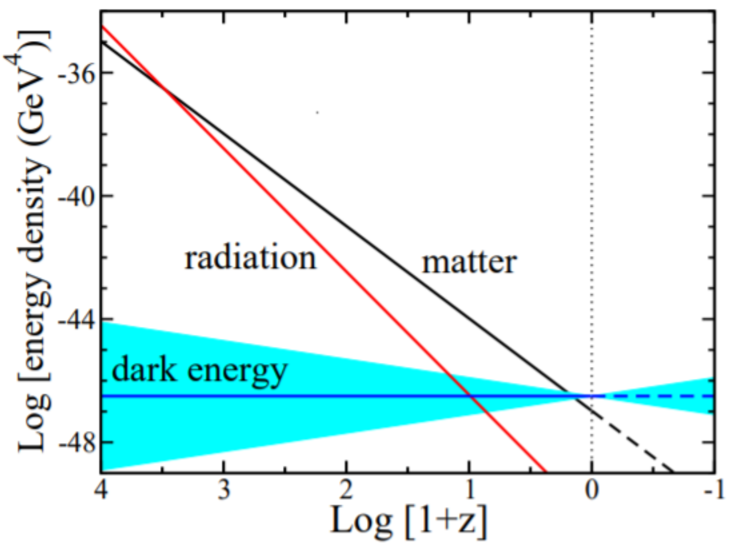

Figure 3.2: Evolution of radiation, matter and dark energy with redshift taken from Frieman et al. (2008). The band for dark energy represents $w_{DE} = -1.0 \pm 0.2$.

Universe and leading to what is known as the "Big Rip" (Caldwell et al., 2003). However, such phantom-like dark energy violates the null dominant energy condition, making it difficult (although not impossible) to construct viable models of dark energy with this EoS parameter (Carroll et al., 2003).

The Universe does not just consists of one of matter, radiation or dark energy, but rather consists of a mixture of them. However, because of the different rates at which their density drops off with the expansion of the Universe, different sources dominate at different times. This is clearly highlighted in Fig. 3.2 which shows the evolution of radiation, matter and dark energy. The times at which the Universe transitions from radiation-dominated to matter-dominated, and then to Λ-dominated can be calculated using the density parameter Ω as will be seen in Sec. 3.1.4.

In a universe dominated by matter or radiation, the scale factor varies polynomially with time, whereas for a universe dominated by a cosmological constant, the scale factor evolves exponentially as,

$$a(t) = e^{H_0(t-t_0)} . \tag{3.24}$$

This is known as a **de Sitter universe**. In line with observations pointing towards the energy density of dark energy being constant with time, and since the density of matter and radiation drops off as the Universe expands, Λ will eventually dominate, and thus our Universe is asymptotically de Sitter (de Sitter, 1917).

3.1.4 | Observational Parameters

Cosmological models, such as the ΛCDM model, have certain parameters which are determined observationally. The first of these is the Hubble constant H_0 which has been described in Sec. 3.1.1. With the rapid improvement of the instruments available to us, there are a wide range of properties of the universe which can now be measured to a high degree of precision, for example anisotropies in the CMB (White et al., 1994). For the scope of this project, the most significant observational parameters are the density parameter Ω and the deceleration parameter q.

Although the first Friedmann equation, Eq. (3.18), has so far been given for a flat universe, for a universe with curvature this equation can be expressed as (Carroll, 2004),

$$\Omega - 1 = \frac{\kappa}{H^2 a^2}\,, \tag{3.25}$$

where Ω is what is known as the **density parameter** of the Universe, given by $\Omega = \rho/\rho_c$. ρ_c is the **critical density** which is the density at which the geometry of the Universe is flat and is given by,

$$\rho_c = \frac{3H^2}{8\pi G}\,. \tag{3.26}$$

Thus we can see that the value of the parameter Ω determines this geometry of the Universe. When $\Omega = 1$, $\kappa = 0$ so the Universe is flat, when $\Omega > 1$, $\kappa > 0$, giving a closed universe, while when $\Omega < 1$, $\kappa < 0$, giving an open universe.

For a flat universe,

$$\Omega = 1 = \Omega_r + \Omega_m + \Omega_\Lambda\,, \tag{3.27}$$

where Ω_r is the density parameter of radiation, Ω_m is that of matter and Ω_Λ is that of dark energy. Note that the present day values of these density parameters will be denoted by a subscript 0. From (Ade et al., 2016), we can infer the present day value of Ω_r, to be about four orders of magnitude less than Ω_{m_0} and thus Eq. (3.27) is very often simplified to $1 = \Omega_m + \Omega_\Lambda$ to describe the late-time behaviour of the Universe, as will be done in this work.

We can use the measured values of the density parameters to estimate the time at which the different energy components started to dominate. At, for example, matter and dark energy equality,

$$\frac{\rho_\Lambda(a)}{\rho_m(a)} = \frac{\rho_{\Lambda_0}}{\rho_{m_0}/a^3} = \frac{\Omega_{\Lambda_0}}{\Omega_{m_0}}a^3\,. \tag{3.28}$$

From the measured values of the density parameters we can calculate the value of the red shift at radiation-matter equality to be $z \approx 3400$. This is located at the intersection of the red and black lines in Fig. 3.2. Similarly we find that dark energy started dominating over matter at $z \approx 0.55$ (Velten et al., 2014), which is extremely recent in cosmological time scales. This point corresponds to the intersection of the black and blue lines in Fig. 3.2, and it is clear from this figure how close to the present time this equality was reached.

In order to quantify the change of the rate at which the Universe is expanding, it is necessary to define the deceleration parameter. We obtain the definition of this parameter by considering the Taylor expansion of the scale factor $a(t)$ about the present time t_0 (Liddle, 2003),

$$a(t) = a(t_0) + \dot{a}(t_0)(t - t_0) + \frac{1}{2}\ddot{a}(t_0)(t - t_0)^2 + \dots . \tag{3.29}$$

Dividing by $a(t_0)$ this becomes,

$$\frac{a(t)}{a(t_0)} = 1 + H_0(t - t_0) - \frac{1}{2}q_0 H_0^2 (t - t_0)^2 + \frac{1}{3!} j_0 H_0^3 (t - t_0)^3 + \dots , \tag{3.30}$$

where we have defined the **deceleration parameter** q as,

$$q(t) = -\frac{1}{a}\frac{d^2 a}{dt^2}\left[\frac{1}{a}\frac{da}{dt}\right]^{-2} . \tag{3.31}$$

q_0 is then the value of this deceleration parameter at present times. We can relate the deceleration parameter and the density parameters via the acceleration equation,

$$q_0 = \frac{1}{2}\Omega_{m_0} + \Omega_{r_0} - \Omega_{\Lambda_0} . \tag{3.32}$$

The motivation behind defining such a parameter comes from a time when the present day Universe was thought to be matter dominated. In such a universe it was to be expected that the expansion will be slowed down because of the gravitational pull of matter i.e. the Universe would be decelerating. Even though this was not what was observed, as will be discussed in the next section, the convention of a positive deceleration parameter indicating a decelerating universe remains.

In Eq. (3.30) we have also defined the **jerk parameter** j as,

$$j(t) = \frac{1}{a}\frac{d^3 a}{dt^3}\left[\frac{1}{a}\frac{da}{dt}\right]^{-3} , \tag{3.33}$$

with $j_0 = j(t_0)$. In the ΛCDM model, the value of the jerk parameter is fixed at one at all times. Alongside the Hubble and deceleration parameters, since j depends only on the scale factor a, it is purely kinematic, meaning that it is independent of any gravitational theory and thus can provide a way to search for departures from the standard model

(Mamon and Bamba, 2018). The value of the jerk parameter from observations is given by 2.7 ± 6.7 (John, 2005). The large error bars of such a measured value means that any results inferred from it will be statistically weak. In order to minimise this error, the value of j_0 is usually derived within the framework of a cosmological model, like ΛCDM (Capozziello et al., 2011). In this work, the order of magnitude will be mainly of importance and thus we will set $j_0 = 1$.

3.1.5 | The Accelerating Universe

The discovery that high-redshift SNIa can be used as standard candles was critical for attempts to measure the deceleration parameter. SNIa had been used for accurate calculation of H_0 but it was due to the work of two collaborations, the Supernova Cosmology Project (Goobar and Perlmutter, 1995) and the High-z Supernova Search Team (Schmidt et al., 1998), that SNIa at high red-shifts were used to probe the acceleration of the expansion. The distances to these supernovae are calculated by measuring the incoming flux and then fitting empirical families of light curves to this flux (Branch and Tammann, 1992). The distance is then derived from the luminosity distance,

$$D_L = \left(\frac{L}{4\pi F} \right)^{1/2}, \tag{3.34}$$

where L is the intrinsic luminosity of the supernova and F is the observed flux (Riess, 2000).

Riess et al. (1998) found that the distances to SNIa at $0.16 \leq z \leq 0.97$ measured by two methods, were around 14% greater than those expected in a flat universe with the same amount of matter, but no cosmological constant. These results were confirmed by Perlmutter et al. (1999) and can be seen in Fig. 3.3a. These two teams used this data to constrain the values of Ω_m and Ω_Λ. Figure 3.3b, indicates that measurements fit an accelerating universe containing a positive cosmological constant, with high statistical significance.

The acceleration of the Universe has since been confirmed by independent studies using alternate probes to SNIa including the CMB and baryon acoustic oscillations (Blake et al., 2011; Percival et al., 2010). Thus, rather than a positive value for the deceleration parameter, we expect to measure $q_0 < 0$. Indeed, recent measurements give $q_0 = -0.51 \pm 0.024$ (Riess et al., 2021). For a de Sitter universe, the deceleration parameter is equal to -1 and since the Universe is asymptotically de Sitter, we expect the value of q to tend towards -1.

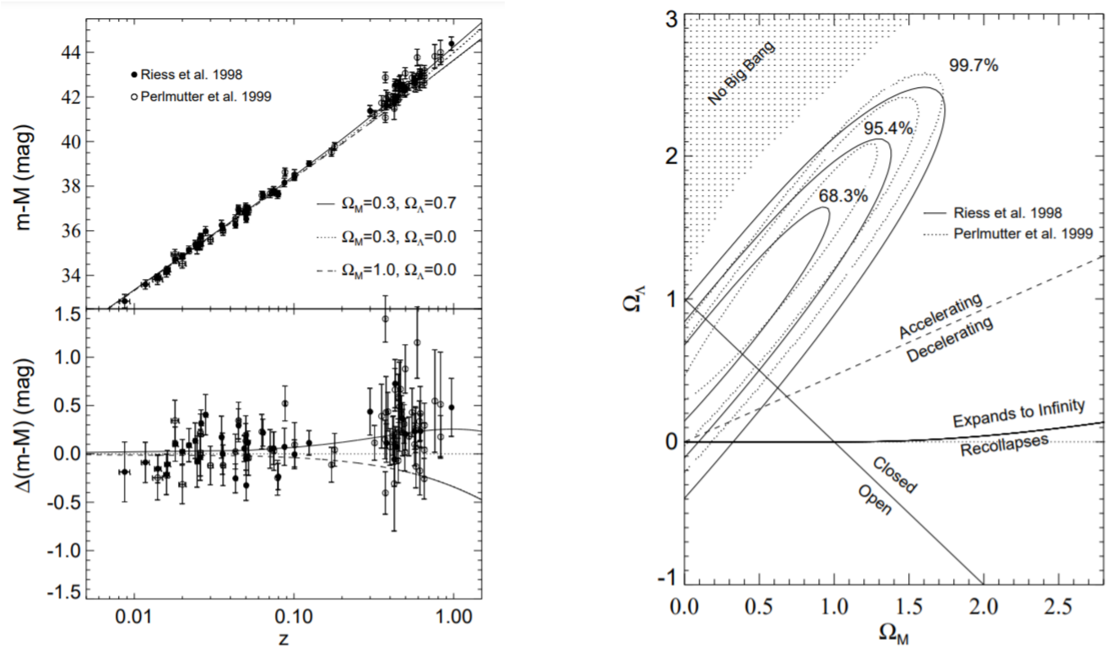

(a) Magnitude of SNIa against redshift. At high redshifts, SNe appear fainter than theoretical predictions in a universe with $\Omega_\Lambda = 0$ indicating an accelerating universe. The best fit for a flat universe is $\Omega_m = 0.3$ and $\Omega_\Lambda = 0.7$

(b) Joint confidence intervals for $(\Omega_m, \Omega_\Lambda)$ from SNIa. Regions representing different cosmological scenarios are labelled.

Figure 3.3: Graphs showing the magnitude of SNIa against redshift and constraints on the matter and dark energy density parameters. Figures taken from Riess (2000) which combine data from Riess et al. (1998) and Perlmutter et al. (1999). The data strongly indicates a non-zero cosmological constant and an accelerating universe.

3.1.6 | Challenges for the Standard Model

The standard cosmological model described in the last few sections explains observations consistently in a simple framework. However, some problems with it remain.

Two of such major problems in cosmology are the flatness and horizon problems. The flatness problem deals with the fact that the geometry of the Universe cannot change over time. Current observations constrain the Universe to be flat, however a small deviation from flatness early on in the Universe would be amplified and thus this poses a fine-tuning problem. The horizon problem deals with the fact that the CMB has a near-uniform temperature, however, there exist points in the sky which are not causally connected and so should not have had enough time to settle into thermal equilibrium. In 1981, Alan Guth proposed **inflation** as the solution to the above problems (Guth, 1981). In simple terms, this is a period of accelerated expansion in the early history of the Universe. Although successful in explaining away these problems, the physics behind inflation is still not understood completely. Moreover, inflation itself requires specific initial conditions to work and so it poses another fine-tuning problem (Penrose, 1989).

One of the biggest problems in cosmology is what is known as the **cosmological constant problem**. Quantum Field Theory predicts that vacuum has an energy originating from quantum fluctuations which should correspond to the cosmological constant. However, the theoretical value of Λ is at least a factor of 10^{120} larger than what the observations constrain it to be (Weinberg, 1989), which is an inadmissible disagreement between theory and observation. The tension in the value of the Hubble parameter discussed in Sec. 3.1.1 casts further doubt over the completeness of the ΛCDM model. Furthermore, although predictions of this model on large scales have been successful so far, it has faced problems on the sub-galaxy scale, including the “cusp-core problem" (Gentile et al., 2004) and the “missing satellites problem" (Klypin et al., 1999) which arise from discrepancies between CDM simulations and observations. Such problems have been coined the **small-scale controversies** (Weinberg et al., 2015). A rather philosophical problem with ΛCDM is known as the **cosmic coincidence** problem. This deals with the fact that the observed value of Λ is the exact one needed for the transition from matter domination to dark-energy domination to have happened very recently, as calculated in Sec. 3.1.4 and highlighted in Fig. 3.2. It would be much more likely for us to exist during a period of dark energy domination and there is no apparent reason as to why we are living at a special period of the cosmic history (Bahamonde et al., 2018; Velten et al., 2014).

Such problems motivate the need to look for modified cosmological models beyond ΛCDM arising from modifications to GR as discussed in Secs. 2.1.5 and 2.2.4. The main motivation behind this work is to look for such modified cosmologies which could explain the late-time acceleration of the Universe by modifying the gravitational theory itself and thus eliminating the need to introduce a cosmological constant.

3.2 | $f(T, T_G)$ Cosmology

The Friedmann equations which govern the dynamics of the Universe are the specific form of Einstein’s field equations using an FLRW metric. Since the field equations are derived from the Einstein-Hilbert action, modifying this action will accordingly give different Friedmann equations and as a consequence the dynamics of the Universe will differ from those described in Sec. 3.1. Since this work focuses on analysing the different cosmological scenarios that can result from the $f(T, T_G)$ modification given in Eq. (2.57), it will be necessary to explicitly describe the dynamics of a universe governed by this gravitational theory. In order to do this, many of the same assumptions taken in Sec. 3.1 in the context of ΛCDM will still hold. In particular, the energy-momentum tensor of a perfect isotropic fluid as given in Eq. (3.17) will again be considered, and the EoS for matter, radiation and dark energy will take on the same form as in Eq. (3.23). The cosmological parameters defined in Sec. 3.1.4 will also be useful in studying the properties of $f(T, T_G)$ cosmology and, as shall be shown, the energy content of the Universe will still satisfy the fluid equation in Eq. (3.22).

The modelled universe is still required to be homogeneous and isotropic and so the FLRW metric will again be used. Since in the teleparallel formulation of gravity, it is the tetrad that is the fundamental dynamical variable, we can use Eq. (2.37) to find the tetrad corresponding to the FLRW metric in Eq. (3.9). This is found to be,

$$e^A{}_\mu = \mathrm{diag}(1, a(t), a(t), a(t)), \tag{3.35}$$

while the dual tetrad field is given by,

$$E_A{}^\mu = \mathrm{diag}(1, a^{-1}(t), a^{-1}(t), a^{-1}(t)). \tag{3.36}$$

Calculating the determinant of $e^A{}_\mu$ gives $e = a^3(t)$.

Using Eqs. (2.51) and (2.55), and the tetrad field defined above, allows us to express the invariants T and T_G in terms of H,

$$T = 6H^2, \tag{3.37}$$

$$T_G = 24H^2(\dot{H} + H^2). \tag{3.38}$$

From these expressions it is easy to recognise that T is of first order in the derivative of the scale factor, and thus the tetrad field, while T_G is of second order.

In order to obtain a realistic cosmological model, we consider a matter action, S_M, in addition to the one defined in Eq. (2.57). As previously indicated, this corresponds to an energy momentum tensor $\Theta^{\mu\nu}$ representing a perfect fluid of energy density ρ_m and pressure p_m. Variation of the total action $S + S_M$ gives the Friedmann equations for $f(T, T_G)$ cosmology,

$$f - 12H^2 f_T - T_G f_{T_G} + 24H^3 \dot{f_{T_G}} = 2\kappa^2 \rho_m, \tag{3.39}$$

$$f - 4(3H^2 + \dot{H}) f_T - 4H\dot{f_T} - T_G f_{T_G} + \frac{2}{3H} T_G \dot{f_{T_G}} + 8H^2 \ddot{f_{T_G}} = -2\kappa^2 p_m, \tag{3.40}$$

where f_T and f_{T_G} denote differentiation of the function $f(T,T_G)$ wrt T and T_G, respectively. The derivation of these Friedmann equations can be found in (Kofinas and Saridakis, 2014).

Making the reasonable assumption that the only two components of the Universe which have a significant effect on its late-time dynamics are matter and dark energy, we can rewrite the Friedmann equations in Eqs. (3.39) and (3.40) in the simpler form (Kofinas et al., 2014),

$$H^2 = \frac{\kappa^2}{3}(\rho_m + \rho_{DE}) \tag{3.41}$$

$$\dot{H} = -\frac{\kappa^2}{2}(\rho_m + p_m + \rho_{DE} + p_{DE})\,, \tag{3.42}$$

where ρ_{DE} and p_{DE} are the effective density and pressure of dark energy given by,

$$\rho_{DE} = \frac{1}{2\kappa^2}(6H^2 - f + 12H^2 f_T + T_G f_{T_G} - 24H^3 \dot{f_{T_G}})\,, \tag{3.43}$$

$$p_{DE} = \frac{1}{2\kappa^2}[-2(2\dot{H} + 3H^2) + f - 4(\dot{H} + 3H^2) f_T - 4H\dot{f_T} - T_G f_{T_G} + \frac{2}{3H} T_G \dot{f_{T_G}} + 8H^2 \ddot{f_{T_G}}]\,. \tag{3.44}$$

From this it follows that both the matter and dark energy sectors individually satisfy the fluid equation in Eq. (3.22) meaning that,

$$\dot{\rho}_m + 3H(\rho_m + p_m) = 0\,, \tag{3.45}$$

$$\dot{\rho}_{DE} + 3H(\rho_{DE} + p_{DE}) = 0\,. \tag{3.46}$$

The EoS parameter of dark energy can be defined in the usual way as $w_{DE} = p_{DE}/\rho_{DE}$. Notice that for $f(T,T_G) = -T - 2\Lambda$, the same Friedmann equations as in Eqs. (3.41) and (3.42) are recovered. This is in line with the dynamical equivalence of GR and TEGR and shows that the $f(T,T_G)$ modification has a ΛCDM limit.

In order to analyse the dynamics which can result from the $f(T,T_G)$ modification, the specific form of the function needs to be defined. There will be four specific models analysed in this study all in the form $f(T,T_G) = -T + F(T,T_G)$. This is so as to parametrise the deviation of the models from GR. In this way the modification is entirely contained in the function F (Kofinas and Saridakis, 2014). The motivation for these models comes from those considered in the literature for the $f(T)$ and $f(T,B)$ TEGR modifications, namely as discussed in (Briffa et al., 2021), (Escamilla-Rivera and Said, 2020) and (Caruana et al., 2020).

The first is the power-law model given by,

$$f_1(T,T_G) = -T + \alpha_1 T_G^{P_1}\,. \tag{3.47}$$

In the $f(T)$ modification, a similar model has been observed to produce late-times acceleration of the Universe (Bengochea and Ferraro, 2009) and thus it will be interesting to study whether even more complex dynamics can be obtained through the inclusion of the T_G invariant.

The second model is given by,

$$f_2(T, T_G) = -T + \alpha_2 e^{-P_2\sqrt{T_G/T_{G_0}}}\,, \tag{3.48}$$

where T_{G_0} is the value of T_G at the present time. This model has been inspired by the Linder model (Linder, 2010) which was also derived to explain the late-times acceleration of the universe in the $f(T)$ modification.

The model given by,

$$f(T, T_G) = -T + \alpha_3\sqrt{T^2 + P_3 T_G}\,, \tag{3.49}$$

is the only $f(T, T_G)$ model whose dynamical behaviour has been previously studied in detail in the literature (Kofinas et al., 2014). The motivation for the form of this specific model is that since T_G contains quartic torsion terms, it is of the same order of T^2. Since T and $\sqrt{T^2 + P_3 T_G}$ are of the same order, both terms should be considered. In order to extend on the study that has already been done, we will generalise this model to,

$$f_3(T, T_G) = -T + \alpha_3(T^2 + P_3 T_G)^{\beta_3}\,. \tag{3.50}$$

The specific case where $\beta_3 = 1/2$ would then correspond to the model studied in Kofinas et al. (2014).

The fourth model is a logarithmic model given by,

$$f_4(T, T_G) = -T + \alpha_4 \ln\left(\frac{P_4 T_G}{T}\right). \tag{3.51}$$

This is motivated by the logarithmic $f(T)$ model investigated in Bamba et al. (2011) which showed consistency with observational data and so, again, it will be interesting to see the effect of incorporating T_G into the model.

The α_i's and P_i's in each model are dimensionless real numbers; varying them results in different dynamics. Indeed, the specific case in which the α_i's are equal to zero give $f(T, T_G) = -T$ which corresponds to the TEGR action and thus produces the same dynamics as GR. Moreover, the ΛCDM model dynamics are achieved when,

$$f(T, T_G) = -T + 6H_0^2(1 - \Omega_{m_0} - \Omega_{r_0})\,. \tag{3.52}$$

Thus, for the first two models in Eqs. (3.47) and (3.48), the ΛCDM limit is achieved by setting $P_i = 0$ and $\alpha_i = 6H_0^2(1 - \Omega_{m_0} - \Omega_{r_0})$. Similarly for f_3 we can set $\beta_3 = 0$

and $\alpha_3 = 6H_0^2(1 - \Omega_{m_0} - \Omega_{r_0})$, however, for a fixed value of β_3, such as in Eq. (3.49), there is no ΛCDM limit. This is also the case for the logarithmic model. These last two models without a ΛCDM limit are of particular interest as the theory cannot feature confirmation bias with the standard model (Briffa et al., 2021).

Although superficially it may seem that the models contain two free variables, α_i and P_i, these parameters can be related through the first Friedmann equation as given in Eq. (3.39), evaluated at the present time t_0. We can thus obtain $\alpha_i = \alpha_i(P_i)$, leaving one free parameter in each model. As an example, for the first model in Eq. (3.47), the relation between the two variables is given by,

$$\alpha_1 = \frac{3H_0^2(\Omega_{m_0} + \Omega_{r_0} - 1)}{\frac{1}{2}(1 - P_1)T_{G_0}^{P_1} + 12P_1(P_1 - 1)H_0^3 T_{G_0}^{(P_1-2)} \dot{T}_G|_{t=t_0}} . \tag{3.53}$$

Although useful when analysing whether these models can fit current observations, the scope of this work is to study the overall dynamics that each of the models has the potential of producing. Moreover, the jerk parameter is involved in this relation in order to calculate the value of $\dot{T}_G|_{t=t_0}$ and, as previously discussed, an accurate observational value of j_0, without specifying a cosmological model, is very hard to obtain. Thus, in order to avoid these complications and focus on the dynamics of the models, both α_i and P_i will be treated as free parameters.

3.3 | Dynamical Systems Applied to Cosmology

The equations that govern the dynamics of the Universe, in the context of both ΛCDM and $f(T, T_G)$ cosmology, take the form of ordinary differential equations. Thus, in order to get a qualitative understanding of the overall dynamics of the models given in Eqs. (3.47) - (3.51) we will utilise the techniques used to study dynamical systems. These techniques have been used extensively in the literature (Coley, 2003; Wainwright and Ellis, 1997) to analyse alternative cosmological models as they provide a way in which models can be ruled out on purely theoretical grounds when the overall dynamics do not agree with observations. On the other hand models whose dynamics look promising can be identified so that further in-depth analysis about the resulting cosmology can be carried out and a qualitative comparison to observational data can be made (Bahamonde et al., 2018).

3.3.1 | Introduction to Dynamical Systems

A dynamical system in n-dimensions is defined as a system consisting of a phase space $X \subset \mathbb{R}$ and a mathematical rule describing the evolution of any point in that space (Böhmer and Chan, 2016). In order to analyse a system, such as the Universe, one must identify specific quantities that describe it. The phase space consists of every possible value that these quantities can take. Note that different quantities can be used to describe the same system, and choosing different variables on which to perform the dynamical analysis, might result in different dynamics of the system being exposed.

Let $\mathbf{x} \in X$ be a point in the phase space. Then an autonomous dynamical system is in general given by (Wiggins, 2003),

$$\dot{\mathbf{x}} = \mathbf{f}(\mathbf{x}) \tag{3.54}$$

where the function $\mathbf{f} : X \mapsto X$ and dot denotes differentiation wrt a suitable time parameter. Note that the function $\mathbf{f}$ does not have a time dependence as this would result in a nonautonomous system which will not be of importance in this work. The function $\mathbf{f}$ is in general smooth almost everywhere, although it might contain some singularities. In this case, the techniques that will be discussed, can be applied away from these singularities, where the function is continuous (Bahamonde et al., 2018). A particular solution of Eq. (3.54) is called a trajectory or orbit in phase space and is denoted by $\psi(t)$.

From Eq. (3.54) one can see that at points $\mathbf{x_0}$ in the phase space such that $\mathbf{f}(\mathbf{x_0}) = 0$, the evolution stops, since $\dot{\mathbf{x}}|_{\mathbf{x}=\mathbf{x_0}} = 0$. Such a point $\mathbf{x_0}$ is called a *critical point* or a *fixed point* of the system. In principle, the system could remain in such states indefinitely. However, one needs to investigate whether such a state is actually attainable and whether the state is stable wrt small perturbations (Bahamonde et al., 2018). This motivates the following definition of a *stable fixed point* (Wiggins, 2003),

Definition 3.3.1 (Stable fixed point) *A fixed point $\mathbf{x_0}$ of the system given in Eq.* (3.54) *is said to be stable if* $\forall\, \epsilon > 0\ \exists\, \delta$ *such that for any solution $\psi(t)$ of Eq.* (3.54) *satisfying $|\psi(t_0) - \mathbf{x_0}| < \delta$, then $|\psi(t) - \mathbf{x_0}| < \epsilon$ for any $t \geq t_0$.*

Conceptually this means that any trajectory that starts close to a stable fixed point will remain nearby. We can further make the following definition of an *asymptotically stable fixed point*.

Definition 3.3.2 (Asymptotically stable fixed point) *A fixed point $\mathbf{x_0}$ of the system given in Eq.* (3.54) *is said to be asymptotically stable if it is stable and* $\exists\, \delta > 0$ *such that if a solution ψ satisfies $|\psi(t_0) - \mathbf{x_0}| < \delta$, then $\lim_{t \to \infty} \psi(t) = \mathbf{x_0}$.*

The difference between these two definitions is that any solutions near an asymptotically stable fixed point will eventually tend to this fixed point while those near a stable fixed point could, for example, circle around it. In cosmology, most of the stable fixed points are asymptotically stable and so we will refer to asymptotically stable fixed points simply as stable. We can also define an *unstable fixed point* as simply a stable fixed point with the time direction reversed, i.e. solutions tend away from the fixed point rather than towards it. Studying the stability of fixed points allows us to make conclusions about the qualitative time evolution of the system without having to specify any initial conditions (Bahamonde et al., 2018).

3.3.2 | Linear Stability Theory

There are multiple techniques that can be employed in order to study the stability of fixed points of a system. Some of these include linear stability theory (LST), Lyapunov's method (Hirsch et al., 2013) and centre manifold theory (Lynch, 2017). The first technique is the simplest and is applicable to so called *hyperbolic* fixed points. While the other two methods allow for the study of the stability of non-hyperbolic fixed points, in this work, such fixed points will not be encountered and thus LST will be sufficient, as it is in most other applications of dynamical systems in cosmology.

The main idea behind LST is to linearise the system described by Eq. (3.54) near a fixed point $\mathbf{x_0}$. Since we are considering functions that are mostly smooth, we can expand each component of $\mathbf{f}$ about $\mathbf{x_0}$ using a Taylor series to obtain (Bahamonde et al., 2018),

$$f_i(\mathbf{x}) = f_i(\mathbf{x_0}) + \sum_{j=1}^{n} \frac{\partial f_i}{\partial x_j}(\mathbf{x_0}) y_j + \frac{1}{2!} \sum_{j,k=1}^{n} \frac{\partial^2 f_i}{\partial x_j \partial x_k}(\mathbf{x_0}) y_j y_k + \ldots, \tag{3.55}$$

where the vector $\mathbf{y}$ is defined as $\mathbf{y} = \mathbf{x} - \mathbf{x_0}$. In LST, the non-linear terms of this expansion are ignored and so the *Jacobian matrix* J, defined as,

$$J = \frac{\partial f_i}{\partial x_j} = \begin{pmatrix} \frac{\partial f_1}{\partial x_1} & \cdots & \frac{\partial f_1}{\partial x_n} \\ \vdots & \ddots & \vdots \\ \frac{\partial f_n}{\partial x_1} & \cdots & \frac{\partial f_n}{\partial x_n} \end{pmatrix}, \tag{3.56}$$

will be of importance. This matrix is also referred to as the *stability matrix* since the stability behaviour around a fixed point will depend on its eigenvalues.

The orbit structure around the fixed point $\mathbf{x_0}$ of the original, non-linear system, is essentially the same as that of the linear one, given that $\mathbf{x_0}$ is hyperbolic. This means that the eigenvalues of J evaluated at $\mathbf{x_0}$ all have non-zero real part (Wiggins, 2003). If this condition is satisfied, then we can determine the stability of the fixed point based on these eigenvalues of $J|_{\mathbf{x}=\mathbf{x_0}}$ (Bahamonde et al., 2018).

- If all the eigenvalues have a positive real part, then $\mathbf{x_0}$ is an *unstable point* or a *repellor*,
- if all the eigenvalues have a negative real part, then $\mathbf{x_0}$ is a *stable point* or an *attractor*,
- otherwise, $\mathbf{x_0}$ is said to be a *saddle*. In this case the fixed point attracts trajectories from certain directions while it repels them in others.

In the case of complex conjugate eigenvalues of J, when all the eigenvalues have a negative real part, the fixed point is called a *stable focus*. When all the eigenvalues have a positive real part, it is called an *unstable focus*. These foci are characterised by the spiralling behaviour of trajectories in the neighbourhood of the fixed point (Lynch, 2017).

An example which highlights the applicability of LST in cosmology, by analysing the ΛCDM model is presented in (Bahamonde et al., 2018). The dynamical variables are identified as the matter and radiation density parameters,

$$x = \Omega_m = \frac{\kappa^2 \rho_m}{3H^2}, \; y = \Omega_r = \frac{\kappa^2 \rho_r}{3H^2}, \tag{3.57}$$

The physical phase space is then represented by $1 = x + y + \Omega_\Lambda$ such that $x, y \geq 0$, since matter and radiation density are positive. Differentiating wrt $\eta = \ln a$, and using the fluid and the Friedmann equations, one obtains the following dynamical system,

$$x' = x(3x + 4y - 3)\,, \tag{3.58}$$

$$y' = y(3x + 4y - 4)\,, \tag{3.59}$$

where prime denotes differentiation wrt η. Solving $x' = y' = 0$ gives three critical points of the system, whose equation of state parameter w_{eff}, eigenvalues of the stability matrix, and stability are summarised in Table 3.1. From the values of Ω_m, Ω_r and w_{eff}, we can identify O, R and M with universes containing only Λ, radiation and matter respectively. The phase plot of this system can be seen in Fig. 3.4.

The line RM in Fig. 3.4 represents a universe containing radiation and matter only. Since the observed value of Λ is very small, the trajectory representing our Universe starts infinitesimally close to RM. From the phase portrait we can see that it is repelled from R towards the saddle point M, resulting in a matter-dominated era, and is finally attracted towards the stable fixed point O giving a dark-energy dominated universe. Apart from those on the boundary of the phase space, all the trajectories eventually

Point	x	y	w_{eff}	Eigenvalues	Stability
O	0	0	-1	$\{-4,-3\}$	Stable point
R	0	1	$1/3$	$\{1,4\}$	Unstable point
M	1	0	0	$\{-1,3\}$	Saddle point

Table 3.1: Fixed points of the system defined in Eqs. (3.58) & (3.59) reproduced from Bahamonde et al. (2018).

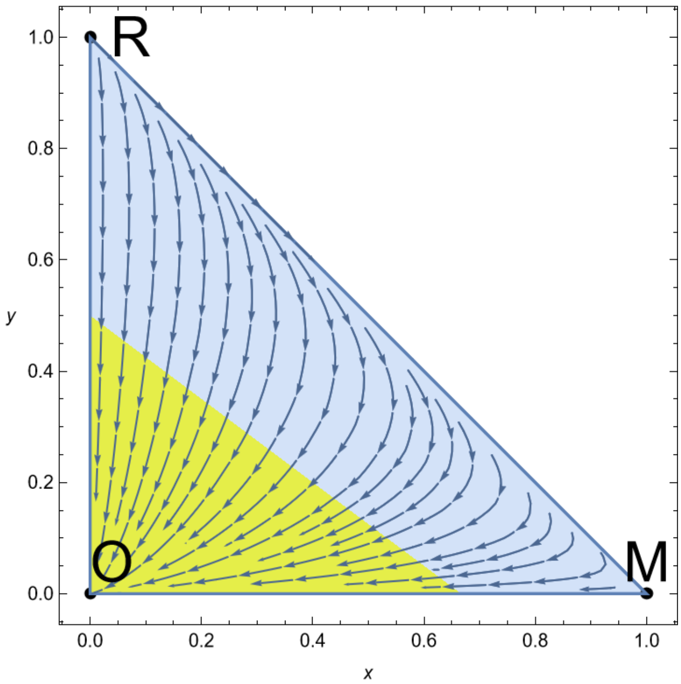

Figure 3.4: Phase space portrait for the system defined in Eqs. (3.58) & (3.59). The yellow-shaded region represents the region in which $w_{eff} < -1/3$, i.e. in this region the Universe is accelerating.

tend towards this point O which represents a de-Sitter universe, thus transitioning from a decelerating universe to an accelerating one (Bahamonde et al., 2018). These critical points are in precise agreement with the standard cosmological model of the history of the Universe from the observational perspective which have been highlighted in Fig. 3.2.

This is the type of qualitative phase space analysis that will be done in Chapter 4 for the models in Eqs. (3.47) - (3.51), although we will see that it will not always be possible to define a dynamical system as simple as in this example in order to analyse these $f(T, T_G)$ models.

3.3.3 | Behaviour at Infinity

Since we will be dealing with non-compact dynamical systems in which one or more of the dynamical variables is unbounded, it is necessary to perform an analysis of the behaviour at infinity as there could be non-trivial dynamical features in this regime (Bahamonde et al., 2018). To do so we will employ the method used by Kofinas et al. (2014) and Xu et al. (2012) which is based on the Poincarè projection method. The essence of this method is that a 2D-phase plane is mapped onto a sphere, transforming the points at infinity into points on the equator of the sphere (Lynch, 2017) . This method can then be extended to a system with three variables.

Consider a dynamical system with two variables, x and y. Then we can transform to the Poincarè plane (R, Θ) using the transformations (Kofinas et al., 2014),

$$x = \frac{R}{1-R}\cos\Theta \tag{3.60}$$

$$y = \frac{R}{1-R}\sin\Theta\,, \tag{3.61}$$

where $R \in [0, 1)$ and $\Theta \in [0, \frac{\pi}{2}]$. Thus, we can see that the limit $r^2 = x^2 + y^2 \to \infty$ corresponds to $R \to 1^-$. We can then use the equations for x' and y' to obtain the dynamical system,

$$R' = f(R, \Theta) \tag{3.62}$$

$$\Theta' = g(R, \Theta)\,. \tag{3.63}$$

The fixed points at infinity are then found by finding the leading terms of Eqs. (3.62) and (3.63) as $R \to 1^-$, setting $\Theta' = 0$ and solving for Θ.

We can also study the stability of a fixed point at $\Theta = \tilde{\Theta}$. This is done by first studying the stability of the angular coordinate, and then from the sign of R', deducing the stability along the radial coordinate (Lynch, 2017). A stable fixed point is one such that,

$$\frac{d\Theta'}{d\Theta}|_{\Theta=\tilde{\Theta}} < 0\,,\; R'|_{\Theta=\tilde{\Theta}} > 0\,, \tag{3.64}$$

an unstable fixed point satisfies the conditions,

$$\frac{d\Theta'}{d\Theta}|_{\Theta=\tilde{\Theta}} > 0\,,\; R'|_{\Theta=\tilde{\Theta}} < 0\,, \tag{3.65}$$

while otherwise, the fixed point is a saddle.

The above procedure will be generalised to systems of three dynamical variables, x, y and z, as follows. We will transform the system into the Poincarè coordinates (R, Θ, Φ)

through the following transformation,

$$x = \frac{R}{1-R}\cos\Theta\sin\Phi \tag{3.66}$$

$$y = \frac{R}{1-R}\sin\Theta\sin\Phi \tag{3.67}$$

$$z = \frac{R}{1-R}\cos\Phi\,. \tag{3.68}$$

We can then obtain expressions for R', Θ' and Φ', thus obtaining a new dynamical system, and then solve for the fixed points at infinity by setting $\Theta' = \Phi' = 0$ in the leading order terms. Note that we are only solving for the values of Θ and Φ at the fixed points, as at infinity, the R coordinate is fixed as one. A fixed point $(1, \tilde{\Theta}, \tilde{\Phi})$ is said to be stable if,

$$\frac{d\Theta'}{d\Theta}|_{(\Theta,\Phi)=(\tilde{\Theta},\tilde{\Phi})} < 0\,, \frac{d\Phi'}{d\Phi}|_{(\Theta,\Phi)=(\tilde{\Theta},\tilde{\Phi})} < 0\,,\ R'|_{(\Theta,\Phi)=(\tilde{\Theta},\tilde{\Phi})} > 0\,. \tag{3.69}$$

Similarly, it is said to be unstable if,

$$\frac{d\Theta'}{d\Theta}|_{(\Theta,\Phi)=(\tilde{\Theta},\tilde{\Phi})} > 0\,, \frac{d\Phi'}{d\Phi}|_{(\Theta,\Phi)=(\tilde{\Theta},\tilde{\Phi})} > 0\,,\ R'|_{(\Theta,\Phi)=(\tilde{\Theta},\tilde{\Phi})} < 0\,. \tag{3.70}$$

Otherwise, the fixed point is a saddle. We will see that in the case of $f(T, T_G)$ models, these fixed points at infinity will correspond to future singularities such as a Big Rip, in which the distances between particles become infinite and the size of the observable universe is zero (Caldwell et al., 2003; Kofinas et al., 2014), or to past singularities such as the Big Bang.

3.3.4 | Dynamical Systems to Probe Novel Cosmologies

The simplicity of the dynamical systems approach along with its practicality in investigating the overall dynamics of a cosmological model, makes it perfectly suited to investigate novel cosmologies such as $f(T, T_G)$. As previously discussed, this method provides a way to identify potentially viable models for further investigation. Dynamical systems techniques have been used extensively for theories like $f(\mathring{R})$ gravity (Amendola et al., 2007; de Souza and Faraoni, 2007), $f(T)$ gravity (Myrzakulov, 2011) and other higher-order theories like $f(T, B)$ (Paliathanasis and Leon, 2021).

However, apart from in (Kofinas et al., 2014), no other attempts have been made to study other viable $f(T, T_G)$ models using dynamical systems. Thus, the main motivation for carrying out this work is to analyse a number of $f(T, T_G)$ models that differ from the one found in the existing literature, using dynamical systems, in order to understand whether this modification has the potential to explain the observed cosmological evolution.

4

Dynamical Analysis of the $f(T, T_G)$ Modification

The dynamical systems approach when applied to cosmological models has been extremely successful in uncovering interesting dynamics of modified theories of gravity (Bahamonde et al., 2018; Wainwright and Ellis, 1997; Xu et al., 2012). In (Kofinas et al., 2014), this technique is specifically applied to the $f(T, T_G)$ teleparallel modification. The promising results obtained in this paper for one form of $f(T, T_G)$ give confidence that this modification can lead to an accurate description of Nature. Thus, in this chapter we will be using the dynamical systems techniques introduced in Sec. 3.3 to study the general late-time behaviour of more $f(T, T_G)$ models, in particular those introduced in Eqs. (3.47) - (3.51). This will be done to reveal further potential cosmological solutions that the $f(T, T_G)$ modification can lead to and will be achieved by incorporating the dynamics of the models, determined by the Friedmann and fluid equations, into a dynamical system. Using this method, we can immediately distinguish those models which have the potential of describing the physical Universe, from those which do not lead to physical solutions, before constraining these models to fit observational data.

It is important to note that what will be analysed in this section is the late-time behaviour of the models rather than the dynamics over the full history of the modelled universes. This is because of the various assumptions that have been made. For example, the density parameter of radiation has been, and will continue to be, taken to be equal to zero. This is a valid assumption for modelling the late-time behaviour, since the contribution of radiation to the energy content of the Universe at present times is negligible. In fact, the measured temperature of the CMB, corresponds to $\Omega_{r_0} = 2.47 \times 10^{-5} h^{-2}$ (Lahav and Liddle, 2019), where h is the dimensionless Hubble constant defined by $H_0 = 100h$ km/s/Mpc (Liddle, 2003). However, radiation was the dominant component of the Universe in early times, as can be seen in Fig. 3.2, and so to accurately give a theoretical description of this early period of the Universe, one needs to consider Ω_r as another dynamical variable. Moreover, additional fields might be required to explain the inflationary period of the Universe. This is indeed something that needs to be added even to the ΛCDM model to accurately describe the inflationary era (Guth and Pi, 1985). These two further terms could be added to any model which shows potential in accurately describing the late-time behaviour in future works, to look for $f(T, T_G)$ models which explain the full history of the Universe.

In the analysis that follows, the software Mathematica 13.0 (Wolfram Research, Inc.) was used to aid in numerical manipulation and to generate the phase portraits of the dynamical systems. [1]

4.1 | Model 1: $f_1(T, T_G) = -T + \alpha_1 T_G^{P_1}$

The first model that will be analysed is the power law model as given in Eq. (3.47). Power law models are used in many areas of physics and act as approximations to more complex theoretical models. Thus, this model is the logical choice for an initial analysis before investigating more complex models.

For this model, the Friedmann equations which govern the dynamics of the universe are those given in Eqs. (3.41) and (3.42), with the specific form of the effective fluid density and pressure, ρ_{DE} and p_{DE} given by,

$$\kappa^2\rho_{DE} = \frac{24^{P_1}\alpha_1(P_1-1)}{2(H^2+\dot{H})^2}(H^2+H^2\dot{H})^{P_1}[H^4+2(1-2P_1)H^2\dot{H}+(1-2P_1)\dot{H}^2-P_1H\ddot{H}] \tag{4.1}$$

$$\begin{aligned}\kappa^2 p_{DE} =& \frac{24^{P_1}\alpha_1(P_1-1)(H^4+H^2\dot{H})^{P_1-1}}{6(H^2+\dot{H})^2} \times \{-3H^8+(8P_1-9)H^6\dot{H}+2P_1(2P_1-1)\dot{H}^4 \\ &+6P_1H^5\ddot{H}+2P_1(4P_1-1)H^3\dot{H}\ddot{H}+4P_1^2H\dot{H}^2\ddot{H}+H^4[(16P_1^2-9)\dot{H}^2+P_1\dddot{H}] \\ &+H^2[(2P_1-1)(3+8P_1)\dot{H}^3+P_1(P_1-2)\ddot{H}^2+P_1\dot{H}\dddot{H}]\}\,.\end{aligned} \tag{4.2}$$

To perform the dynamical analysis, the unitless auxiliary variables,

$$x = \left(1+\frac{\dot{H}}{H^2}\right)^{P_1/2} \tag{4.3}$$

$$\Omega_m = \frac{\kappa^2\rho_m}{3H^2}\,, \tag{4.4}$$

[1] The code used for the first model can be accessed on the following link: `https://github.com/s-buttigieg/dynamical_systems`. The code for the other models follows the same pattern.

are introduced. These variables were chosen in order to expose the dynamical features of the model through an autonomous dynamical system, as defined in Eq. (3.54), with fixed points that are hyperbolic. In particular, Ω_m is the matter density parameter introduced in Sec. 3.1.4 and its value will directly show whether the modelled universe is matter-dominated, dark-energy-dominated, or a mixture of the two. x does not have a specific physical significance but was rather chosen based on the terms in Eqs. (4.1) and (4.2) with the aim of simplifying the obtained dynamical system. Because of this, x will vary for different models, while Ω_m will always be taken as one of the dynamical variables, as shall be seen in the following sections. Note that choosing different dynamical variables for the same model, might uncover different dynamics and so the dynamics that are presented in this section do not exhaust the full list of different dynamical behaviour that the model can result in.

The dynamical system will be obtained wrt the time variable $\eta = \ln a$. Prime will denote differentiation wrt η while dot will denote differentiation wrt t. For a general function f, the relation between the two is given by,

$$f' = \frac{1}{H}\dot{f}\,, \tag{4.5}$$

after a simple application of the chain rule.

The evolution of Ω_m wrt η is obtained as follows,

$$\begin{aligned} \Omega_m' &= \frac{1}{H}\dot{\Omega}_m \\ &= \frac{\kappa^2}{3H}\left(\frac{\dot{\rho_m}}{H^2} - \frac{2\rho_m \dot{H}}{H^3}\right)\,. \end{aligned} \tag{4.6}$$

Now, using Eq. (3.45), it follows that,

$$\Omega_m' = \frac{\kappa^2}{3H^4}(-3H^2(\rho_m + p_m) - 2\rho_m \dot{H})\,. \tag{4.7}$$

In this step, the fluid equation is being incorporated into the dynamical system. Using the definition of x in Eq. (4.3) allows us to write $\dot{H}$ in terms of H and x,

$$\dot{H} = H^2(x^{\frac{2}{p_1}} - 1)\,. \tag{4.8}$$

Thus,

$$\Omega_m' = \frac{\kappa^2\rho_m}{3H^2}(-3(1+\omega_m) - 2(x^{\frac{2}{p_1}} - 1))\,, \tag{4.9}$$

where $\omega_m = \frac{p_m}{\rho_m}$ is the equation of state parameter for matter, giving,

$$\Omega_m' = -\Omega_m(1 + 3\omega_m + 2x^{\frac{2}{p_1}})\,. \tag{4.10}$$

We can obtain the evolution of x in a similar way,

$$\begin{aligned} x' &= \frac{1}{H}\dot{x} \\ &= \frac{P_1}{2H}\left(1+\frac{\dot{H}}{H^2}\right)^{\frac{P_1}{2}-1}\left(\frac{\ddot{H}}{H^2}-\frac{2\dot{H}^2}{H^3}\right) \\ &= \frac{P_1 x^{1-\frac{2}{P_1}}}{2H^4}(\ddot{H}H-2\dot{H}^2)\,. \end{aligned} \tag{4.11}$$

Our aim is to express the evolution of x purely in terms of x, H and Ω_m and thus we need to eliminate $\ddot{H}$ and $\dot{H}$. Using Eq. (4.1), we can obtain an expression for $\ddot{H}$,

$$P_1 H\ddot{H} = H^4 + 2(1-2P_1)H^2\dot{H} + (1-2P_1)\dot{H}^2 - \frac{2\kappa^2\rho_{DE}(H^2+\dot{H})^2}{24^{P_1}\alpha_1(P_1-1)(H^4+H^2\dot{H})^{P_1}}\,, \tag{4.12}$$

where using the first Friedmann equation in Eq. (3.41),

$$\begin{aligned} \rho_{DE} &= \frac{3H^2}{\kappa^2} - \rho_m \\ &= \frac{3H^2}{\kappa^2}(1-\Omega_m)\,. \end{aligned} \tag{4.13}$$

Using Eqs. (4.8), (4.12) and (4.13), Eq. (4.11) becomes,

$$x' = \frac{x}{2}\left[4P_1 + x^{\frac{2}{P_1}}\left(1-4P_1+\frac{6H^{2-4P_1}(\Omega_m-1)}{24^{P_1}x^2\alpha_1(P_1-1)}\right)\right]\,. \tag{4.14}$$

Notice how the first Friedmann equation for the $f(T,T_G)$ modification is being directly incorporated into the expression for the evolution of x.

The final equation needed is that governing the evolution of H which is simply given by,

$$H' = H(x^{\frac{2}{P_1}}-1)\,. \tag{4.15}$$

In this way, the dynamics of the model are contained in the dynamical system given by Eqs. (4.14), (4.15) and (4.10). This dynamical system is defined on the phase space,

$$S = \{(x,H,\Omega_m)|x\in(0,\infty), H\in[0,\infty), \Omega_m\in[0,\infty)\}\,, \tag{4.16}$$

however, the range of H needs to be restricted to $(0,\infty)$ for $P_1 > \frac{1}{2}$. Notice that in Eq. (4.14), H can be completely eliminated from the dynamical system for $P_1 = \frac{1}{2}$, reducing the 3D system to a 2D one. This specific case requires a different analysis that will be done in Sec. 4.1.4 so in the remainder of this section, $P_1 \neq \frac{1}{2}$ will be assumed.

We can obtain expressions for observable parameters in terms of the dynamical variables. In particular the deceleration parameter $q \equiv -1 - \frac{\dot{H}}{H^2}$ is given by,

$$q = -x^{\frac{2}{P_1}}\,. \tag{4.17}$$

The dark energy density parameter is simply given by,

$$\Omega_{DE} = 1 - \Omega_m \,, \tag{4.18}$$

while the dark energy equation of state can be found using the relation,

$$2q = 1 + 3(\omega_m \Omega_m + \omega_{DE}\Omega_{DE}) \tag{4.19}$$

giving,

$$\omega_{DE} = \frac{-2x^{\frac{2}{P_1}} - 1 - 3\omega_m\Omega_m}{3(\Omega_m - 1)} \,. \tag{4.20}$$

These expressions will be used to calculate these cosmological parameters at fixed points of interest, to then infer the cosmological implications of the dynamical system. In the rest of the work, dust matter will be assumed, i.e. $\omega_m = 0$ without loss of generality. This is because matter in the Universe can be approximated in this way and an extension to the analysis with a non-zero value of ω_m is straightforward.

4.1.1 | Finite Phase Space Analysis

The finite phase space analysis is performed by first finding the real fixed points of the autonomous system defined in Eqs. (4.10), (4.14) and (4.15). We will then use techniques from LST described in Sec. 3.3 to study the stability of these fixed points. The deceleration and dark energy equation of state parameters at the fixed point will also be computed in order to investigate the cosmological implications of the dynamics of the model.

The first fixed point of the system is at $C_1 = (1, H_1, 0)$ where $H_1 = \left(\frac{24^{P_1}\alpha_1(P_1-1)}{6}\right)^{\frac{1}{2-4P_1}}$. The existence of this fixed point is not guaranteed but rather depends on the values of α_1 and P_1. The existence conditions are complex, however, the existence of C_1 will be guaranteed if one of the following conditions is satisfied;

- $P_1 = \frac{2n-1}{4n}$ for $n \in \mathbb{N}$,
- $\alpha_1 > 0$ and $P_1 > 1$,
- $\alpha_1 < 0$ and $P_1 < 1$.

The other fixed point, is at $C_2 = (x_2, 0, 0)$ where $x_2 = \left(\frac{4P_1}{4P_1-1}\right)^{\frac{P_1}{2}}$. A sufficient condition for the existence of C_2 is that $P_1 < 0$ or $\frac{1}{4} < P_1 < \frac{1}{2}$.

The stability of these fixed points will be studied using the stability matrix J, which was defined in Eq. (3.56) for a general dynamical system. The specific form of J for a dynamical system in terms of x, H and Ω_m becomes,

$$J = \begin{pmatrix} \frac{\partial x'}{\partial x} & \frac{\partial x'}{\partial H} & \frac{\partial x'}{\partial \Omega_m} \\ \frac{\partial H'}{\partial x} & \frac{\partial H'}{\partial H} & \frac{\partial H'}{\partial \Omega_m} \\ \frac{\partial \Omega_m'}{\partial x} & \frac{\partial \Omega_m'}{\partial H} & \frac{\partial \Omega_m'}{\partial \Omega_m} \end{pmatrix} . \tag{4.21}$$

This form of J will also be valid for all the other models that will be analysed in the subsequent sections. J will be evaluated, and the stability of the fixed points will be analysed, for specific values of α_1 and P_1. This is because the expressions in Eq. (4.21) for general values of these parameters would make the investigation complex, and thus specifying these values makes it possible to study the stability effectively.

Notice that the value of q at the fixed points will always be equal to -1. This follows from the fact that $H' = 0$, which directly implies that $\dot{H} = 0$, and $q = -1 - \frac{\dot{H}}{H^2}$. It then also follows from Eq. (4.19) that at fixed points with a non-zero value of H, $\omega_{DE} = -1$. So any such fixed point, will represent a de Sitter universe in which the expansion is exponential, as described in Eq. (3.24). In particular, this is the case for C_1 for this $f_1(T, T_G)$ model. The exception to this is at fixed points with $H = 0$ at which q and ω_{DE} are undefined.

As can be seen in Eq. (4.17), $q < 0$ in all of the phase space for this model, meaning that the expansion of the modeled universe is always accelerating. Although we know that throughout the history of the Universe there were periods of matter domination in which the expansion was decelerating, in this work these models are being studied for the predicted late-time behaviour, as previously mentioned, and so this does not reflect a deficiency of the model itself. Since we cannot have a positive value of q, points with $H = 0$ are disconnected from the boundary conditions as they can never be realised by a physical universe, i.e. although certain trajectories do approach such fixed points, these are isolated trajectories, which do not correspond to the initial conditions of our Universe. These points are rather mathematical artefacts of the dynamical analysis, and do not have a direct physical interpretation. This is also reflected in the fact that at these fixed points, q and ω_{DE} are undefined.

4.1.2 | Analysis at Infinity

Apart from the fixed points in the finite phase space, the dynamical system might also have fixed points at infinity. At these points one or more of the dynamical variables x,

H and Ω_m are infinite. These fixed points could represent future singularities and thus warrant an extensive investigation.

In order to study this dynamical behaviour at infinity, we transform to the (R, Θ, Φ) co-ordinates defined in Eqs. (3.66)-(3.68). For this specific dynamical system we take,

$$x = \frac{R}{1-R} \cos\Theta \sin\Phi \tag{4.22}$$
$$H = \frac{R}{1-R} \sin\Theta \sin\Phi \tag{4.23}$$
$$\Omega_m = \frac{R}{1-R} \cos\Phi \,. \tag{4.24}$$

The region of the (R, Θ, Φ) plane which corresponds to S defined in Eq. (4.16), is given by,

$$\begin{gathered}\{(R,\Theta,\Phi) : 0 \leq R \leq \frac{1}{2}, 0 \leq \Theta \leq \frac{\pi}{2}, 0 \leq \Phi \leq \frac{\pi}{2}\} \cup \\ \left\{(R,\Theta,\Phi) : \frac{1}{2} < R < 1, 0 \leq \Theta \leq \frac{\pi}{2}, 0 \leq \Phi \leq \arccos\left(\frac{1-R}{R}\right)\right\} ,\end{gathered} \tag{4.25}$$

where $\Theta = 0$ is not in the phase space for $P_1 > \frac{1}{2}$. Differentiating Eqs. (4.22)-(4.24) wrt η we find that,

$$R' = (1-R)^2[\Omega_m' \cos\Phi + \sin\Phi(x'\cos\Theta + H'\sin\Theta)] \tag{4.26}$$
$$\Theta' = \frac{R-1}{R\sin\Phi}\left[x'\sin\Theta - H'\cos\Theta\right] \tag{4.27}$$
$$\Phi' = \frac{R-1}{R}\left[\Omega_m'\sin\Phi - \cos\Phi(x'\cos\Theta + H'\sin\Theta)\right] . \tag{4.28}$$

Substituting in the expressions for x',H' and Ω_m' from Eqs. (4.14), (4.15) and (4.10) respectively, and again using the substitutions in Eqs. (4.22)-(4.24), we obtain the dynamical system in the (R, Θ, Φ) space,

$$\begin{aligned}R' = (1-R)\Bigg\{ & -R\cos^2\Phi\left[1 + 2\left(\frac{R\cos\Theta\sin\Phi}{1-R}\right)^{\frac{2}{P_1}}\right] \\ & + \frac{1}{2}R\sin^2\Phi\Bigg[2\sin^2\Theta\left(-1 + \left(\frac{R\cos\Theta\sin\Phi}{1-R}\right)^{\frac{2}{P_1}}\right) \\ & + \cos^2\Theta\Bigg[4P_1 + \left(\frac{R\cos\Theta\sin\Phi}{1-R}\right)^{\frac{2}{P_1}}\left(1 - 4P_1 + \frac{6\left(\frac{R\cos\Phi}{1-R} - 1\right)\tan^2\Theta}{24^{P_1}\alpha_1(P_1-1)\left(\frac{R\sin\Theta\sin\Phi}{1-R}\right)^{4P_1}}\right)\Bigg]\Bigg]\Bigg\}\end{aligned} \tag{4.29}$$

$$\Theta' = -\frac{1}{2}\cos\Theta\sin\Theta\Bigg\{2 + 4P_1 - 2\left(\frac{R\cos\Theta\sin\Phi}{1-R}\right)^{\frac{2}{P_1}}$$

$$+\left(\frac{R\cos\Theta\sin\Phi}{1-R}\right)^{\frac{2}{P_1}}\left[1-4P_1+\frac{6\left(\frac{R\cos\Phi}{1-R}-1\right)\tan^2\Theta}{24^{P_1}\alpha_1(P_1-1)\left(\frac{R\sin\Theta\sin\Phi}{1-R}\right)^{4P_1}}\right]\Bigg\} \tag{4.30}$$

$$\begin{aligned}\Phi' = &-\frac{1}{2}\cos\Phi\sin\Phi\Bigg\{-2-4\left(\frac{R\cos\Theta\sin\Phi}{1-R}\right)^{\frac{2}{P_1}} \\ &-2\sin^2\Theta\left[\left(\frac{R\cos\Theta\sin\Phi}{1-R}\right)^{\frac{2}{P_1}}-1\right] \\ &-\cos^2\Theta\left[4P_1+\left(\frac{R\cos\Theta\sin\Phi}{1-R}\right)^{\frac{2}{P_1}}\left(1-4P_1+\frac{6\left(\frac{R\cos\Phi}{1-R}-1\right)\tan^2\Theta}{24^{P_1}\alpha_1(P_1-1)\left(\frac{R\sin\Theta\sin\Phi}{1-R}\right)^{4P_1}}\right)\right]\Bigg\}.\end{aligned} \tag{4.31}$$

We can also obtain expressions for q, Ω_{DE} and ω_{DE} in the (R,Θ,Φ) coordinate system, by substituting Eqs. (4.22)-(4.24) into Eqs. (4.17), (4.18) and (4.20) respectively,

$$q = -\left(\frac{R\cos\Theta\sin\Phi}{1-R}\right)^{\frac{2}{P_1}} \tag{4.32}$$

$$\Omega_{DE} = \frac{1-R(1+\cos\Phi)}{1-R} \tag{4.33}$$

$$\omega_{DE} = \frac{(R-1)\left(1+2\left(\frac{R\cos\Theta\sin\Phi}{1-R}\right)^{\frac{2}{P_1}}\right)}{3(R(\cos\Phi+1)-1)}. \tag{4.34}$$

These expressions will allow us to interpret the cosmological implications of these infinite fixed points.

The behaviour at infinity occurs as $R\to 1^-$, as discussed in Sec. 3.3.3. Thus, in order to find the fixed points at infinity, only the leading terms of Eqs. (4.29)-(4.31), in the limit as $R\to 1^-$, are required. These leading terms depend on the value of P_1. As an example, the analysis for $0<P_1<2$ is given below. In this case the leading terms are,

$$\begin{aligned}R' \to &\cos\Theta\sin\Phi\left(\frac{\cos\Theta\sin\Phi}{1-R}\right)^{\frac{2}{P_1}-1}\Bigg[-2\cos^2\Phi+\frac{1}{2}\cos^2\Theta\sin^2\Phi(1-4P_1) \\ &+\sin^2\Theta\sin^2\Phi\Bigg]\end{aligned} \tag{4.35}$$

$$\Theta' \to \sin\Theta\cos\Theta\left(\frac{\cos\Theta\sin\Phi}{1-R}\right)^{\frac{2}{P_1}}\left(\frac{1}{2}+2P_1\right) \tag{4.36}$$

$$\Phi' \to \left(\frac{\cos\Theta\sin\Phi}{1-R}\right)^{\frac{2}{P_1}}\cos\Phi\sin\Phi\left(2+\frac{\cos^2\Theta}{2}(1-4P_1)+\sin^2\Theta\right). \tag{4.37}$$

The fixed points at infinity occur when $\Theta'=\Phi'=0$ and thus we can find these critical points by setting Eqs. (4.36) and (4.37) equal to zero. The critical points at infinity along with their existence and stability conditions are presented in Table 4.1. The values of q, ω_{DE}, Ω_{DE} and H at these fixed points are then presented in Table 4.2.

Critical Point	Θ	Φ	Existence	Stability
Q_1	0	$\frac{\pi}{2}$	Always	Unstable if $P_1 > \frac{5}{4}$. Saddle otherwise.
Q_2	$\frac{\pi}{2}$	$[0, \frac{\pi}{2}]$	$P_1 > 0$	Inconclusive since $\frac{d\Theta'}{d\Theta} = \frac{d\Phi'}{d\Phi} = 0$.
Q_3	$[0, \frac{\pi}{2}]$	0	$P_1 > 0$	Inconclusive since $\frac{d\Theta'}{d\Theta} = \frac{d\Phi'}{d\Phi} = 0$.

Table 4.1: The critical points at infinity alongside their existence and stability conditions for $f_1(T, T_G)$. Note that Q_2 and Q_3 are lines of fixed points. The stability of these last two sets of critical points cannot be studied analytically and thus they can only be classified by investigation of the phase portrait.

The stability of point Q_1 was inferred from the signs of $\frac{d\Theta'}{d\Theta}$ and $\frac{d\Phi'}{d\Phi}$ calculated from Eqs. (4.36) and (4.37), as discussed in Sec. 3.3.3. Evaluated at Q_1, these are,

$$\frac{d\Theta'}{d\Theta} = \frac{1}{2}\left(\frac{1}{1-R}\right)^{\frac{2}{P_1}}(1+4P_1) \tag{4.38}$$

$$\frac{d\Phi'}{d\Phi} = \frac{1}{4}\left(\frac{1}{1-R}\right)^{\frac{2}{P_1}}(8P_1-10)\,, \tag{4.39}$$

while,

$$R' = \frac{1}{2}\left(\frac{1}{1-R}\right)^{\frac{2}{P_1}-1}(1-4P_1)\,. \tag{4.40}$$

The values of P_1 satisfying the stability conditions in Eqs. (3.69) and (3.70) are as given in Table 4.1.

Notice how since Q_1 and Q_3 correspond to a zero value of H, the values of q and ω_{DE} at these points are undefined, and, in line with the discussion in Sec. 4.1.1, these fixed points do not have a direct physical interpretation. The cosmology that fixed points along the line Q_2 can represent varies depending on the exact coordinates and so, this interpretation will be done for particular values of α_1 and P_1 where fixed points of interest are identified.

4.1.3 | Cosmological Implications

We now investigate the cosmological implications of the dynamical system analysed above. This will be done by fixing specific values of the parameters α_1 and P_1 and investigating the phase portraits of the resulting models. The choice of parameters was done

Cr. Point	Θ	Φ	Ω_{DE}	q	ω_{DE}	H
Q_1	0	$\frac{\pi}{2}$	1	Undefined	Undefined	0
Q_2	$\frac{\pi}{2}$	$[0, \frac{\pi}{2}]$	1 if $\Phi = \frac{\pi}{2}$ ∞ otherwise	See note in caption	See note in caption	0 when $\Phi = 0$ ∞ otherwise
Q_3	$[0, \frac{\pi}{2}]$	0	∞	Undefined	Undefined	0

Table 4.2: Values of the dark energy density parameter, deceleration parameter and dark energy equation-of-state parameter at the infinite fixed points of $f_1(T, T_G)$. Note that the values of q and ω_{DE} at the line of fixed points Q_2 depend on both the value of P_1 and Φ and are too complex to list in this table. Instead, they will be explicitly evaluated for cases of interest, if any, in Sec. 4.1.3.

based on the stability criteria that were discussed in Secs. 4.1.1 and 4.1.2. However, in certain cases the stability of fixed points could not be studied before fixing the values of α_1 and P_1. In this case, different values of the parameters were tried out and the resulting phase portraits were used to study the type of dynamics that they produce. Different combinations of positive and negative values, and integers and fractional values, were tested. This trial-and-error method was also employed for the other models, as will be seen in the following sections. For $f_1(T, T_G)$, three different parameter choices, which lead to qualitatively different dynamics, are presented.

4.1.3.1 | Case 1: $\alpha_1 = -1$ & $P_1 = \frac{1}{3}$

We start the analysis for the parameter choice $\alpha_1 = -1$ and $P_1 = \frac{1}{3}$ by computing the stability matrix J given in Eq. (4.21), which, as discussed in Sec. 3.3.2, allows for the study of the stability of the fixed points,

$$J = \begin{pmatrix} \frac{1}{12}\left(8 - 14x^6 + 45(3H)^{\frac{2}{3}}x^4(\Omega_m - 1)\right) & \frac{3^{\frac{2}{3}}x^5(\Omega_m - 1)}{2H^{\frac{1}{3}}} & \frac{3}{4}(3H)^{\frac{2}{3}}x^5 \\ 6Hx^5 & x^6 - 1 & 0 \\ -12x^5\Omega_m & 0 & -1 - 2x^6 \end{pmatrix}. \tag{4.41}$$

The set of eigenvalues of J evaluated at the fixed point C_1 is found to be $\{-3, -2, -1\}$. Thus, the point C_1 is a stable fixed point. This behaviour is indeed observed in the 3D phase portrait which can be seen in Fig. 4.1a and is more evident in the trajectories contained within the $\Omega_m = 0$ plane shown in Fig. 4.1b. Notice that for this choice of parameters, the other fixed point C_2 results in the second entry of the first row of J being infinite. Hence, the stability of this fixed points cannot be investigated analytically. However, from the phase portraits, it is easy to see that C_2 is a saddle, as trajectories are first attracted towards it and then are repelled away.

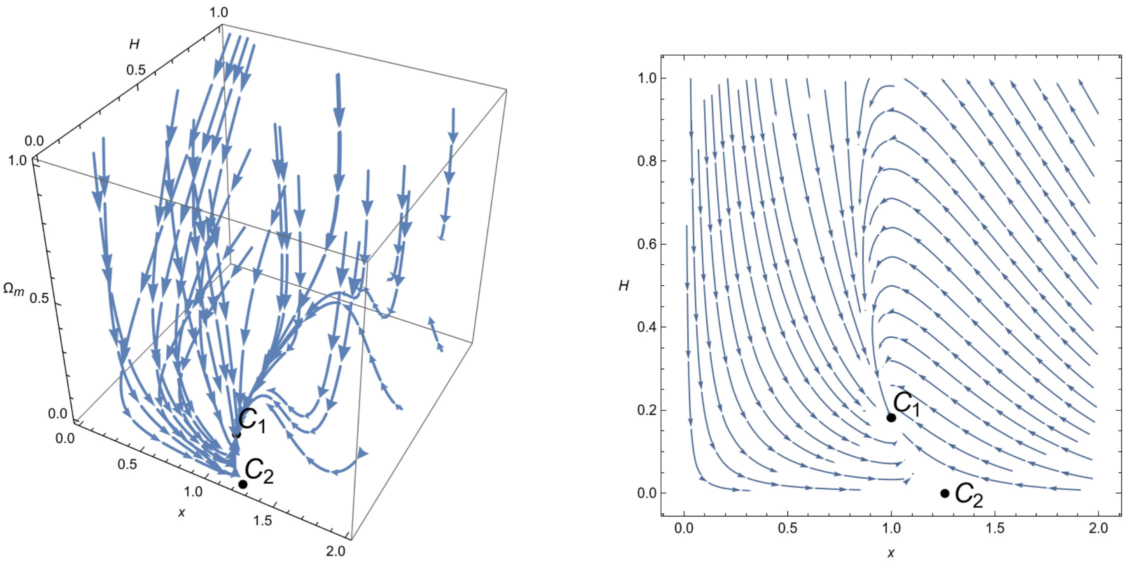

(a) Full 3D phase portrait. (b) 2D phase portrait in the plane $\Omega_m = 0$.

Figure 4.1: Trajectories in the phase space for the $f_1(T, T_G)$ cosmological scenario defined by Eqs. (4.14)-(4.10) with parameters $\alpha_1 = -1, P_1 = \frac{1}{3}$. The fixed points C_2 is a saddle while C_1 is an attractor.

The dynamics of the finite phase space are clearly reflected in the global phase portrait in the (R, Θ, Φ) coordinate system, as can be seen in Fig. 4.2. The fixed points along the line Q_2 seem to be behaving like unstable fixed points, while the point $(1, \frac{\pi}{2}, \frac{\pi}{2})$ is behaving like a saddle. Note that from Eqs. (4.32) and (4.34), at $(1, \frac{\pi}{2}, \frac{\pi}{2})$, $q = 0$ and $\omega_{DE} = \frac{1}{3}$. However, since at this point $H = \infty$, the values of these observable parameters do not seem to be consistent and thus this point would require further investigation. As mentioned previously, there is no way to analytically study the stability of these fixed points since $\frac{d\Theta'}{d\Theta} = \frac{d\Phi'}{d\Phi} = 0$. The point Q_1 should be behaving like a saddle, however, because of numerical instability, the trajectories at $R = 1$ are not being plotted accurately, making it impossible to confirm the stability of this fixed point. Likewise, the stability of the points along Q_3 is not clear.

From the two phase portraits in Figs. 4.1 and 4.2, we can get an idea of the type of cosmology that this model with this choice of parameters can represent. The value of Ω_m is decreasing from one to zero for all the trajectories, meaning that the universe is going from matter domination to dark-energy domination. Moreover, all the trajectories are eventually tending towards C_1 which has $q = \omega_{DE} = -1$. This means that the future dynamics of the modeled universe are like those of a de Sitter universe with a cosmological constant. Although the value of $H \approx 0.2$ towards which the modeled universe is tending towards is not in line with the expected value of H in S.I. units, what

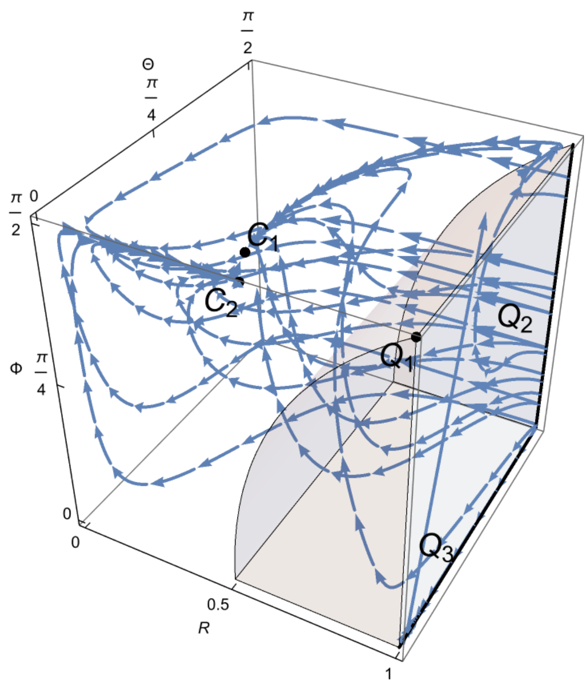

Figure 4.2: Global phase portrait for $f_1(T, T_G)$ with parameters $\alpha_1 = -1, P_1 = \frac{1}{3}$ in the (R, Θ, Φ) coordinates. The gray shaded region represents the volume of the space which results in $\Omega_m > 1$ and the universe may result in future singularities. This region will be similarly shaded in all the following global phase portraits and will have the same physical significance. Notice that the trajectories around the plane $R = 1$, i.e. at infinity, are not being plotted accurately because of numerical instability arising from the software used. This makes it hard to verify the stability of the fixed point Q_1 which is expected to be a saddle.

is of importance in this analysis is that the model results in a non-zero, positive value of H. This analysis gives an indication that the model can produce physical dynamics which describe the observable universe. The model would then need to be constrained with data such as from type Ia Supernovae and the CMB in order to tune α_1 and P_1 in order to fit parameters such as the value of H_0 to observations before it can be considered as a correct description of our Universe. This will also be true for the other three $f(T, T_G)$ models.

It is important to note that although from the global phase portrait in Fig. 4.2, the trajectories all seem to originate from a past singularity, this singularity might be simply an algebraic one rather than a physical one, like for example the Big Bang. This, once again, comes down to the fact that in this work it is the late-time Universe that is being modeled, and different assumptions, such as considering the radiation component, need to be taken in order to study the early Universe. If, in future works, these assumptions

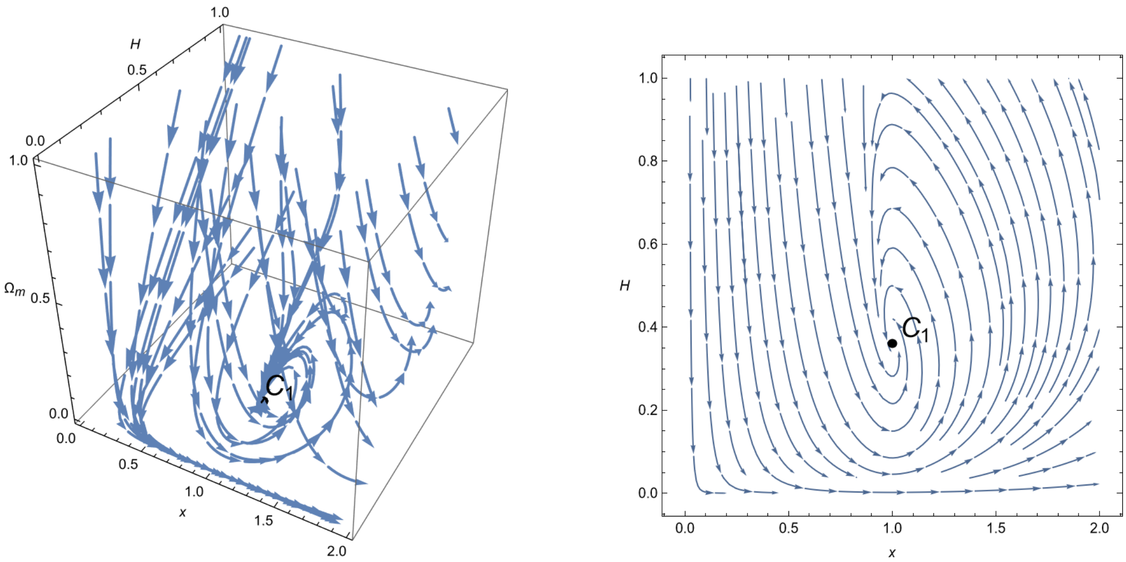

(a) Full 3D phase portrait. (b) 2D phase portrait in the plane $\Omega_m = 0$.

Figure 4.3: Trajectories in the phase space for the $f_1(T, T_G)$ cosmological scenario defined by Eqs. (4.14)-(4.10) with parameters $\alpha_1 = -1, P_1 = \frac{1}{8}$. The fixed point C_1 is an attractor of the system.

are taken into consideration and the past singularity is still a dynamical feature of the model, this could then be interpreted with certainty as a physical past singularity.

4.1.3.2 | Case 2: $\alpha_1 = -1$ & $P_1 = \frac{1}{8}$

Similar dynamics to those seen in the previous section can be obtained by setting $\alpha_1 = -1$ and $P_1 = \frac{1}{8}$, however, in this case, the critical point C_3 does not exist. The stability matrix is given by,

$$J = \begin{pmatrix} \frac{1}{4} + \frac{17x^{16}}{4} + \frac{60}{7}(2^{\frac{5}{8}})(3^{\frac{7}{8}})H^{\frac{3}{2}}x^{14}(\Omega_m - 1) & \frac{6}{7}(2^{\frac{5}{8}})(3^{\frac{7}{8}})\sqrt{H}x^{15}(\Omega_m - 1) & \frac{4}{7}(2^{\frac{5}{8}})(3^{\frac{7}{8}})H^{\frac{3}{2}}x^{15} \\ 16Hx^{15} & x^{16} - 1 & 0 \\ -32x^{15}\Omega_m & 0 & -1 - 2x^{16} \end{pmatrix}. \tag{4.42}$$

At C_1, the set of eigenvalues of J are $\{-1.5 \pm 3.12i, -3\}$, meaning that this point is a stable focus. This is indeed reflected in the phase portraits as can be seen in Fig 4.3. Notice the spiral formed around the critical point which is a result of J having a complex conjugate pair of eigenvalues (see Sec. 3.3.2).

The global dynamics of the model, as can be seen in the global phase portrait in Fig. 4.4, are very similar to those resulting from the parameters considered in Sec. 4.1.3.1

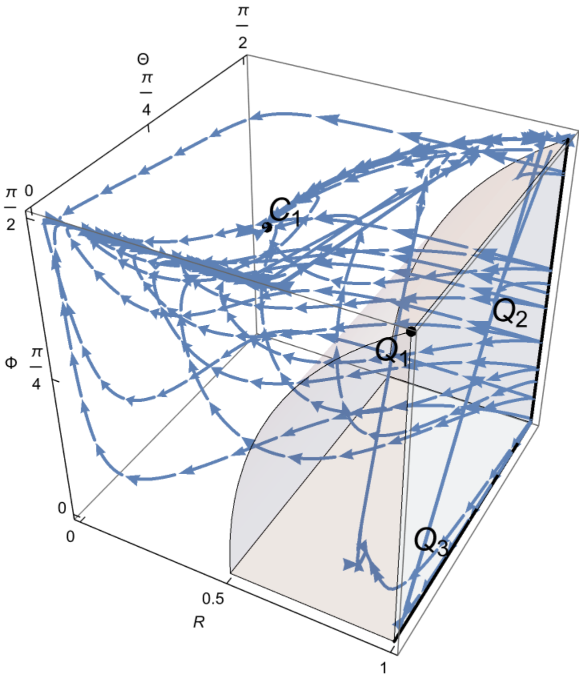

Figure 4.4: Global phase portrait for $f_1(T, T_G)$ with parameters $\alpha_1 = -1, P_1 = \frac{1}{8}$ in the (R, Θ, Φ) coordinates. The numerical instability as $R = 1$ is approached is very evident in this case which once again makes it hard to study the stability of fixed points at infinity.

and thus the cosmological implications are as discussed there. In particular, the universe is evolving towards a de Sitter one.

4.1.3.3 | Case 3: $\alpha_1 = \frac{1}{2}$ & $P_1 = 2$

It is also interesting to study the case for which the critical point C_1 is not a stable fixed point. This can be achieved by setting $\alpha_1 = \frac{1}{2}$ and $P_1 = 2$. The stability matrix in this case is,

$$J = \begin{pmatrix} 4-7x & \frac{\Omega_m - 1}{16H^7} & \frac{1}{96H^6} \\ H & x-1 & 0 \\ -2\Omega_m & 0 & -1-2x \end{pmatrix}. \tag{4.43}$$

At C_1, the only fixed point of the system, the eigenvalues of J are $\{-3.8, -3, 0.8\}$ and so this point is now a saddle. The behaviour in the finite phase space can be seen in Fig. 4.5 while the global dynamics can be seen in Fig. 4.6. From this global phase portrait, the fixed points at infinity of particular interest are Q_1 which is acting like a saddle as expected, and the point $(1, \frac{\pi}{2}, \frac{\pi}{2})$ which is acting like a stable fixed point, although the

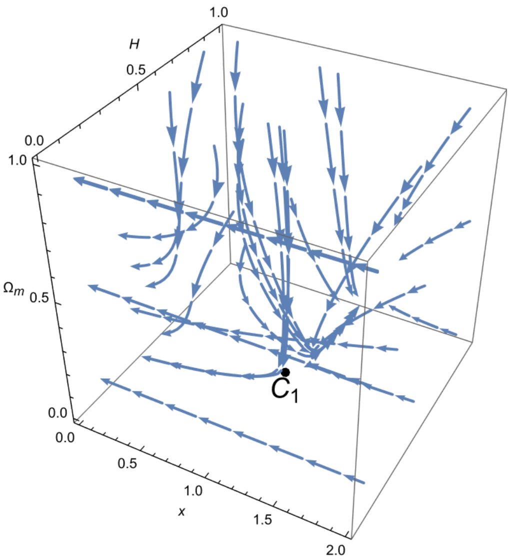

(a) Full 3D phase portrait.

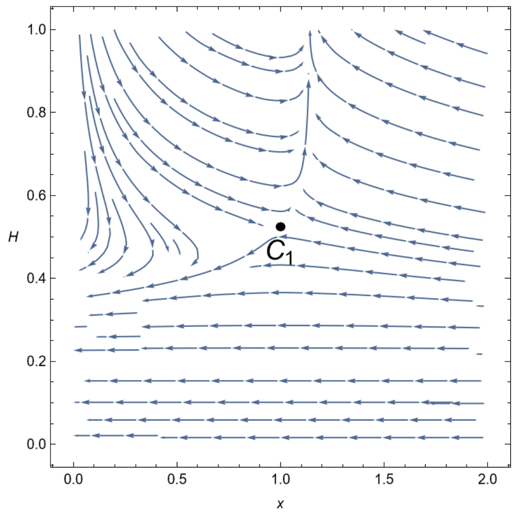

(b) 2D phase portrait in the plane $\Omega_m = 0$.

Figure 4.5: Trajectories in the phase space for the $f_1(T, T_G)$ cosmological scenario defined by Eqs. (4.14)-(4.10) with parameters $\alpha_1 = \frac{1}{2}, P_1 = 2$. C_1 is a saddle in this case.

stability of the latter cannot be confirmed analytically. Moreover, trajectories seem to be originating from the line of fixed points Q_2.

At the stable fixed point at infinity we find that $\Omega_{DE} = 1$ and $H = \infty$. This implies that the expansion of the universe becomes infinite, and thus this point could represent something similar to a Big Rip. However, from Eqs. (4.32) and (4.34), $q = 0$ and $\omega_{DE} = \frac{1}{3}$. Hence, further analysis would be needed to confirm what type of future cosmology this point represents. Since Q_1 represents a point with $H = 0$, this fixed point is inaccessible to the system from the allowed initial conditions. As in the other cases, at the finite fixed point C_1, $q = \omega_{DE} = -1$. Thus this model represents a universe which first tends towards a de Sitter universe and then could evolve into a future singularity.

4.1.4 | Model 1 Variation

As previously indicated, for $P_1 = \frac{1}{2}$, H is eliminated from Eq. (4.14) and so the dynamical system reduces to a 2D one, in terms of x and Ω_m only. In this case the model becomes $f(T, T_G) = -T + \alpha_1\sqrt{T_G}$ and the dynamical system containing its dynamics is now,

$$x' = \frac{x}{2}\left[2 - x^4\left(1 + \frac{\sqrt{6}(\Omega_m - 1)}{x^2\alpha_1}\right)\right] \tag{4.44}$$

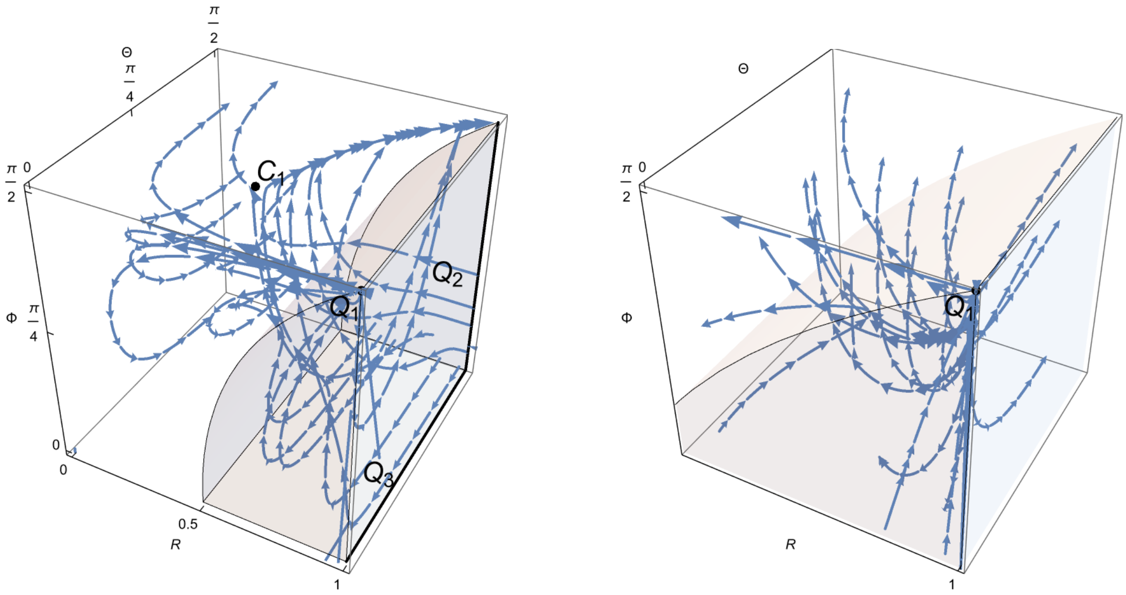

(a) (b)

Figure 4.6: Global phase portrait for $f_1(T, T_G)$ with parameters $\alpha_1 = \frac{1}{2}, P_1 = 2$ in the (R, Θ, Φ) coordinates. Q_1 is behaving as a saddle as expected while there is a stable fixed point at infinity at $(1, \frac{\pi}{2}, \frac{\pi}{2})$. Fig. 4.6b shows an enlarged section around the fixed point Q_1. Notice how although most trajectories seem to be originating from Q_1, trajectories in the $\Theta = 0$ plane show the saddle nature of this fixed point.

$$\Omega_m' = -\Omega_m(1 + 3\omega_m + 2x^4)\,, \tag{4.45}$$

where,

$$x = \left(1 + \frac{\dot{H}}{H^2}\right)^{\frac{1}{4}}\,, \tag{4.46}$$

and Ω_m is as defined in Eq. (4.4). This system is defined on the phase space,

$$S = \{(x, \Omega_m) | x \in [0, \infty), \Omega_m \in [0, \infty)\}\,. \tag{4.47}$$

The critical points of the system are at $C_1 = (0, 0)$ and $C_2 = (x_2, 0)$, where

$$x_2 = \begin{cases} \sqrt{\frac{\sqrt{3}+\sqrt{3+4\alpha_1^2}}{\sqrt{2}\alpha_1}} & \text{if } \alpha_1 > 0 \\ \sqrt{\frac{\sqrt{3}-\sqrt{3+4\alpha_1^2}}{\sqrt{2}\alpha_1}} & \text{if } \alpha_1 < 0\,. \end{cases} \tag{4.48}$$

The stability matrix is given by,

$$J = \begin{pmatrix} 1 - \frac{5x^4}{2} - \frac{3\sqrt{\frac{3}{2}}x^2(\Omega_m - 1)}{\alpha_1} & -\frac{\sqrt{\frac{3}{2}}x^3}{\alpha_1} \\ -8x^3\Omega_m & -1 - 2x^4 \end{pmatrix}\,. \tag{4.49}$$

At C_1, the eigenvalues of this matrix are always ± 1 meaning that the origin is always a saddle. The eigenvalues of J at C_2 are,

$$\left\{ -\frac{3+4\alpha_1^2+\sqrt{3(3+4\alpha_1^2)}}{\alpha_1^2}, -\frac{6+5\alpha_1^2+2\sqrt{3(3+4\alpha_1^2)}}{\alpha_1^2} \right\}, \tag{4.50}$$

when $\alpha_1 > 0$, and,

$$\left\{ \frac{-3-4\alpha_1^2+\sqrt{3(3+4\alpha_1^2)}}{\alpha_1^2}, \frac{-6-5\alpha_1^2+2\sqrt{3(3+4\alpha_1^2)}}{\alpha_1^2} \right\}, \tag{4.51}$$

when $\alpha_1 < 0$. In both cases, both eigenvalues are negative for any value of α_1 and thus C_2 is always a stable fixed point.

The deceleration and dark-energy equation-of-state parameters are given by,

$$q = -x^4 \tag{4.52}$$

$$\omega_{DE} = \frac{2x^4+1}{3(\Omega_m - 1)}\,. \tag{4.53}$$

At C_1, $q = 0$ and $\omega_{DE} = -\frac{1}{3}$ for any value of α_1, while at C_2,

$$q = -\frac{\left(\sqrt{3} \pm \sqrt{3+4\alpha_1^2}\right)^2}{2\alpha_1^2} \tag{4.54}$$

$$\omega_{DE} = -\frac{1}{3}\left(1 + \frac{\left(\sqrt{3} \pm \sqrt{3+4\alpha_1^2}\right)^2}{\alpha_1^2}\right), \tag{4.55}$$

where the $+$ sign in Eqs. (4.54) and (4.55) corresponds to $\alpha_1 > 0$ and the $-$ sign corresponds to $\alpha_1 < 0$. Notice that at C_2, $q < 0$ for any value of α_1 implying that this fixed point represents an accelerating universe in all cases. At C_2, $\omega_{DE} < -1$ for $\alpha_1 > 0$ or $\alpha_1 < -\sqrt{6}$, i.e. this fixed point represents a universe with phantom dark energy for these ranges of α_1. For $\alpha_1 = -\sqrt{6}$, the fixed point represents a de Sitter universe, while the remaining values of α_1 give a fixed point with quintessence-like dark energy.

We can also investigate the behaviour at infinity by transforming to the (R, Θ) coordinates via,

$$x = \frac{R}{1-R}\cos\Theta \tag{4.56}$$

$$\Omega_m = \frac{R}{1-R}\sin\Theta\,. \tag{4.57}$$

This gives the dynamical system,

$$R' = \frac{R}{2\alpha_1(R-1)^3}[-2\alpha_2(r-1)^4\cos^2\Theta + R^4\alpha_1\cos^6\Theta + 2\alpha_1(R-1)^4\sin^2\Theta \\ -R^2\cos^4\Theta(\sqrt{6}(R-1)^2 + \sqrt{6}R(R-1)\sin\Theta - 4R^2\alpha_2\sin^2\Theta)] \tag{4.58}$$

$$\Theta' = -\frac{\cos\Theta\sin\Theta}{2\alpha_2(R-1)^4}[4\alpha_1(R-1)^4 + 3R^4\alpha_1\cos^4\Theta \\ +\sqrt{6}R^2(R-1)\cos^2\Theta(R+R\sin\Theta-1)]\,. \tag{4.59}$$

The parameters q, Ω_{DE} and ω_{DE} in this coordinate system are given by,

$$q = -\left(\frac{R\cos^4\Theta}{1-R}\right)^4 \tag{4.60}$$

$$\Omega_{DE} = \frac{1-R(1+\sin\Theta)}{1-R} \tag{4.61}$$

$$\omega_{DE} = \frac{(R-1)^4 + 2R^4\cos^4\Theta}{3(R-1)^3(R+R\sin\Theta-1)}\,. \tag{4.62}$$

In order to investigate the fixed points at infinity, we consider the leading terms in Eqs. (4.58) and (4.59) as $R \to 1^-$,

$$R' \to \frac{\alpha_1\cos^6\Theta + 4\alpha_1\cos^4\Theta\sin^2\Theta}{2\alpha_1(R-1)^3} \tag{4.63}$$

$$\Theta' \to -\frac{3\cos^5\Theta\sin\Theta}{2(R-1)^4}\,. \tag{4.64}$$

Solving for $\Theta' = 0$, gives the fixed point $Q_1 = (1, \frac{\pi}{2})$. At this point $q = 0 = \omega_{DE}$, while $\Omega_{DE} = -\infty$. The infinite value of $\Omega_m = 1 - \Omega_{DE}$, implies that this point represents a past singularity, however, the nature of this singularity is not clear from this analysis. $\frac{d\Theta'}{d\Theta} = 0$ at Q_1 and thus the stability of this point can only be investigated through the phase portrait for specific values of α_1.

Since the dynamics are expected to be the same for any value of α_1, a representative case which leads to a phantom-like solution, with $\alpha_1 = -3$ is presented here. The phase portrait in the (x, Ω_m) coordinates can be seen in Fig. 4.7a, while its projection on the Poincaré plane (R, Θ) can be seen in Fig. 4.7b. All trajectories are originating from a past singularity at Q_1 and are then tending towards the global attractor C_2. Since for this value of α_1, C_2 represents a phantom-like solution, we can conclude that this cosmological model represents an accelerating universe that is evolving from matter-dominated to dark-energy-dominated with phantom-like behaviour. The model cannot result in a future singularity since there are no stable fixed points at infinity. This model is an example of how a simple modification to the teleparallel action can lead to a universe in which the effective dark energy produces dynamics like those of a cosmological

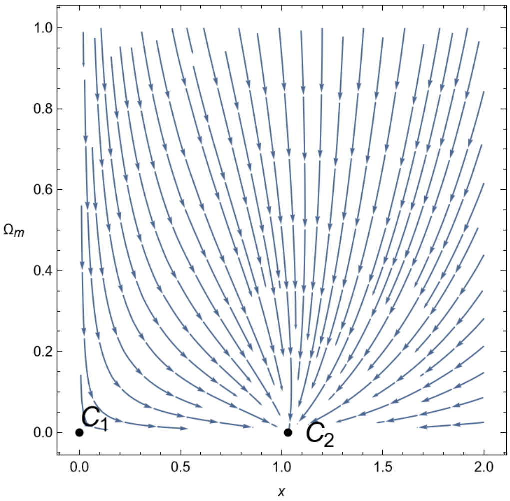

(a) Phase space portrait in the (x, Ω_m) plane.

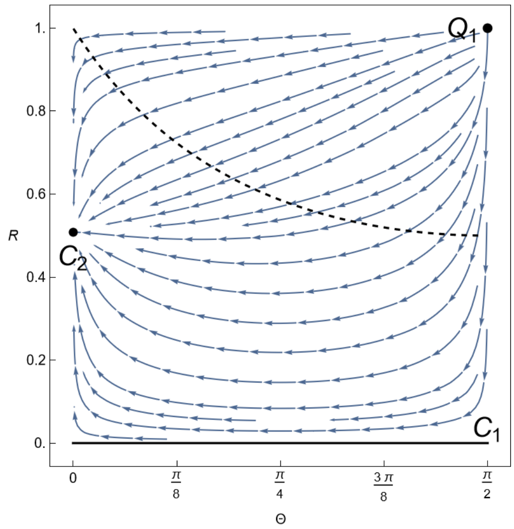

(b) Projection of the phase space onto the Poincaré plane, (R, Θ). The region above the dashed line represents a past singularity.

Figure 4.7: Trajectories in the phase space for the $f_1(T, T_G)$ cosmological scenario defined by Eqs. (4.44)-(4.45) with $\alpha_1 = -\sqrt{6}$. The finite fixed point C_1 acts like a saddle while C_2 acts like a global attractor. The fixed point Q_1 at infinity is unstable.

constant or a phantom/quintessence scalar field, without having to implicitly add such terms to the theory.

4.2 | Model 2: $f_2(T, T_G) = -T + \alpha_2 e^{-P_2\sqrt{\frac{T_G}{T_{G0}}}}$

The next model to be analysed is the one inspired by the Linder model as given in Eq. (3.48). This adds some more complexity to the power law model analysed in the previous section. Here T_{G_0} is the present day value of the T_G invariant. T_{G_0} can be calculated using Eq. (3.38) by substituting the values of H_0 and $\dot{H}|_{t=t_0}$. The latter can be calculated using the value of the deceleration parameter at the present time q_0. In order to obtain an estimate of T_{G_0} we can take $H_0 = 73.3$km/s/Mpc and $q_0 = -0.51$. These values were taken from Riess et al. (2021) and give $T_{G_0} \approx 350 \times 10^6 \text{km}^4/\text{s}^4/\text{Mpc}^4$. Although the initial dynamical analysis will be performed without fixing the value of T_{G_0}, when investigating the cosmological implications of this model, T_{G_0} will be set equal to one. This is because, since it is the dynamics of the model that are being investigated, we can scale this constant to simplify calculations and avoid numerical instability while not affecting the resulting dynamics. To constrain the model to fit observations, the value of T_{G_0} calculated above would then need to be used.

Once again, the dynamics of the model are governed by the Friedmann equations as given in Eqs. (3.41) and (3.42), with the dark-energy effective fluid density and pressure given by,

$$\kappa^2\rho_{DE} = \frac{\alpha_2 e^{-2\sqrt{6}P_2 D} H^2}{4T_{G_0}^2 D^3}\{2\sqrt{6}P_2 H^6 + 2T_{G_0}\dot{H}D + 8P_2 H^4\dot{H}(\sqrt{6}+6P_2 D) + 2H^2[T_{G_0}D + 2P_2\dot{H}^2(\sqrt{6}+6P_2D)] + P_2H^3(\sqrt{6}+12P_2D)\ddot{H}\} \tag{4.65}$$

$$\kappa^2 p_{DE} = \frac{e^{-2\sqrt{6}P_2D}\alpha_2}{24T_{G_0}^2\kappa^2(H^2+\dot{H})^2D}\Big\{12T_{G_0}^2H^4D + 24T_{G_0}^2H^2\dot{H}D + 192T_{G_0}P_2^2H^6\dot{H}D + 12T_{G_0}^2\dot{H}^2D + 192T_{G_0}P_2^2H^4\dot{H}^2D + 144T_{G_0}P_2^2H^2\dot{H}^3D + 144T_{G_0}P_2^2H^5\ddot{H}D + 48T_{G_0}P_2^2H^3\dot{H}\ddot{H}D + 48T_{G_0}P_2^2H\dot{H}^2\ddot{H}D - 36T_{G_0}P_2^2H^2\ddot{H}^2D - 24\sqrt{6}P_2^3H^2(H^2+\dot{H})[2\dot{H}(2H^2+\dot{H}) + H\ddot{H}]^2 + 24T_{G_0}P_2^2H^4\dddot{H}D + 24T_{G_0}P_2^2H^2\dot{H}\dddot{H}D + \sqrt{6}T_{G_0}P_2H[12H^7 + 52H^5\dot{H} + 12H^4\ddot{H} + 4H^2\dot{H}\ddot{H} + 4\dot{H}^2\ddot{H} + 2H^3(26\dot{H}^2 + \dddot{H}) + H(24\dot{H}^3 - 3\ddot{H}^2 + 2\dot{H}\dddot{H})\Big\}, \tag{4.66}$$

where we are defining $D = \sqrt{\frac{H^2(H^2+\dot{H})}{T_{G_0}}}$.

To perform the dynamical analysis, two auxiliary, unitless variables, are introduced,

$$x = \frac{D}{H^2} = \sqrt{\frac{1+\frac{\dot{H}}{H^2}}{T_{G_0}}} \tag{4.67}$$

$$\Omega_m = \frac{\kappa^2\rho_m}{3H^2}\,. \tag{4.68}$$

Notice that although the same dynamical variable x is used, this is defined differently than how it was in Sec. 4.1 for the first model. The evolution of these two variables will be obtained, as before, wrt η. Notice that Ω_m is defined in the same way as it was defined for $f_1(T, T_G)$. This will also be the case for the remaining two models. Thus, in order to obtain the evolution of Ω_m, we can start from Eq. (4.7). To substitute for $\dot{H}$ in this equation, we can use the definition of x in Eq. (4.67) to get,

$$\dot{H} = H^2(T_{G_0}x^2 - 1)\,. \tag{4.69}$$

Substituting and simplifying gives,

$$\Omega_m' = -\Omega_m(1 + 3\omega_m + 2T_{G_0}x^2)\,. \tag{4.70}$$

The evolution of x is obtained using a similar method to that used in Sec. 4.1,

$$x' = \frac{1}{H}\dot{x} \tag{4.71}$$

$$= \frac{1}{2T_{G_0}xH^2}(\ddot{H}H - 2\dot{H}^2)\,. \tag{4.72}$$

We can use the expression for the effective fluid density in Eq. (4.65) to obtain an expression for $\ddot{H}$,

$$\ddot{H} = \frac{1}{P_2H^3(\sqrt{6}+12P_2D)}\left\{\frac{4T_{G_0}^2D^3\kappa^2\rho_{DE}}{\alpha_2H^2e^{-2\sqrt{6}\alpha_2D}} - 2\sqrt{6}P_2H^6 - 2T_{G_0}\dot{H}D\right.$$
$$\left. - 8P_2H^4\dot{H}(\sqrt{6}+6P_2D) - 2H^2[T_{G_0}D + 2P_2\dot{H}^2(\sqrt{6}+6P_2D)]\right\}. \tag{4.73}$$

Using $D = H^2x$ alongside Eqs. (4.69) and the first Friedmann equation, (4.13), the expression for x' simplifies to,

$$x' = \frac{x}{H\alpha_2P_2(\sqrt{6}+12H^2xP_2)}\left\{-\alpha_2[T_{G_0}x + \sqrt{6}H^2(3T_{G_0}x^2-2)P_2\right.$$
$$\left. + 24H^4x(T_{G_0}x^2-1)P_2^2] + 6e^{2\sqrt{6}H^2xP_2}H^2T_{G_0}x(\Omega_m-1)\right\}. \tag{4.74}$$

Finally, the equation,

$$H' = H(T_{G_0}x^2-1)\,, \tag{4.75}$$

completes the dynamical system given by Eqs. (4.74), (4.70) and (4.75) which incorporates the dynamics of the model through the fluid and Friedmann equations. This system is defined on the phase space given by,

$$S = \{(x, H, \Omega_m)|x \in [0,\infty), H \in (0,\infty), \Omega_m \in [0,\infty)\}\,. \tag{4.76}$$

We can, once again, obtain expressions for the observable parameters q, Ω_{DE} and ω_{DE} in order to obtain comparisons between the theoretical predictions and observations,

$$q = -T_{G_0}x^2 \tag{4.77}$$

$$\omega_{DE} = \frac{1+2T_{G_0}x^2+3\omega_m\Omega_m}{3(\Omega_m-1)} \tag{4.78}$$

$$\Omega_{DE} = 1-\Omega_m\,. \tag{4.79}$$

Notice how for this model, the expressions for these observational parameters are independent of the parameters α_2 and P_2 which is in contrast with the equivalent expressions for the first model which had a dependency on P_1. In the case of $f_2(T, T_G)$, the dependency on these parameters will be introduced when solving for the fixed points of the system. As before, dust matter with $\omega_m = 0$ will be assumed for the dynamical analysis.

4.2.1 | Finite Phase Space Analysis

As was done in Sec. 4.1.1, the first step in the analysis of the dynamics of $f_2(T, T_G)$ is to find the fixed points in the finite phase space. In this case, finding these fixed points is not as straightforward as for $f_1(T, T_G)$ and thus the method is discussed in more detail here. Firstly, it follows directly from Eq. (4.70) that $\Omega_m' = 0 \iff \Omega_m = 0$. Moreover, using Eq. (4.75) we see that $H' = 0 \iff H = 0$ or $x = \sqrt{\frac{1}{T_{G_0}}}$. However, $H = 0$ would result in an undefined equation for x' and thus this value is not allowed. Finally, substituting for $x = \sqrt{\frac{1}{T_{G_0}}}$ in the equation for x' and setting $x' = 0$, one obtains the following transcendental equation,

$$6e^{2\sqrt{\frac{6}{T_{G_0}}}H^2P_2}H^2 + \alpha_2 + \sqrt{\frac{6}{T_{G_0}}}H^2\alpha_2 P_2 = 0\,. \tag{4.80}$$

This equation has no analytical solution and thus the only way to find the coordinates of the fixed point of the system is to solve Eq. (4.80) using numerical methods after specifying the values of α_2 and P_2. This was done using the FindRoot method in Mathematica with an appropriate starting point (Wolfram Research, 2003).

In summary, the system has one fixed point at $C_1 = \left(\sqrt{\frac{1}{T_{G_0}}}, H_1, 0\right)$ where the value of H_1 will be explicitly given in the relevant sections. This real fixed point exists for any value of α_2 and P_2. Notice that the stability of this fixed point using the stability matrix cannot be investigated at this stage because of this transcendental equation but will rather be studied for specific values of α_2 and P_2. Nonetheless, it is useful to give the general form of the stability matrix J,

$$J = \begin{pmatrix} J_{11} & J_{12} & \frac{6e^{2\sqrt{6}H^2xP-2}Hx^2}{\sqrt{6}\alpha_2 P_2 + 12H^2x\alpha_2 P_2^2} \\ 2Hx & x^2-1 & 0 \\ -4x\Omega_m & 0 & -1-2x^2\,, \end{pmatrix} \tag{4.81}$$

where,

$$\begin{aligned} J_{11} = {}& \frac{1}{H\alpha_2 P_2(\sqrt{6}+12H^2xP_2)^2}\Big\{-2\alpha_2\big\{-6H^2P_2 + x\big[\sqrt{6} + 3H^2P_2\big(11x \\ & + 4\sqrt{6}H^2(7x^2-1)P_2 + 48H^4x(3x^2-1)P_2^2\big)\big]\big\} + 12e^{2\sqrt{6}H^2xP_2}H^2x(\sqrt{6} \\ & + 12H^2xP_2(1+\sqrt{6}H^2xP_2))(\Omega_m - 1)\Big\} \end{aligned} \tag{4.82}$$

$$\begin{aligned} J_{12} = {}& \frac{x}{H^2\alpha_2 P_2(\sqrt{6}+12H^2xP_2)^2}\Big\{\alpha_2\big\{12H^2P_2 + x\big[\sqrt{6} + 6H^2P_2\big(3x \\ & + 2\sqrt{6}H^2(4-3x^2)P_2 - 48H^4x(x^2-1)P_2^2\big)\big]\big\} + 6e^{2\sqrt{6}H^2xP_2}H^2x\big[\sqrt{6} \end{aligned}$$

$$+12H^2xP_2(1+4\sqrt{6}H^2xP_2)\big](1-\Omega_m)\Big\}. \tag{4.83}$$

J is being defined in this general way since fixing the numerical values of α_2 and P_2 does not significantly simplify the expressions in the matrix as was the case for $f_1(T, T_G)$. The eigenvalues of J evaluated at the fixed point C_1 will then be computed for the specific cases investigated in Sec. 4.2.3.

Reiterating, the values of q and ω_{DE} at any fixed point, and specifically at C_1, are equal to -1. It is also important to note that, as in the case of the first model, for this second model, $q < 0$ in all of the physical phase space, i.e. the modeled universe is always accelerating. At C_1, $\Omega_{DE} = 1 - \Omega_m = 1$. Thus, this fixed point represents a dark-energy dominated, de Sitter universe. To conclude whether such a universe is theoretically possible we will have to investigate the dynamics for specific values of the parameters, as will be done in Sec. 4.2.3.

4.2.2 | Analysis at Infinity

For a complete analysis of the phase space, we need to find fixed points at infinity as was done for the previous model by compactifying the phase space. Once again, this is achieved by using the transformations given in Eqs. (4.22) - (4.24). The region corresponding to the physical phase space is given by,

$$\begin{aligned}&\{(R,\Theta,\Phi): 0 \leq R \leq \frac{1}{2}, 0 < \Theta \leq \frac{\pi}{2}, 0 \leq \Phi \leq \frac{\pi}{2}\} \cup \\ &\left\{(R,\Theta,\Phi): \frac{1}{2} < R < 1, 0 < \Theta \leq \frac{\pi}{2}, 0 \leq \Phi \leq \arccos\left(\frac{1-R}{R}\right)\right\}.\end{aligned} \tag{4.84}$$

The dynamical system defined by Eqs. (4.74), (4.75) and (4.70) becomes,

$$\begin{aligned}R' = (1-R)^2\Bigg\{ &-\frac{R\cos\Phi\big(1+\frac{2R^2\cos^2\Theta\sin^2\Phi}{(1-R)^2}\big)}{1-R} \\ &+\sin\Phi\Bigg[\frac{R\sin^2\Theta\sin\Phi\big(-1+\frac{R^2\cos^2\Theta\sin^2\Phi}{(1-R)^2}\big)}{1-R} + \frac{\cos\Theta\cot\Theta}{\alpha_2 P_2\big(\sqrt{6}+\frac{12R^3P_2\cos\Theta\sin^2\Theta\sin^3\Phi}{(1-R)^3}\big)} \\ &\Bigg(\frac{1}{(1-R)^3}6e^{\frac{2\sqrt{6}R^3P_2\cos\Theta\sin^2\Theta\sin^3\Phi}{(1-R)^3}}R^3\cos\Theta\Big(-1+\frac{R\cos\Phi}{1-R}\Big)\sin^2\Theta\sin^3\Phi \\ &-\alpha_2\Bigg\{\frac{R\cos\Theta\sin\Phi}{1-R} + \frac{24R^5P_2^5\cos\Theta\sin^4\Theta\sin^5\Phi\big(-1+\frac{R^2\cos^2\Theta\sin^2\Phi}{(1-R)^2}\big)}{(1-R)^5} \\ &+\frac{\sqrt{6}R^2P_2\sin^2\Theta\sin^2\Phi\big(-2+\frac{3R^2\cos^2\Theta\sin^2\Phi}{(1-R)^2}\big)}{(1-R)^2}\Bigg\}\Bigg)\Bigg]\Bigg\}\end{aligned} \tag{4.85}$$

$$
\begin{aligned}
\Theta' = \frac{R-1}{R\sin\Phi}\Bigg\{ &- \frac{R\cos\Theta\sin\Theta\sin\Phi\left(\frac{R^2\cos^2\Theta\sin^2\Phi}{(1-R)^2}-1\right)}{1-R} \\
&+ \frac{\cos\Theta}{\alpha_2 P_2\left(\sqrt{6}+\frac{12R^3P_2\cos\Theta\sin^2\Theta\sin^3\Phi}{(1-R)^3}\right)}\Bigg[\frac{1}{(1-R)^3}6e^{\frac{2\sqrt{6}R^3P_2\cos\Theta\sin^2\Theta\sin^3\Phi}{(1-R)^3}}R^3\cos\Theta \\
&\left(\frac{R\cos\Phi}{1-R}-1\right)\sin^2\Theta\sin^3\Phi - \alpha_2\Bigg(\frac{R\cos\Theta\sin\Phi}{1-R} \\
&+ \frac{24R^5P_2^2\cos\Theta\sin^4\Theta\sin^5\Phi\left(\frac{R^2\cos^2\Theta\sin^2\Phi}{(1-R)^2}\right)}{(1-R)^5} \\
&+ \frac{\sqrt{6}R^2P_2\sin^2\Theta\sin^2\Phi\left(\frac{3R^2\cos^2\Theta\sin^2\Phi}{(1-R)^2}-2\right)}{(1-R)^2}\Bigg)\Bigg]\Bigg\}
\end{aligned} \tag{4.86}
$$

$$
\begin{aligned}
\Phi' = \frac{R-1}{R}\Bigg\{ &- \frac{R\cos\Phi\sin\Phi\left(1+\frac{2R^2\cos^2\Theta\sin^2\Phi}{(1-R)^2}\right)}{1-R} \\
&- \cos\Phi\Bigg[\frac{R\sin^2\Theta\sin\Phi\left(\frac{R^2\cos^2\Theta\sin^2\Phi}{(1-R)^2}-1\right)}{1-R} + \frac{\cos\Theta\cot\Theta}{\alpha_2P_2\left(\sqrt{6}+\frac{12R^3P_2\cos\Theta\sin^2\Theta\sin^3\Phi}{(1-R)^3}\right)} \\
&\Bigg(\frac{1}{(1-R)^3}6e^{\frac{2\sqrt{6}R^3P_2\cos\Theta\sin^2\Theta\sin^3\Phi}{(1-R)^3}}R^3\cos\Theta\left(\frac{R\cos\Phi}{1-R}-1\right)\sin^2\Theta\sin^3\Phi \\
&- \alpha_2\Bigg\{\frac{R\cos\Theta\sin\Phi}{1-R} + \frac{24R^5P_2^2\cos\Theta\sin^4\Theta\sin^5\Phi\left(\frac{R^2\cos^2\Theta\sin^2\Phi}{(1-R)^2}-1\right)}{(1-R)^5} \\
&+ \frac{\sqrt{6}R^2P_2\sin^2\Theta\sin^2\Phi\left(\frac{3R^2\cos^2\Theta\sin^2\Phi}{(1-R)^2}-1\right)}{(1-R)^2}\Bigg\}\Bigg)\Bigg]\Bigg\}
\end{aligned} \tag{4.87}
$$

in the (R, Θ, Φ) coordinates.

We can also obtain expressions for q, ω_{DE} and Ω_{DE} in terms of R, Θ and Φ,

$$q = -\frac{T_{G_0}R^2\cos^2\Theta\sin^2\Phi}{(1-R)^2} \tag{4.88}$$

$$\omega_{DE} = -\frac{(R-1)^2+2R^2T_{G_0}\cos^2\Theta\sin^2\Phi}{3(R-1)(R-1+R\cos\Phi)} \tag{4.89}$$

$$\Omega_{DE} = 1+\frac{R\cos\Phi}{R-1}\,. \tag{4.90}$$

Since the behaviour at infinity occurs at $R \to 1^-$, the leading terms of Eqs. (4.85)-(4.87) are required. For $P_2 > 0$ these are,

$$R' \to \frac{6e^{\frac{2\sqrt{6}P_2\cos\Theta\sin^2\Theta\sin^3\Phi}{(1-R)^3}}\cos^3\Theta\cos\Phi\sin\Theta\sin^4\Phi}{(1-R)^2\alpha_2P_2\left(\sqrt{6}+\frac{12P_2\cos\Theta\sin^2\Theta\sin^3\Phi}{(1-R)^3}\right)} \tag{4.91}$$

$$\Theta' \to -\frac{6e^{\frac{2\sqrt{6}P_2\cos\Theta\sin^2\Theta\sin^3\Phi}{(1-R)^3}}\cos^2\Theta\cos\Phi\sin^2\Theta\sin^2\Phi}{(1-R)^3\alpha_2 P_2\left(\sqrt{6}+\frac{12P_2\cos\Theta\sin^2\Theta\sin^3\Phi}{(1-R)^3}\right)} \tag{4.92}$$

$$\Phi' \to -\frac{6e^{\frac{2\sqrt{6}P_2\cos\Theta\sin^2\Theta\sin^3\Phi}{(1-R)^3}}\cos^3\Theta\cos^2\Phi\sin\Theta\sin^3\Phi}{(1-R)^2\alpha_2 P_2\left(\sqrt{6}+\frac{12P_2\cos\Theta\sin^2\Theta\sin^3\Phi}{(1-R)^3}\right)}. \tag{4.93}$$

Thus, for this range of values of P_2, there are four lines of fixed points at infinity; Q_1 at $\Theta = 0$, Q_2 at $\Phi = 0$, Q_3 at $\Theta = \frac{\pi}{2}$ and Q_4 at $\Phi = \frac{\pi}{2}$, which were found by setting $\Theta' = 0 = \Phi'$. Evaluating $\frac{d\Theta'}{d\Theta}$ and $\frac{d\Phi'}{d\Phi}$ at these fixed points always results in both derivatives being equal to zero. This means that the stability of the fixed points at infinity cannot be studied using the method introduced in Sec. 3.3.3. Instead, the stability will be investigated directly using the phase portraits for specific values of α_2 and P_2 in Sec. 4.2.3. The values of q, ω_{DE} and Ω_{DE} will also be calculated in Sec. 4.2.3 for any particular fixed points at infinity of interest.

If, on the other hand $P_2 < 0$, the exponential term does not dominate but rather the leading terms of Eqs. (4.85)-(4.87) become,

$$R' \to \frac{24P_2\cos^5\Theta\sin^3\Theta\sin^8\Phi}{(R-1)^2(\sqrt{6}(R-1)^3-6P_2\sin\Theta\sin(2\Theta)\sin^3\Phi)} \tag{4.94}$$

$$\Theta' \to \frac{24P_2\cos^4\Theta\sin^4\Theta\sin^6\Phi}{(R-1)^3(\sqrt{6}(R-1)^3-6P_2\sin\Theta\sin(2\Theta)\sin^3\Phi)} \tag{4.95}$$

$$\Phi' \to -\frac{24P_2\cos^5\Theta\cos\Phi\sin^3\Theta\sin^7\Phi}{(R-1)^3(\sqrt{6}(R-1)^3-6P_2\sin\Theta\sin(2\Theta)\sin^3\Phi)}. \tag{4.96}$$

In this case, the fixed points at infinity occur at the lines $\Theta = 0$, $\Phi = \frac{\pi}{2}$ and $\Theta = \frac{\pi}{2}$ which will be labelled Q_1, Q_2 and Q_3, respectively. Once again, at these lines of fixed points $\frac{d\Theta'}{d\Theta}$ and $\frac{d\Phi'}{d\Phi}$ are equal to zero and so their stability can only be inferred from investigation of the global phase portrait.

4.2.3 | Cosmological Implications

The cosmological implications of this dynamical analysis will be investigated in the same way as was done in Sec. 4.1.3, namely, the phase portraits of two specific sets of parameter values will be studied, and their cosmological implications interpreted. The choice of values for α_2 and P_2 was done in a way which produced different qualitative dynamics. In what follows the value of T_{G_0} was set to one in all cases as previously mentioned.

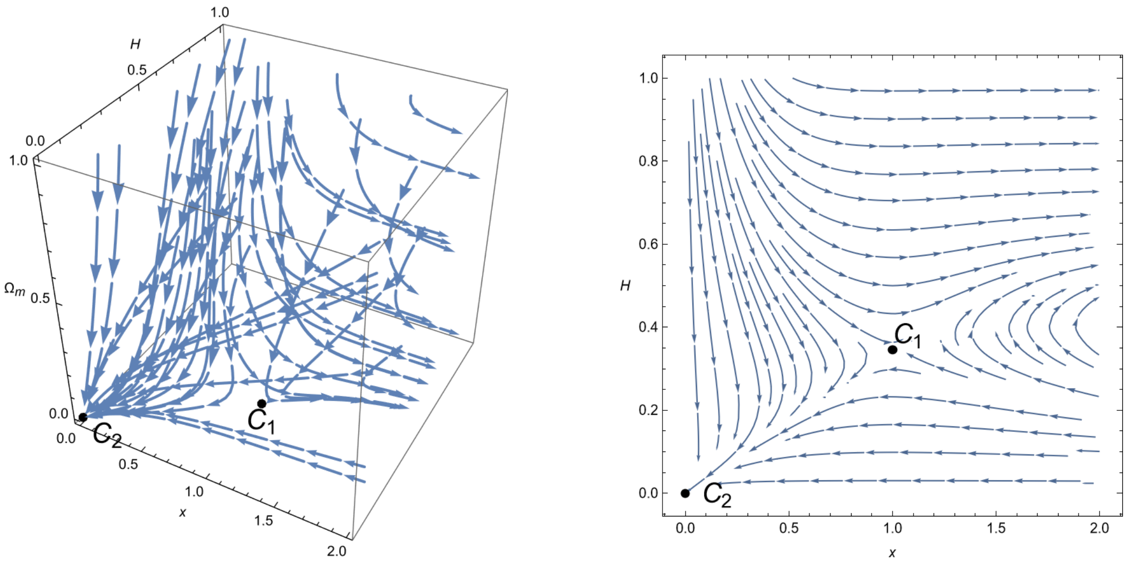

(a) Full 3D phase portrait. (b) 2D phase portrait in the plane $\Omega_m = 0$.

Figure 4.8: Trajectories in the phase space for the $f_2(T, T_G)$ cosmological scenario defined by Eqs. (4.74), (4.75) and (4.70) with parameters $\alpha_2 = -1, P_2 = 1$. The point $C_1 = (1, H_1, 0)$ is a saddle while the origin at C_2 seems to be behaving like a stable fixed point.

4.2.3.1 | Case 1: $\alpha_2 = -1$ & $P_2 = 1$

We begin the analysis for the case $\alpha_2 = -1$ and $P_2 = 1$ by numerically computing the value of H_1 at the fixed point C_1. This is found to be $H_1 = 0.346196$, although it is the existence of a fixed point with a non-zero value of H which is important rather than the exact numerical value of H_1. Next, by plugging in the values of α_2 and P_2 in the stability matrix given in Eq. (4.81), we can compute its eigenvalues at C_1. These are found to be $\{-3, -2.86, 1.83\}$. Since this set of eigenvalues consists of both positive and negative values, C_1 is a saddle, attracting trajectories along particular directions and repelling them along others. As discussed in the general analysis, at C_1, $q = \omega_{DE} = -1$ and $\Omega_{DE} = 1$ and so this point represents a de Sitter universe.

The phase portrait can be seen in Fig. 4.8 and the saddle nature of C_1 can indeed be confirmed. Note that from these phase portraits, it is evident that the point $(0, 0, 0)$, labelled as C_2 in the figures, is behaving like a stable fixed point even though this lies outside of the phase space S, as defined in Eq. (4.76), and leads to an undefined expression for x' (Eq. (4.74)). Thus, we will ignore the trajectories tending towards C_2 and focus our attention on the trajectories above the fixed point C_1 which seem to be tending towards infinity. Consequently, in order for the phase space analysis to be complete, we need to also investigate the behaviour at infinity to check whether there are any stable fixed points.

The global phase portrait in the (R, Θ, Φ) coordinates can be seen in Fig. 4.9. The dynamics of the finite phase portrait in Fig. 4.8 are clearly reflected in this coordinate system, with C_1 acting like a saddle and C_2, which is now mapped to the plane $R = 0$, acting like a stable fixed point. The infinite fixed point $(1, 0, 0)$ is behaving like an unstable fixed point while $(1, 0, \frac{\pi}{2})$ seems to be a saddle, as can be seen in Fig. 4.9b, although this cannot be confirmed analytically. Since these points both correspond to $H = 0$, q and ω_{DE} are undefined. The global dynamics of the model can now be inferred; since C_2 is the only point behaving like an attractor, any trajectory falls into one of the following scenarios;

- The trajectory eventually tends towards the point C_2 which has $H = 0$ and so lies outside of the phase space of the dynamical system. Moreover, the value $H = 0$ is disconnected from the allowed boundary conditions, as has been previously discussed.

- The trajectory oscillates between the saddles C_1 and the infinite fixed point $(1, 0, \frac{\pi}{2})$. This means that the value of the Hubble parameter does not tend towards a fixed value, but rather keeps oscillating.

The latter scenario should be confirmed in future studies by employing analytical techniques to ensure that there are indeed trajectories that do not eventually tend towards the origin. However, from this preliminary investigation it is evident from Fig. 4.9 that most trajectories do tend towards $H = 0$, and so although this choice of parameters can describe the current Universe, it does not have a lot of potential at explaining its asymptotic behaviour.

4.2.3.2 | Case 2: $\alpha_2 = -1$ & $P_2 = -\frac{1}{10}$

A desired modeled universe resulting from these cosmological models is one which is asymptotically de Sitter, as this matches the prediction from ΛCDM. This scenario can be achieved using this second model by setting $\alpha_2 = -1$ and $P_2 = -\frac{1}{10}$ as will be investigated in this section.

Numerically solving Eq. (4.80) for this choice of parameters, gives a value of $H_1 = 0.42$ at the fixed point C_1. Evaluating the eigenvalues of the stability matrix in Eq. (4.81) at this fixed point C_1 gives $\{-0.63 \pm 6.24i, -2\}$. Thus C_1 is a stable focus as can be observed in Fig. 4.10. At this point, $q = \omega_{DE} = -1$ and $\Omega_{DE} = 1$, and so, as before, this point represents a de Sitter universe. In this case, all trajectories are eventually tending

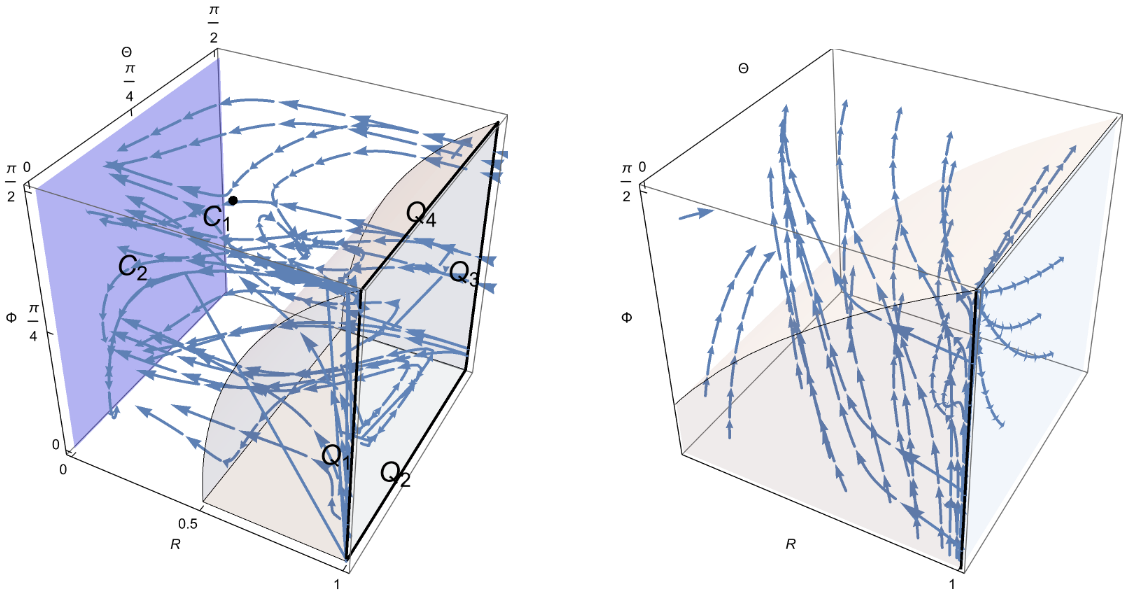

(a) (b)

Figure 4.9: Global phase portrait for $f_2(T, T_G)$ with parameters $\alpha_1 = -1, P_2 = 1$ in the (R, Θ, Φ) coordinates. The four lines of fixed points at infinity as defined in Sec. 4.2.2 are labelled. Fig.4.9b shows the trajectories around $(1, 0, \frac{\pi}{2})$ in more detail.

towards this cosmology irrespective of the initial conditions. For this reason, it is not expected for there to be any stable fixed points at infinity. This is confirmed by the global phase portrait in Fig. 4.11.

All trajectories seem to be originating from the line Q_3 of fixed points at infinity. Apart from the endpoints, $q = \omega_{DE} = -\infty$, while the values of x, H and Ω_m are infinite along this line. This shows that trajectories are originating from a past singularity. Another fixed point at infinity of particular importance is $(1, 0, \frac{\pi}{2})$ which seems to be acting like a saddle. $H = 0$, while q and ω_{DE} are undefined at this point, and thus this point can never be realised by our physical Universe.

In conclusion, this choice of parameters warrants a more in-detail analysis due to its potential to explain an asymptotically de Sitter universe.

4.3 | Model 3: $f_3(T, T_G) = -T + \alpha_3(T^2 + P_3 T_G)^{\beta_3}$

The third model to be analysed is the generalisation to the model analysed in Kofinas et al. (2014). As was previously discussed in Sec. 3.2, setting $\beta_3 = \frac{1}{2}$ would give the exact model which was studied in that work. Since this is the only $f(T, T_G)$ model that has been studied in detail using dynamical systems, it will be interesting to see whether

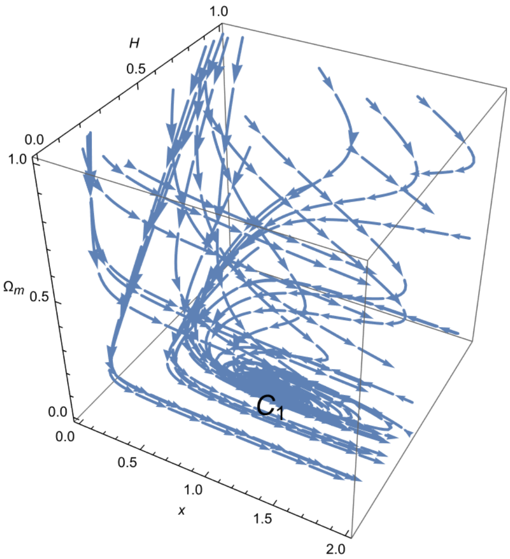

(a) Full 3D phase portrait in the (x, H, Ω_m) space.

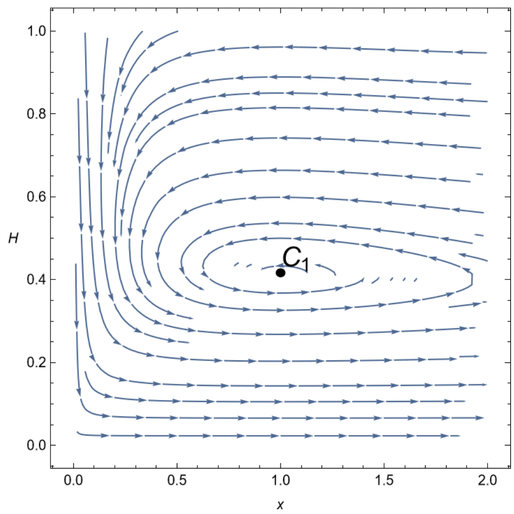

(b) 2D phase portrait in the plane $\Omega_m = 0$.

Figure 4.10: Trajectories in the phase space for the $f_2(T, T_G)$ cosmological scenario defined by Eqs. (4.74), (4.75) and (4.70) with parameters $\alpha_2 = -1, P_2 = -\frac{1}{10}$. The fixed point $C_1 = (1, H_1, 0)$ is a stable focus.

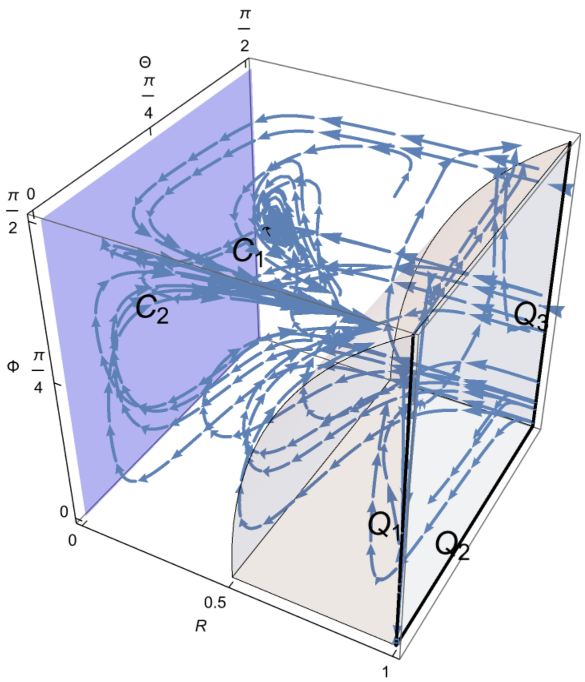

Figure 4.11: Global phase portrait for $f_2(T, T_G)$ with parameters $\alpha_2 = -1, P_2 = -\frac{1}{10}$ in the (R, Θ, Φ) coordinates. The three lines of fixed points at infinity as defined in Sec. 4.2.2 are labelled.

different, and potentially more interesting, dynamics arise from different values of β_3, or whether the specific case which was already analysed gives the best results.

As for the other models, the dynamics of the modeled universe are given by the Friedmann equations in Eqs. (3.41) and (3.42), with the dark-energy effective fluid density and pressure taking on the following form,

$$\kappa^2\rho_{DE} = \frac{\alpha_3}{2}\left(12H^2D\right)^{\beta_3}\Bigg\{-1+\frac{2\beta_3}{D^2}\Big[(6+P_3)(3+2P_3)H^4 \\ +P_3(27+P_3(12-8\beta_3)-12\beta_3)H^2\dot{H}+2P_3^2(3-2\beta_3)\dot{H}^2-2P_3^2(\beta_3-1)H\ddot{H}\Big]\Bigg\} \tag{4.97}$$

$$\kappa^2 p_{DE} = \frac{\alpha_3}{6}\left(12H^2D\right)^{\beta_3}\Bigg\{3+\frac{2\beta_3}{H^2D^3}\Big[-3(6+P_3)(3+2P_3)^2H^8+(3+P_3)\big(18-93P_3 \\ -34P_3^2+8(P_3-3)(3+2P_3)\beta_3\big)H^6\dot{H}+8P_3^3(\beta_3-1)(2\beta_3-1)\dot{H}^4 \\ +12P_3^2(3+2P_3)(\beta_3-1)H^5\ddot{H}+8P_3^2(\beta_3-1)(-6-P_3+6\beta_3+4P_3\beta_3)H^3\dot{H}\ddot{H} \\ +16P_3^3(\beta_3-1)\beta_3H\dot{H}^2\ddot{H}+2P_3H^4[2(-9(-3+P_3+P_3^2)-(3+2P_3)(39+8P_3)\beta_3 \\ +4(3+2P_3)^2\beta_3^2)\dot{H}^2+P_3(3+2P_3)(\beta_3-1)\dddot{H}]+4P_3^2H^2[(3-P_3-9(5+2P_3)\beta_3 \\ +8(3+2P_3)\beta_3^2)\dot{H}^3+P_3(\beta_3-2)(\beta_3-1)\ddot{H}^2+P_3(\beta_3-1)\dot{H}\dddot{H}]\Big]\Bigg\}, \tag{4.98}$$

where we are defining $D = 3H^2 + 2P_3(\dot{H} + H^2)$. Notice that in this case, these equations are significantly more complex than those describing ρ_{DE} and p_{DE} for the previous two models. This was to be expected since by adding a third parameter β_3, an extra degree of freedom is introduced.

Alongside Ω_m as defined for the previous two models, see for example Eq. (4.68), we define the following unitless variable to perform the dynamical analysis,

$$x = \left(\frac{D}{3H^2}\right)^{\beta_3} \\ = \left[1+\frac{2P_3}{3}\left(1+\frac{\dot{H}}{H^2}\right)\right]^{\beta_3}. \tag{4.99}$$

Rearranging Eq. (4.99) gives an equation for $\dot{H}$ in terms of x which will be useful when deriving the dynamical system,

$$\dot{H} = H^2\left[\frac{3}{2P_3}\left(x^{\frac{1}{\beta_3}}-1\right)-1\right]. \tag{4.100}$$

Substituting Eq. (4.100) into Eq. (4.7), gives the evolution of Ω_m in accordance with the fluid equation,

$$\Omega_m' = \Omega_m \left[-1 - 3\omega_m - \frac{3}{P_3}\left(x^{\frac{1}{\beta_3}} - 1 \right) \right] . \tag{4.101}$$

The evolution of x is obtained using the usual method. First differentiating Eq. (4.99),

$$x' = \frac{2P_3\beta_3}{3H^4}\left(\frac{D}{3H^2} \right)^{\beta_3 - 1} \left(H\ddot{H} - 2\dot{H}^2 \right) . \tag{4.102}$$

Rearranging Eq. (4.97) to obtain an equation for $\ddot{H}$ gives,

$$\begin{aligned} H\ddot{H} = \frac{1}{-2P_3^2(\beta_3 - 1)} \Bigg\{ & \frac{D^2}{2\beta_3}\left[\frac{2\kappa^2 \rho_{DE}}{\alpha_3 (12DH^2)^{\beta_3}} + 1 \right] - (6 + P_3)(3 + 2P_3)H^4 \\ & - P_3(27 + P_3(12 - 8\beta_3) - 12\beta_3)H^2\dot{H} - 2P_3^2(3 - 2\beta_3)\dot{H}^2 \Bigg\} . \end{aligned} \tag{4.103}$$

Substituting this into Eq. (4.102) and performing the usual simplifications gives,

$$x' = \frac{1}{2P_3}\left\{ x\left[x^{\frac{1}{\beta_3}}(3 - 12\beta_3) + \left(12 + 8P_3 + \frac{9}{\beta_3 - 1} \right)\beta_3 \right] + \frac{18H^{2-4\beta_3}x^{\frac{1}{\beta_3}}(\Omega_m - 1)}{36^{\beta_3}\alpha_3(\beta_3 - 1)} \right\} , \tag{4.104}$$

in which the first Friedmann equation is incorporated. The equation which completes the dynamical system is that for H' which follows directly from Eq. (4.100),

$$H' = H\left[\frac{3}{2P_3}\left(x^{\frac{1}{\beta_3}} - 1 \right) - 1 \right] . \tag{4.105}$$

Notice how for the specific case of $\beta_3 = \frac{1}{2}$, H is completely eliminated from Eq. (4.104) and thus the dynamical system can be reduced to a 2D one with Eq. (4.105) not being needed. Since the dynamical system for this particular value of β_3 is different, it will be discussed separately in Sec. 4.3.4.

We will limit our investigation to the phase space,

$$S = \{ (x, H, \Omega_m) | x \in [0, \infty), H \in [0, \infty), \Omega_m \in [0, \infty) \} . \tag{4.106}$$

Notice that however, H needs to be restricted to the range $(0, \infty)$ for values of $\beta_3 > \frac{1}{2}$. The observables q and ω_{DE} are given by,

$$q = -\frac{3}{2P_3}\left(x^{\frac{1}{\beta_3}} - 1 \right) \tag{4.107}$$

$$\omega_{DE} = \frac{3 - 3x^{\frac{1}{\beta_3}} - P_3 - 3P_3\omega_m\Omega_m}{3P_3(1 - \Omega_m)} . \tag{4.108}$$

Notice that when P_3 and β_3 are both negative or both positive, $q < 0$ for $x > 1$, whereas when P_3 and β_3 have different signs, $q < 0$ for $x < 1$. This means that the model can describe a universe transitioning from a deceleration phase to an acceleration phase, which has so far not been possible with the other theoretical models, and as will be seen in Sec. 4.4, will not be possible for $f_4(T, T_G)$ either. Dust matter with $\omega_m = 0$ will be assumed for the remainder of the analysis.

4.3.1 | Finite Phase Space Analysis

We start the analysis by investigating the finite fixed points of the system. By setting Eqs. (4.104), (4.105) and (4.101) equal to 0, we find that there are three fixed points of the system for $\beta_3 < \frac{1}{2}$ at $C_1 = (0,0,0)$, $C_2 = (x_2, 0, 0)$ and $C_3 = (x_3, H_3, 0)$ where,

$$x_2 = \left[\frac{\left(12 + 8P_3 + \frac{9}{\beta_3 - 1}\right)\beta_3}{12\beta_3 - 3}\right]^{\beta_3} \tag{4.109}$$

$$H_3 = \left\{\frac{\alpha_3(\beta_3 - 1)}{6^{1-2\beta_3}(3 + 2P_3)}\left[\left(1 + \frac{2P_3}{3}\right)^{\beta_3}\left((3 + 2P_3)(1 - 4\beta_3)\right.\right.\right.$$
$$\left.\left.\left. + \left(12 + 8P_3 + \frac{9}{\beta_3 - 1}\right)\beta_3\right)\right]\right\}^{\frac{1}{2-4\beta_3}} \tag{4.110}$$

$$x_3 = \left[\frac{2P_3}{3} + 1\right]^{\beta_3}. \tag{4.111}$$

In the case that $\beta_3 > \frac{1}{2}$, only the point C_3 is in the phase space of the system. Notice that these fixed points do not exist for all values of α_3, β_3 and P_3. It is straightforward to see that C_2 does not exist for $\beta_3 = \frac{1}{4}$. The existence conditions of x_2 depend on the value of β_3, for example, for $\beta_3 = \frac{1}{2n}$ where $n \in \mathbb{N}$, one must ensure that the term enclosed in the square bracket in Eq. (4.109) is positive to give a real value of x_2. This happens for $P_3 > \frac{3-6n}{-8+4n}$. The existence of C_3 also depends on the values of the parameters in a similar way however it is not straightforward to give the general existence conditions in this case. Since C_3 is the only fixed point of the system with a non-zero value of H in line with the allowed boundary conditions, for any combination of the parameters, it was first ensured that C_3 does indeed exist, i.e. that the x and H coordinates at this fixed point are real.

One can calculate the stability matrix J at this stage, evaluate it at the fixed points, find the eigenvalues and deduce the stability conditions. However, this would lead to complicated expressions since the system has three free parameters. Thus, this process will be done explicitly for the different parameter values investigated in Sec. 4.3.3.

Since at C_1 and C_2, $H = 0$, q and ω_{DE} are undefined. At the point C_3, $q = \omega_{DE} = -1$ while $\Omega_{DE} = 1$ meaning that this fixed point represents a de Sitter solution.

4.3.2 | Analysis at Infinity

We perform the analysis at infinity using the usual coordinate transformation defined in Eqs. (4.22) - (4.24). We find that the dynamical system in the (R, Θ, Φ) coordinates becomes,

$$\begin{aligned} R' =& \frac{(R-1)R\sin^2\Theta\sin^2\Phi\left(3+2P_3-4\left(\frac{R\cos\Theta\sin\Phi}{1-R}\right)^{\frac{1}{\beta_3}}\right)}{2P_3} \\ &+ \frac{(R-1)R\cos^2\Phi\left(-3+P_3+3\left(\frac{R\cos\Theta\sin\Phi}{1-R}\right)^{\frac{1}{\beta_3}}\right)}{P_3} + \frac{(R-1)^2\cos\Theta\sin\Phi}{2P_3} \\ &\left\{\frac{18\left(\frac{R\cos\Phi}{1-R}-1\right)\left(\frac{R\cos\Theta\sin\Phi}{1-R}\right)^{\frac{1}{\beta_3}}\left(\frac{R\sin\Theta\sin\Phi}{1-R}\right)^{2-4\beta_3}}{36^{\beta_3}\alpha_3(\beta_3-1)}\right. \\ &\left.+\frac{R\cos\Theta\sin\Phi}{1-R}\left[\left(12+8P_3+\frac{9}{\beta_3-1}\right)\beta_3+(3-12\beta_3)\left(\frac{R\cos\Theta\sin\Phi}{1-R}\right)^{\frac{1}{\beta_3}}\right]\right\} \end{aligned} \tag{4.112}$$

$$\begin{aligned} \Theta' =& \frac{R-1}{R\sin\Phi}\left\{\frac{R\cos\Theta\sin\Theta\sin\Phi\left(-3-2P_3+3\left(\frac{R\cos\Theta\sin\Phi}{1-R}\right)^{\frac{1}{\beta_3}}\right)}{2P_3(R-1)}\right. \\ &+\frac{\sin\Theta}{2P_3}\left[\frac{18\left(\frac{R\cos\Phi}{1-R}-1\right)\left(\frac{R\cos\Theta\sin\Phi}{1-R}\right)^{\frac{1}{\beta_3}}\left(\frac{R\sin\Theta\sin\Phi}{1-R}\right)^{2-4\beta_3}}{36^{\beta_3}\alpha_3(\beta_3-1)}\right. \\ &\left.\left.+\frac{R\cos\Theta\sin\Phi}{1-R}\left\{\left(12+8P_3+\frac{9}{\beta_3-1}\right)\beta_3+(3-12\beta_3)\left(\frac{R\cos\Theta\sin\Phi}{1-R}\right)^{\frac{1}{\beta_3}}\right\}\right]\right\} \end{aligned} \tag{4.113}$$

$$\begin{aligned} \Phi' =& \frac{R-1}{R}\left\{\frac{R\cos\Phi\sin\Phi\left(-3+P_3+3\left(\frac{R\cos\Theta\sin\Phi}{1-R}\right)^{\frac{1}{\beta_3}}\right)}{P_3(R-1)}\right. \\ &-\cos\Phi\left[\frac{R\sin^2\Theta\sin\Phi\left(3+2P_3-3\left(\frac{R\cos\Theta\sin\Phi}{1-R}\right)^{\frac{1}{\beta_3}}\right)}{2P_3(R-1)}\right. \\ &+\frac{\cos\Theta}{2P_3}\left\{\frac{18\left(\frac{R\cos\Phi}{1-R}-1\right)\left(\frac{R\cos\Theta\sin\Phi}{1-R}\right)^{\frac{1}{\beta_3}}\left(\frac{R\sin\Theta\sin\Phi}{1-R}\right)^{2-4\beta_3}}{36^{\beta_3}\alpha_3(\beta_3-1)}\right. \\ &\left.\left.\left.+\frac{R\cos\Theta\sin\Phi}{1-R}\left[\left(12+8P_3+\frac{9}{\beta_3-1}\right)\beta_3+(3-12\beta_3)\left(\frac{R\cos\Theta\sin\Phi}{1-R}\right)^{\frac{1}{\beta_3}}\right]\right\}\right]\right\} \end{aligned} \tag{4.114}$$

The leading terms of these expressions depend explicitly on the value of β_3 and thus, in order to simplify matters, they will be given in Sec. 4.3.3 for specific parameter values of α_3, β_3 and P_3. This means that the fixed points at infinity will also have to be evaluated at this later stage.

In this coordinate system, the deceleration and equation-of-state parameters are given by,

$$q = -\frac{3}{2P_3}\left[-1 + \left(\frac{R\cos\Theta\sin\Phi}{1-R}\right)^{\frac{1}{\beta_3}}\right] \tag{4.115}$$

$$\omega_{DE} = -\frac{P_3}{3(R-1)}\left[-1 + R(1+\cos\Phi)\right]\left[-3 + P_3 + 3\left(\frac{R\cos\Theta\sin\Phi}{1-R}\right)^{\frac{1}{\beta_3}}\right], \tag{4.116}$$

while Ω_{DE} is as given in Eq. (4.90). These expressions will be used to calculate the values of these observable parameters at any interesting fixed points at infinity.

4.3.3 | Cosmological Implications

We now investigate two different cosmological scenarios that can result from $f_3(T, T_G)$ by fixing specific values of the free parameters in the model. The two parameter choices given here will both result in an asymptotically de Sitter universe in line with observations. The model can also produce cosmologies with less meaningful cosmological interpretations, for example trajectories tending towards the origin, however these specific cases were omitted here.

4.3.3.1 | Case 1: $\alpha_3 = -1$, $P_3 = 1$ & $\beta_3 = \frac{1}{3}$

We can obtain an asymptotically de Sitter universe transitioning from a deceleration phase to an acceleration phase by setting $\alpha_3 = -1$, $P_3 = 1$ and $\beta_3 = \frac{1}{3}$. The stability matrix in this case becomes,

$$J = \begin{pmatrix} \frac{-3x^4 + x\left(\frac{13}{6} - x^3\right) + \frac{27(3H^2)^{\frac{1}{3}}x^3(\Omega_m - 1)}{2^{\frac{2}{3}}}}{2x} & \frac{3^{\frac{4}{3}}x^3(\Omega_m - 1)}{(4H)^{\frac{1}{3}}} & \frac{3^{\frac{7}{3}}H^{\frac{2}{3}}x^3}{2^{\frac{5}{4}}} \\ \frac{9Hx^2}{2} & -1 + \frac{3}{2}(x^3 - 1) & 0 \\ -9x^2\Omega_m & 0 & 2 - 3x^2 \end{pmatrix}. \tag{4.117}$$

Notice that the matrix is not well-defined at the fixed points C_1 and C_2 since $H = 0$, and thus the stability of these fixed points cannot be studied analytically. From the phase portraits in Fig. 4.12, we can infer that these points behave like saddles. Evaluating the eigenvalues of J at C_3 gives the set $\{-3, -2.5, -0.5\}$, meaning that C_3 is a stable fixed point.

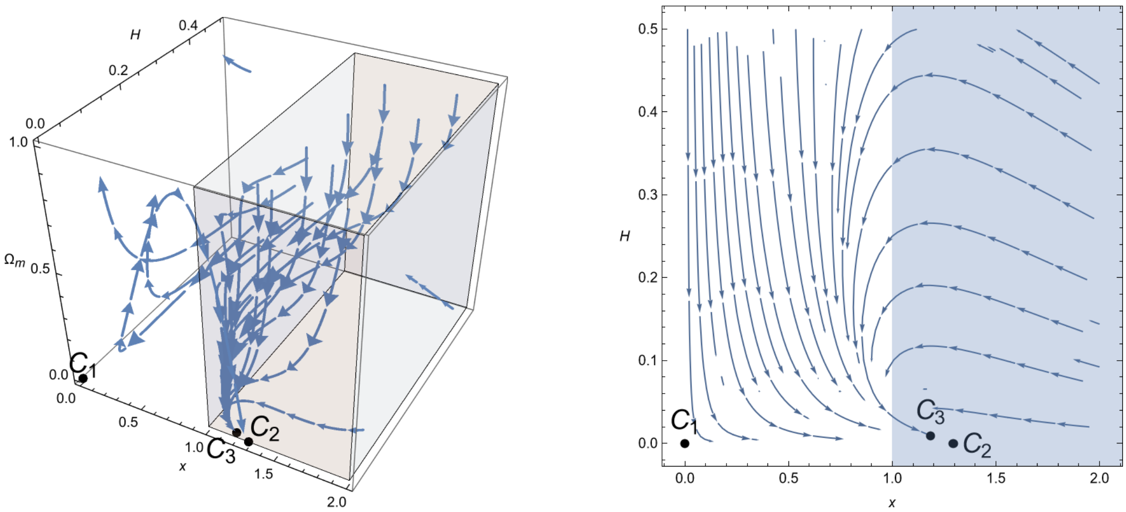

(a) Full 3D phase portrait. (b) 2D phase portrait in the plane $\Omega_m = 0$.

Figure 4.12: Trajectories in the phase space for the $f_3(T, T_G)$ cosmological scenario defined by Eqs. (4.104), (4.105) and (4.101) with parameters $\alpha_3 = -1, P_3 = 1, \beta_3 = \frac{1}{3}$. The fixed point $C_3 = (x_3, H_3, 0)$ is an attractor of the system and represents a de Sitter universe while C_1 and C_2 are saddles. The shaded region represents the section of the phase space in which $q < 0$, i.e. the universe is accelerating.

From Fig. 4.12 we can see that most trajectories start from an accelerating universe, enter a deceleration phase, then tend towards C_3 which represents an accelerating de Sitter solution. Notice also how for all trajectories, Ω_m is decreasing from one to zero, in agreement with observations. For certain trajectories this is not happening monotonically, meaning that the density of matter in the universe is fluctuating before tending towards zero.

At this stage, having fixed the values of the parameters, it is possible to calculate the leading terms of Eqs. (4.112) - (4.114) as,

$$R' \to \frac{3^{\frac{7}{3}} \cos^4\Theta \cos\Phi \sin^4\Theta (\sin\Theta \sin\Phi)^{\frac{2}{3}}}{2^{\frac{5}{3}}(1-R)^{\frac{8}{3}}} \tag{4.118}$$

$$\Theta' \to -\frac{3^{\frac{7}{3}} \cos^3\Theta \cos\Phi \sin\Theta \sin^2\Phi (\sin\Theta \sin\Phi)^{\frac{2}{3}}}{2^{\frac{5}{3}}(1-R)^{\frac{11}{3}}} \tag{4.119}$$

$$\Phi' \to \frac{3^{\frac{7}{3}} \cos^4\Theta \cos^2\Phi \sin^3\Phi (\sin\Theta \sin\Phi)^{\frac{2}{3}}}{2^{\frac{5}{3}}(1-R)^{\frac{11}{3}}}\,. \tag{4.120}$$

Thus, there are four lines of fixed points at infinity; Q_1 at $\Theta = 0$, Q_2 at $\Phi = 0$, Q_3 at $\Theta = \frac{\pi}{2}$ and Q_4 at $\Phi = \frac{\pi}{2}$. Notice that at these lines of fixed points $\frac{d\Theta'}{d\Theta} = \frac{d\Phi'}{d\Phi} = 0$ and so the stability of these fixed points cannot be studied analytically.

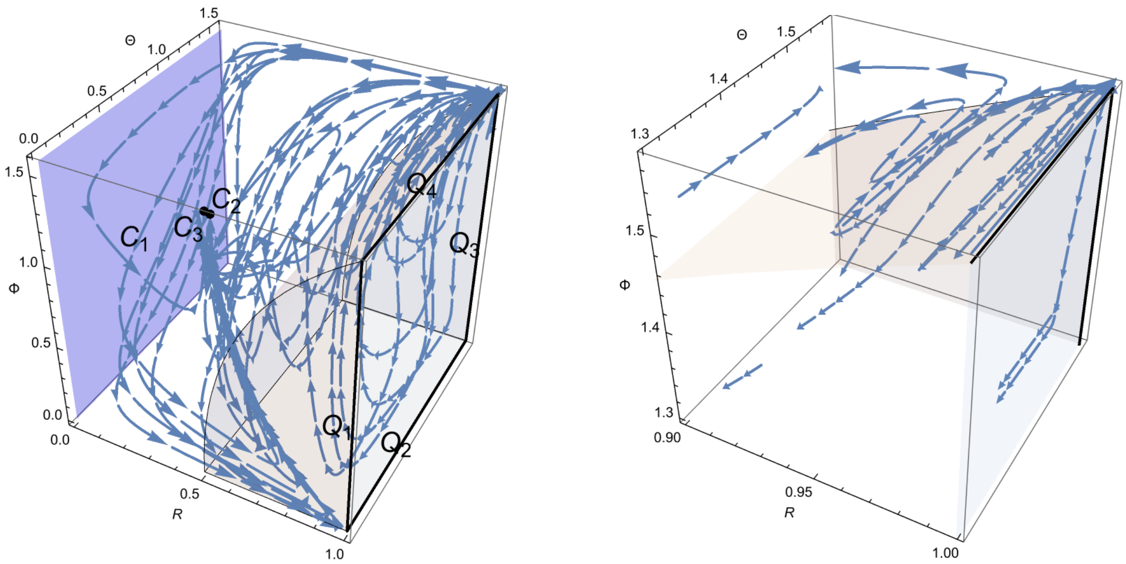

(a) (b)

Figure 4.13: Global phase portrait for $f_3(T, T_G)$ with parameters $\alpha_3 = -1, P_3 = 1, \beta_3 = \frac{1}{3}$ in the (R, Θ, Φ) coordinates. There are four lines of fixed points at infinity, shown by Q_1 - Q_4. Fig. 4.13b shows the saddle nature of $(1, \frac{\pi}{2}, \frac{\pi}{2})$ in more detail.

The global phase portrait in the (R, Θ, Φ) coordinates can be seen in Fig. 4.13. Trajectories all seem to be originating from a past singularity, i.e. from the shaded region, before tending towards C_3. At infinity, there are two fixed points of particular importance, at $(1, 0, 0)$ and at $(1, \frac{\pi}{2}, \frac{\pi}{2})$. Both of these are behaving as saddles. At the first fixed point, q and ω_{DE} are undefined since $H = 0$. At the second fixed point, $q = \frac{3}{2}$, $\omega_{DE} = \frac{2}{3}$ and $\Omega_{DE} = 1$. These parameters indicate a decelerating universe, although at $(1, \frac{\pi}{2}, \frac{\pi}{2})$, $H = \infty$, which makes the interpretation unclear. Since $(1, 0, 0)$ and $(1, \frac{\pi}{2}, \frac{\pi}{2})$ are saddles, they do not influence the type of cosmology that this model represents; a universe going from a deceleration phase to an acceleration phase, which is asymptotically de Sitter.

4.3.3.2 | Case 2: $\alpha_3 = 1$, $P_3 = 2$ & $\beta_3 = \frac{2}{3}$

The second case that will be briefly studied will be for the parameter choice $\alpha_3 = 1$, $P_3 = 2$ and $\beta_3 = \frac{2}{3}$. According to the analysis in Sec. 4.3.1, the only finite fixed point of the system is at the point C_3. Evaluating the stability matrix,

$$J = \begin{pmatrix} \frac{-\frac{15}{2}x^{\frac{5}{2}} + x\left(\frac{2}{3} - 5x^{\frac{3}{2}}\right) - \frac{3^{\frac{8}{3}} x^{\frac{3}{2}} (\Omega_m - 1)}{2^{\frac{4}{3}} H^{\frac{2}{3}}}}{4x} & \frac{3^{\frac{2}{3}} x^{\frac{3}{2}} (\Omega_m - 1)}{2^{\frac{4}{3}} H^{\frac{5}{3}}} & -\frac{3^{\frac{5}{3}} x^{\frac{3}{2}}}{2^{\frac{7}{3}} H^{\frac{2}{3}}} \\ \frac{9H\sqrt{x}}{8} & -1 + \frac{3}{4}(x^{\frac{3}{2}} - 1) & 0 \\ \frac{9\sqrt{x}\Omega_m}{4} & 0 & \frac{1}{2}\left(1 - 3x^{\frac{3}{2}}\right) \end{pmatrix}, \tag{4.121}$$

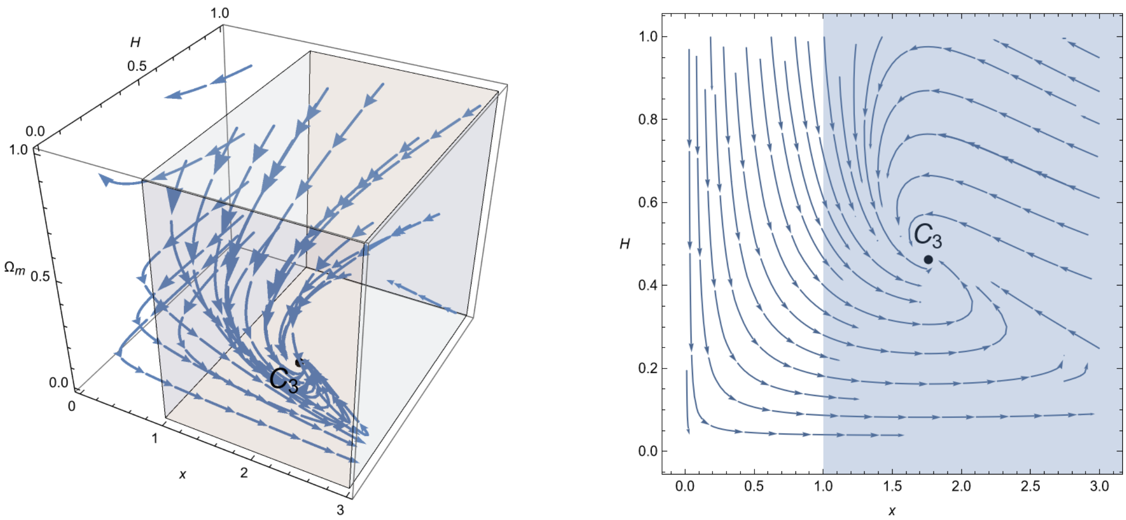

(a) Full 3D phase portrait in the (x, H, Ω_m) space.

(b) 2D phase portrait in the plane $\Omega_m = 0$.

Figure 4.14: Trajectories in the phase space for the $f_3(T, T_G)$ cosmological scenario defined by Eqs. (4.104), (4.105) and (4.101) with parameters $\alpha_3 = 1, P_3 = 2, \beta_3 = \frac{2}{3}$. The fixed point $C_3 = (x_3, H_3, 0)$ is a stable focus and represents a de Sitter universe. Notice how for all trajectories Ω_m is decreasing from 1 to 0, in agreement with observations. The shaded region represents the section of the phase space in which $q < 0$, i.e. the universe is accelerating.

at this fixed point and finding the eigenvalues, gives the set $\{-3, -1.5 + 1.6i, -1.5 - 1.6i\}$ meaning that this fixed point is a stable focus. This behaviour is indeed observed in the phase portrait as can be seen in Fig. 4.14. From these figures we can see that certain trajectories are passing through the region $x < 1$, representing a decelerating universe, before tending towards the stable fixed point, which represents an accelerating universe.

The leading terms of Eqs. (4.112), (4.113) and (4.114) for this choice of parameters become,

$$R' \to \frac{\cos\Theta\sin\Phi}{4(1-R)^{\frac{1}{2}}}\left[-2(\cos\Theta\sin\Phi)^{\frac{5}{2}} + 3(\cos\Theta\sin\Phi)^{\frac{1}{2}}(-2\cos^2\Phi + \sin^2\Theta\sin^2\Phi)\right] \tag{4.122}$$

$$\Theta' \to \frac{\sin\Theta(\cos\Theta\sin\Phi)^{\frac{5}{2}}}{4(1-R)^{\frac{3}{2}}}(3 - 5\csc\Phi) \tag{4.123}$$

$$\Phi' \to \frac{\cos\Phi\sin\Phi}{8}\left(\frac{\cos\Theta\sin\Phi}{1-R}\right)^{\frac{3}{2}}\left(-3(3+\cos 2\Theta) - 10\cos^2\Theta\right) . \tag{4.124}$$

As a consequence, at infinity there is a line of fixed points $Q_1 = (1, \frac{\pi}{2}, \Phi)$, where $\Phi \in [0, \frac{\pi}{2}]$, alongside the fixed point $Q_2 = (1, 0, \frac{\pi}{2})$. For the line of fixed points Q_1, $\frac{d\Theta'}{d\Theta} =$

$\frac{d\Phi'}{d\Phi} = 0$ meaning their stability cannot be found analytically. Using Eqs. (4.115) and (4.116), we find that $q = \frac{3}{4}$ and $\omega_{DE} = -\infty$ for $\Phi \neq \frac{\pi}{2}$. These values do not seem to be consistent and thus this fixed point would require further investigation to understand its cosmological implications. On the other hand, at Q_2, $R' = -\frac{5}{4}$, $\frac{d\Theta'}{d\Theta} = -\frac{1}{2}$ and $\frac{d\Phi'}{d\Phi} = \frac{25}{8}$, so this point is a saddle. $H = 0$ at Q_2 and so q and ω_{DE} are undefined, with this point being disconnected from the allowed initial conditions.

Although it was attempted, the global phase portrait for this choice of parameters could not be generated using Mathematica. This could be due to numerical instability and warrants a further investigation in future works. However, since C_3 is a global attractor, it is not expected that there will be any stable fixed points representing future singularities at infinity and as for the case in Sec. 4.3.3.1, from the finite phase space we can conclude that this choice of parameters can lead to an asymptotically de Sitter universe, going from a deceleration to an acceleration phase.

4.3.4 | Model 3 Variation

For $\beta_3 = \frac{1}{2}$, the dynamical system reduces to a two-dimensional one in terms of x and Ω_m only. In this case, the model becomes $f_3(T, T_G) = -T + \alpha_3\sqrt{T^2 + P_3 T_G}$ which is the exact model that was investigated using dynamical systems in Kofinas et al. (2014). The dynamical system in this case reduces to,

$$x' = -\frac{x\left[3\alpha_3 x^2 - 6(1-\Omega_m)x + \alpha_3(3-4P_3)\right]}{2\alpha_3 P_3} \tag{4.125}$$

$$\Omega_m' = -\frac{\Omega_m(3x^2 + P_3 + 3P_3\omega_m - 3)}{P_3}\,. \tag{4.126}$$

These equations were obtained by setting $\beta_3 = \frac{1}{2}$ in Eqs. (4.104) and (4.101) respectively.

The analysis in Kofinas et al. (2014) was repeated and all the results were in agreement with those in this paper. It was noted that this model can produce various cosmological scenarios, specifically ones in which the universe results in a dark-energy dominated universe which is accelerating. The equation of state parameter can also lie within the quintessence regime, be equal to the cosmological constant value -1, or lie in the phantom regime. This model can also result in a dark energy - dark matter scaling solution, something not seen in the other models. Future singularities, such as the Big Rip, can also be theoretically predicted by this model.

4.4 | Model 4: $f_4(T, T_G) = -T + \alpha_4 \ln \frac{P_4 T_G}{T}$

As was the case for the $f_3(T, T_G)$ modification studied in Sec. 4.3.4, the model that will be investigated in this section has no ΛCDM limit. Thus, it is of particular interest as it avoids confirmation bias with the standard cosmological model. Furthermore, if dynamics which agree with observations can arise from this model, it is an indication that a gravitational theory significantly different from GR could indeed be the correct description of Nature.

Notice that special care is required when fixing the value of P_4 in order for the model to be well-defined. If the range of P_4 is restricted to the positive real line, then it will always be the case that $\frac{P_4 T_G}{T} > 0$ as will be explicitly shown further on. Thus, for the remainder of this section, a positive value of P_4 will be assumed.

As usual, the dynamics of this model are governed by the Friedmann equations in Eqs. (3.41) and (3.42), with the effective fluid density and pressure of dark energy given by,

$$\kappa^2 \rho_{DE} = -\frac{\alpha_4}{2(H^2+\dot{H})^2}\left\{H^4(1+D) + 2H^2\dot{H}(D-1) + \dot{H}^2(D-1) - H\ddot{H}\right\} \tag{4.127}$$

$$\begin{aligned}\kappa^2 p_{DE} = \frac{\alpha_4}{6(H^2+\dot{H})^3}&\Big\{3H^6(1+D) + H^4\dot{H}(9D-1) + \dot{H}^3(3D-1) - 6H^3\ddot{H} \\ &+ 2H\dot{H}\ddot{H} + 2\ddot{H}^2 + H^2((3+9D)\dot{H}^2 - \dddot{H}) - \dot{H}\dddot{H}\Big\},\end{aligned} \tag{4.128}$$

where we are defining,

$$D = \ln\left[4P_4(H^2+\dot{H})\right]. \tag{4.129}$$

For this model, we introduce the auxiliary dynamical variables given by,

$$\begin{aligned} x &= D - 2\ln H \\ &= \ln\left[4P_4\left(1+\frac{\dot{H}}{H^2}\right)\right] \end{aligned} \tag{4.130}$$

$$\Omega_m = \frac{\kappa^2 \rho_m}{3H^2}. \tag{4.131}$$

As for the previous models, the dynamics of the model are obtained wrt η. In order to derive the dynamical system we first obtain an expression for $\dot{H}$ in terms of H and x by rearranging Eq. (4.130),

$$\dot{H} = H^2\left(\frac{e^x}{4P_4} - 1\right). \tag{4.132}$$

Note that using this equation and the expressions for T and T_G in Eqs. (3.37) and (3.38), we can see that,

$$\begin{aligned}\frac{T_G}{T} &= 4(\dot{H}+H^2)\\ &= \frac{H^2 e^x}{P_4} > 0\,,\end{aligned} \tag{4.133}$$

for $P_4 > 0$, thus justifying the restriction of P_4 to positive values only.

Substituting Eq. (4.132) into Eq. (4.7) and simplifying gives the evolution of Ω_m wrt η,

$$\Omega_m' = -\Omega_m\left(1+3\omega_m+\frac{e^x}{2P_4}\right)\,, \tag{4.134}$$

which incorporates the dynamics dictated by the Friedmann equation. Next we obtain an expression for the evolution of x,

$$\begin{aligned}x' &= \frac{1}{H}\dot{x}\\ &= \frac{1}{H^4+H^2\dot{H}}(\ddot{H}H-2\dot{H}^2)\,.\end{aligned} \tag{4.135}$$

Rearranging Eq. (4.127) to obtain an expression for $\ddot{H}$ gives,

$$H\ddot{H} = \frac{2\kappa^2\rho_{DE}(H^2+\dot{H})^2}{\alpha_4} + H^4(1+D) + 2H^2\dot{H}(D-1) + \dot{H}^2(D-1)\,. \tag{4.136}$$

Substituting Eq. (4.136) into Eq. (4.135), and using $D = x + 2\ln H$, $\rho_{DE} = \frac{3H^2}{\kappa^2}(1-\Omega_m)$, and Eq. (4.132), gives,

$$x' = 4 + \frac{e^x\left[\alpha_4(x-3) - 6H^2(\Omega_m-1) + 2\alpha_4\ln H\right]}{4\alpha_4 P_4}\,. \tag{4.137}$$

The final equation which completes the dynamical system is that for the evolution of H wrt η,

$$H' = H\left(\frac{e^x}{4P_4}-1\right)\,. \tag{4.138}$$

The dynamical system defined in Eqs. (4.137), (4.138) and (4.134) is defined on the phase space S, given by,

$$S = \{(x,H,\Omega_m)|x\in(-\infty,\infty), H\in(0,\infty), \Omega_m\in[0,\infty)\}\,. \tag{4.139}$$

Notice how in this case, the range of x is not limited to the positive real line, however since x is an arbitrary variable simply used for the dynamical analysis, this does not have any physical implications related to it. In this section we will limit our investigation to $x \in [0,\infty)$. This is because if we consider the full real line as the domain of x, the usual transformation to the (R, Θ, Φ) space will no longer be adequate to study the behaviour at infinity. Since as mentioned, negative values of x have no special physical significance, introducing another method for studying this behaviour at infinity can be justifiably avoided.

Finally, the specific form of the important observable parameters is,

$$q = -\frac{e^x}{4P_4} \tag{4.140}$$

$$\omega_{DE} = \frac{e^x + 2P_4 + 6P_4\omega_m\Omega_m}{6P_4(\Omega_m - 1)}. \tag{4.141}$$

These were obtained using the same method as described in detail for $f_1(T, T_G)$ in Sec. 4.1. As for the other cases, from this point onward, dust matter will be assumed and thus, ω_m will be set to zero.

4.4.1 | Finite Phase Space Analysis

We will initiate the analysis for this model by first finding the finite fixed points of the system and studying their stability using the linear stability method. Starting with $H' = 0$, this immediately implies that at the fixed points, $x = \ln(4P_4)$ since $H = 0$ is not allowed. Substituting this value of x into Eq. (4.134) and setting $\Omega_m' = 0$ gives $\Omega_m = 0$. Finally, substituting $x = \ln(4P_4)$ and $\Omega_m = 0$ into Eq. (4.137) and setting $x' = 0$ results in the following transcendental equation,

$$2\alpha_4 \ln H - 6H^2 = -\alpha_4(1 + \ln 4P_4) \tag{4.142}$$

This case is similar to the transcendental equation in Eq. (4.80) encountered for the $f_2(T, T_G)$ model. As in this previous case the system only has one fixed point within the phase space at $C_1 = (\ln(4P_4), H_1, 0)$ which exists for any value of $P_4 > 0$. The value of H_1 can only be found by solving Eq. (4.142) numerically after fixing the values of the parameters α_4 and P_4. Note that the x-coordinate of this fixed point is negative for values of P_4 within the range $0 < P_4 < \frac{1}{4}$ so values of P_4 within this range will not be considered.

The values of q and ω_{DE} at the fixed point C_1 are both equal to -1 meaning that this point will always represent a de Sitter universe regardless of the values of the parameters. Moreover, $q < 0$ in all of the phase space so the model represents an accelerating universe at all points.

The general form of the stability matrix is,

$$J = \begin{pmatrix} \frac{e^x\left[(x-2)\alpha_4 - 6H^2(\Omega_m - 1) + 2\alpha_4 \ln H\right]}{4\alpha_4 P_4} & \frac{e^x\left[\alpha_4 - 6H^2(\Omega_m - 1)\right]}{2H\alpha_4 P_4} & -\frac{3e^x H^2}{2\alpha_4 P_4} \\ \frac{e^x H}{4P_4} & \frac{e^x}{4P_4} - 1 & 0 \\ -\frac{e^x \Omega_m}{2P_4} & 0 & -1 - \frac{e^x}{2P_4} \end{pmatrix} \tag{4.143}$$

Notice that, even in this general form, the stability matrix for this model is significantly simpler than the corresponding matrices for the previous models with two free parameters; see for example Eq. (4.81). This is a result of the simple expressions in the dynamical system given by Eqs. (4.137), (4.138) and (4.134). This is an advantage of $f_4(T, T_G)$ over the previous models, provided that the dynamics it produces are in-line with observations, since simpler models are always preferred over more complicated ones if the results are comparable to each other. Nevertheless, it might be the case that choosing different dynamical variables for the previous models would have resulted in simpler dynamical systems and so further investigation would be required to conclude that this model is indeed more elegant than the others.

The eigenvalues of the matrix J at the fixed point C_1 will be computed in the following sections for fixed values of α_4 and P_4. This is due to the fact that a general expression for H_1 cannot be obtained at this point.

4.4.2 | Analysis at Infinity

Analysis at infinity by transformation to the (R, Θ, Φ) coordinates through Eqs. (4.22) - (4.24) was also performed for this model. Obtaining the equations for R', Θ' and Φ' using the same method as for the previous models gives,

$$\begin{aligned} R' = (1-R)^2 \Bigg\{ & -\frac{R\left(1+\exp\left(\frac{R\cos\Theta\sin\Phi}{2P_4}\right)\right)\cos^2\Phi}{1-R} \\ & + \sin\Phi \left[\frac{R\left(\frac{\exp\left(\frac{R\cos\Theta\sin\Phi}{1-R}\right)}{4P_4} - 1\right)\sin^2\Theta\sin\Phi}{1-R} + \frac{\cos\Theta}{4P_4}\left(16P_4 + \exp\left(\frac{R\cos\Theta\sin\Phi}{1-R}\right)\right.\right. \\ & \left[2\ln\left[\frac{R\sin\Theta\sin\Phi}{1-R}\right] - 3\right] + \frac{\exp\left(\frac{R\cos\Theta\sin\Phi}{1-R}\right)R\sin\Phi}{\alpha_4(R-1)^3}\Big\{ -\alpha_4(R-1)^2\cos\Theta \\ & \left.\left. + 6R(-1+R(1+\cos\Phi))\sin^2\Theta\sin\Phi\Big\}\right)\right]\Bigg\} \end{aligned} \tag{4.144}$$

$$\Theta' = \frac{R-1}{R\sin\Phi}\Bigg\{ -\frac{R\left(\frac{\exp\left(\frac{R\cos\Theta\sin\Phi}{1-R}\right)}{4P_4}\right)\cos\Theta\sin\Theta\sin\Phi}{1-R} + \frac{\sin\Theta}{4P_4}\Big[16P_4$$

$$+\exp\left(\frac{R\cos\Theta\sin\Phi}{1-R}\right)\left(2\ln\left[\frac{R\sin\Theta\sin\Phi}{1-R}\right]-3\right)+\frac{\exp\left(\frac{R\cos\Theta\sin\Phi}{1-R}\right)R\sin\Phi}{\alpha_4(R-1)^3}$$
$$\left(-(R-1)^2\alpha_4\cos\Theta+6R(-1+R(1+\cos\Phi))\sin^2\Theta\sin\Phi\right)\Bigg]\Bigg\} \tag{4.145}$$

$$\Phi'=\frac{R-1}{R}\Bigg\{-\frac{R\left(1+\frac{\exp\left(\frac{R\cos\Theta\sin\Phi}{1-R}\right)}{2P_4}\right)\cos\Phi\sin\Phi}{1-R}$$
$$-\cos\Phi\left[\frac{R\left(\frac{\exp\left(\frac{R\cos\Theta\sin\Phi}{1-R}\right)}{4P_4}-1\right)\sin^2\Theta\sin\Phi}{1-R}+\frac{\cos\Theta}{4P_4}\left(16P_4+\exp\left(\frac{R\cos\Theta\sin\Phi}{1-R}\right)\right.\right.$$
$$\left(2\ln\left[\frac{R\sin\Theta\sin\Phi}{1-R}\right]-3\right)+\frac{\exp\left(\frac{R\cos\Theta\sin\Phi}{1-R}\right)R\sin\Phi}{(R-1)^3\alpha_4}\left[-(R-1)^2\alpha_4\cos\Theta\right.$$
$$\left.\left.\left.+6R(-1+R(1+\cos\Phi))\sin^2\Theta\sin\Phi\right]\right)\right]\Bigg\}. \tag{4.146}$$

The expressions for q, ω_{DE} and Ω_{DE} in this coordinate system become,

$$q=-\frac{\exp\left(\frac{R\cos\Theta\sin\Phi}{1-R}\right)}{4P_4} \tag{4.147}$$
$$\omega_{DE}=-\frac{\left(\exp\left(\frac{R\cos\Theta\sin\Phi}{1-R}\right)+2P_4\right)(R-1)}{6P_4(-1+R(1+\cos\Phi))} \tag{4.148}$$
$$\Omega_{DE}=1+\frac{R\cos\Phi}{R-1}. \tag{4.149}$$

In order to find the fixed points at infinity and analyse their stability, the leading terms in Eqs. (4.144) - (4.146) are required. These are the exponential terms multiplied by the largest power of $(1-R)$ in the denominator, i.e.,

$$R'\to\frac{3\exp\left(\frac{\cos\Theta\sin\Phi}{1-R}\right)\cos\Theta\cos\Phi\sin^2\Theta\sin^3\Phi}{2(R-1)\alpha_4P_4} \tag{4.150}$$
$$\Theta'\to\frac{\exp\left(\frac{\cos\Theta\sin\Phi}{1-R}\right)\sin\Theta\left(\alpha_4\cos\Theta+3\cos\Phi\sin^2\Theta\sin\Phi\right)}{2(R-1)^2\alpha_4P_4} \tag{4.151}$$
$$\Phi'\to-\frac{3\exp\left(\frac{\cos\Theta\sin\Phi}{1-R}\right)\cos\Theta\cos^2\Phi\sin^2\Theta\sin^2\Phi}{2(R-1)^2\alpha_4P_4}. \tag{4.152}$$

Setting $\Theta'=0=\Phi'$ to find the fixed points at infinity shows that the line $\Theta=0$ is a line of fixed points which will be labelled as Q_1. The other fixed points at infinity are located at $Q_2=\left(1,\frac{\pi}{2},0\right)$ and $Q_3=\left(1,\frac{\pi}{2},\frac{\pi}{2}\right)$. Calculating $\frac{d\Theta'}{d\Theta}$ and $\frac{d\Phi'}{d\Phi}$, and evaluating at these fixed points separately using Mathematica shows that at every infinite fixed point, these derivatives are equal to zero. This means that, as in most previous cases, the stability of such infinite fixed points cannot be studied analytically but can only be investigated using the phase portraits in each specific case. Likewise, the values of q, ω_{DE} and Ω_{DE} using Eqs. (4.147) - (4.149) will be calculated for specific fixed points of interest in the following sections.

4.4.3 | Cosmological Implications

A range of different cosmological scenarios can be achieved using this theoretical model. This includes cases in which the modelled universe is tending towards a de Sitter universe, in agreement with observations. This is of significant importance as the model does not have a ΛCDM limit but can still theoretically represent physical solutions. In this section, two cases arising from different parameter values will be investigated in detail.

4.4.3.1 | Case 1: $\alpha_4 = -1$ & $P_4 = 10$

We start the analysis with $\alpha_4 = -1$ and $P_4 = 10$ since these parameter values lead to a modelled universe tending towards a de Sitter solution. Solving Eq. (4.142) numerically for these parameter values gives a value of H_1 at the fixed point of 0.854. The set of eigenvalues of the stability matrix J in Eq. (4.143) evaluated at the fixed point C_1 is $\{-3, -1.5 \pm 2.12i\}$. Since all eigenvalues have a negative real part, this means that C_1 is a stable focus. Indeed, this behaviour can be seen in the phase portrait in Fig. 4.15. Since at this point $q = \omega_{DE} = -1$, C_1 represents a de Sitter solution.

C_1 seems to be a global attractor (with the exception of a small number of trajectories which seem to be tending towards the origin), and thus, no stable fixed points at infinity are to be expected. This is confirmed by the global phase portrait in the (R, Θ, Φ) coordinate system as can be seen in Fig. 4.16. From this phase portrait we can see that as opposed to all previous cases that have been investigated, not all the trajectories are originating from a singularity. Moreover, the only fixed point at infinity which seems to be of particular importance is Q_3 which is behaving like a saddle. At this point, which corresponds to an infinite H, we find that $q = -\frac{1}{40}$, $\omega_{DE} = -\frac{7}{20}$ and $\Omega_{DE} = 1$. These are interesting results as from the value of ω_{DE} we could conclude that this point represents a universe with quintessence-like dark energy, however, the infinite value of H hints that this point could represent some form of singularity. This means that for certain initial conditions, this model could describe a universe which tends towards a singularity and then evolves towards a de Sitter universe. Further investigation using techniques beyond dynamical systems would be required to understand the exact cosmological scenario that Q_3 represents.

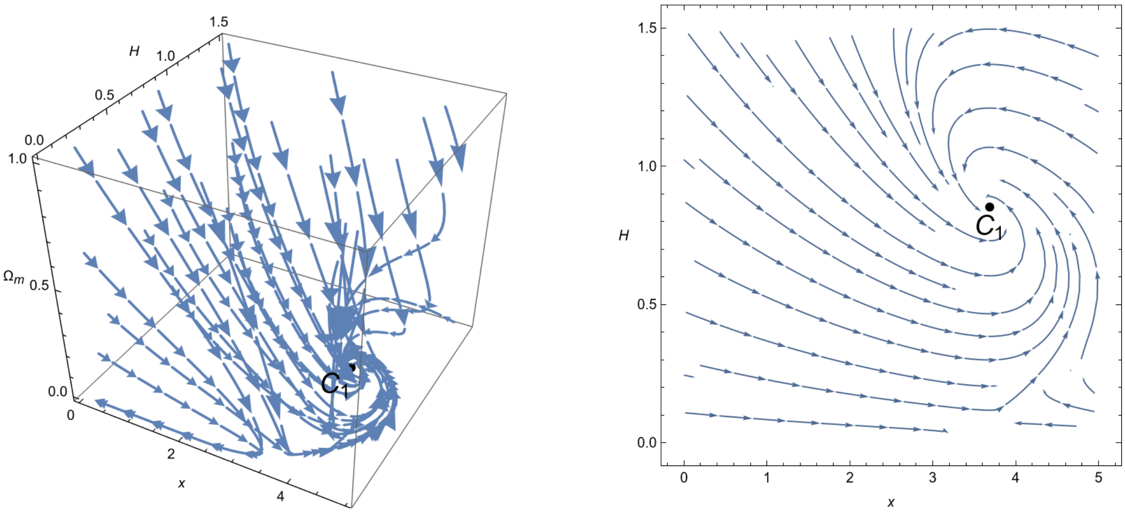

(a) Full 3D phase portrait in the (x, H, Ω_m) space.

(b) 2D phase portrait in the plane $\Omega_m = 0$.

Figure 4.15: Trajectories in the phase space for the $f_4(T, T_G)$ cosmological scenario defined by Eqs. (4.137), (4.138) and (4.134) with parameters $\alpha_4 = -1, P_4 = 10$. The fixed point $C_1 = (1, H_1, 0)$ is an attractor of the system and represents a de Sitter universe. Notice how for all trajectories Ω_m is decreasing from one to zero, in agreement with observations. There seems to be another fixed point behaving like a saddle at roughly $(3.5, 0, 0)$. This fixed point was not seen from the analytical analysis since, $H = 0$ is not within the physical phase space of the system.

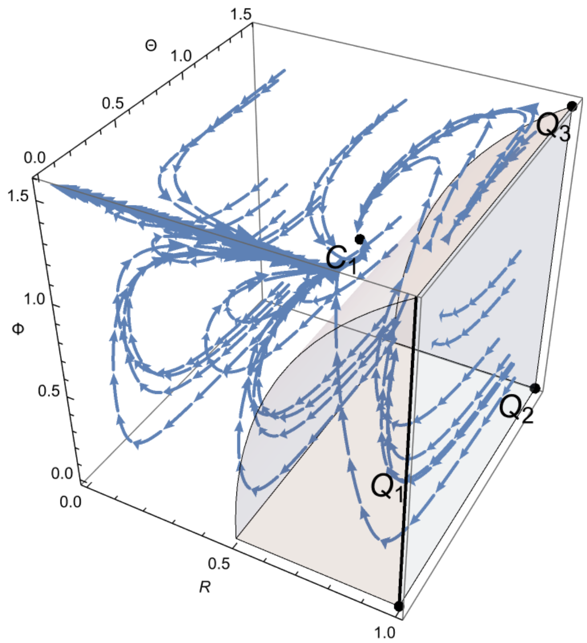

Figure 4.16: Global phase portrait for $f_4(T, T_G)$ with parameters $\alpha_4 = -1, P_4 = 10$ in the (R, Θ, Φ) coordinates.

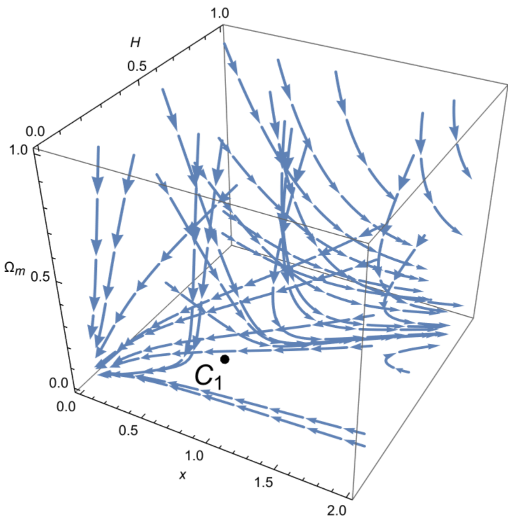

(a) Full 3D phase portrait in the (x, H, Ω_m) space.

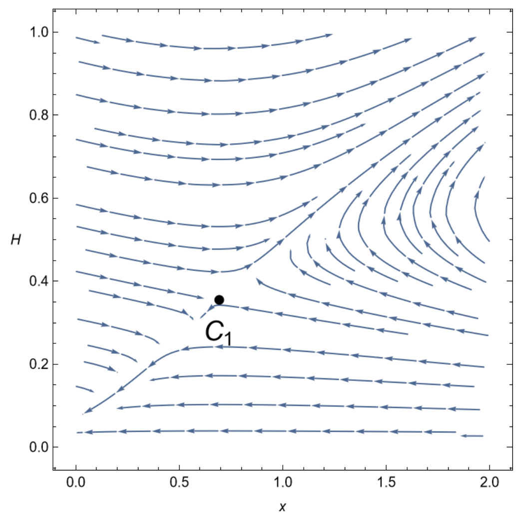

(b) 2D phase portrait in the plane $\Omega_m = 0$.

Figure 4.17: Trajectories in the phase space for the $f_4(T, T_G)$ cosmological scenario defined by Eqs. (4.137), (4.138) and (4.134) with parameters $\alpha_4 = 2, P_4 = \frac{1}{2}$. The fixed point $C_1 = (1, H_1, 0)$, which represents a de Sitter universe, is a saddle. Notice how for all trajectories Ω_m is decreasing from 1 to 0, in agreement with observations.

4.4.3.2 | Case 2: $\alpha_4 = 2$ & $P_4 = \frac{1}{2}$

Although other values of α_4 and P_4 also lead to a stable fixed point representing a de Sitter universe, we present here a different dynamical scenario by setting $\alpha_4 = 2$ and $P_4 = \frac{1}{2}$. The numerical value of H at the fixed point C_1 was found to be 0.355. The set of eigenvalues of J evaluated at this point is $\{-3.74, -3., 0.74\}$ and so the fixed point C_1 is a saddle. This behaviour can be clearly seen in the phase portrait in Fig. 4.17. The values of q and ω_{DE} are both -1 at C_1 meaning that this point represents a dark-energy-dominated de Sitter universe.

Since there are no stable fixed points in the finite phase space, studying the global phase portrait in the (R, Θ, Φ) coordinates is especially important in this case. This can be seen in Fig. 4.18. The global phase portrait shows that the fixed point at infinity $(1, 0, 0)$ is a source. At this point $x = H = 0$ while $\Omega_m = \infty$. Further analysis would need to be done to determine whether this could represent a physical singularity or whether this point is simply an algebraic singularity. For this model, the end-points of the trajectories depends on the initial conditions since there is no stable fixed point in all of the global phase space. Notice for example, how some trajectories lead to a future singularity while others do not.

In summary, this parameter choice leads to a universe potentially originating from

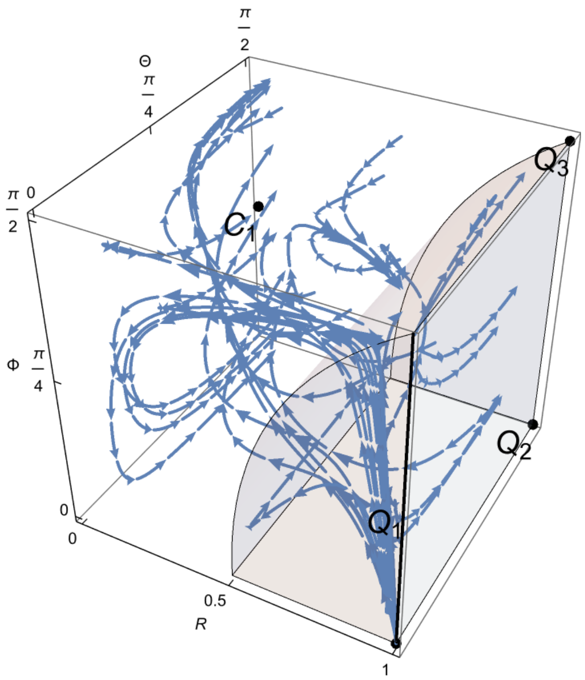

Figure 4.18: Global phase portrait for $f_4(T, T_G)$ with parameters $\alpha_4 = 2, P_4 = \frac{1}{2}$ in the (R, Θ, Φ) coordinates. The only significant fixed point at infinity is at $(1, 0, 0)$ and is a source.

a past singularity and then tending towards a de Sitter universe before moving away from it. The model needs to be constrained with initial conditions for the future of the modelled universe to be studied.

4.5 | Summary

In this chapter, the dynamical behaviour of four $f(T, T_G)$ models was analysed in a qualitative way. This was done through the use of a dynamical systems approach which exposed the dynamics of this modification on purely theoretical grounds. It was seen that all the models can result in an asymptotically de Sitter universe in which dark energy dominates, without the need to introduce a cosmological constant. That is, these models have the potential of explaining late-times acceleration by modifying the gravitational theory underpinning the dynamics of the Universe, rather than modifying the energy content, as is done in the ΛCDM model.

Apart from the asymptotically de Sitter universe, the models were found to have the potential at describing other interesting cosmologies, with each model having certain unique features which were not seen in the other models. $f_1(T, T_G)$ resulted in an asymptotically de Sitter universe for various parameter choices. Moreover, when studying its behaviour at infinity, it was seen that the model can also potentially result in a future singularity, in particular a Big Rip, where the rate of expansion of the universe becomes infinite. The dynamical system was reduced to a two-dimensional one for $P_1 = \frac{1}{2}$, and in this case a dark-energy dominated universe with phantom-like or quintessence-like behaviour could also be modelled. $f_2(T, T_G)$ showed the same potential in modelling an asymptotically de Sitter universe. Through the analysis at infinity, this model also showed the potential of producing a universe which does not tend towards having a fixed value of H, although further analysis would need to be done to confirm this. The defining feature of $f_3(T, T_G)$ is its ability to model a universe transitioning between a decelerating and an accelerating one. This was not observed with the other models where in these cases, all trajectories represented an accelerating universe in all of the phase space. A modification of $f_3(T, T_G)$ can simplify the dynamical system needed to study this model, which allows for solutions such as a phantom or quintessence dark energy dominated universe. This was also the case for $f_1(T, T_G)$. Finally, $f_4(T, T_G)$ showed that even models without a ΛCDM limit could lead to dynamics which are like those of a universe with a cosmological constant, indicating that a significant deviation from the standard ΛCDM model might be needed in order to theoretically explain the features of the observed Universe.

The dynamical analysis done in this chapter shows that the $f(T, T_G)$ modification does indeed have the potential of being the correct description of gravity on cosmological scales. Since all of the models analysed exhibit dynamics in line with those of the observed Universe, none of them can be ruled out at this stage. This means that further investigations, as will be discussed in Chapter 5, are needed to identify which $f(T, T_G)$ modification fits observations best.

5

Conclusions

In this work the dynamical behaviour of the $f(T, T_G)$ modification of TEGR was studied in the context of a flat FLRW Universe. This modification is based on the torsion scalar T which is the Lagrangian of the TEGR action, as well as the T_G invariant which is quartic in the torsion tensor. This class of modifications is analogous to the $f(\mathring{R}, \mathring{G})$ modification of GR, however, since the equations of motion are intrinsically different, these two theories lead to different dynamics. The $f(T, T_G)$ modification is an extension of the $f(T)$ modification, with the introduction of the T_G invariant making it possible to produce different dynamics from the latter lower order theory.

In particular, four $f(T, T_G)$ models, which had not yet been studied in the literature, were analysed. These were inspired by different modifications of TEGR including the $f(T)$ and $f(T, B)$ modifications. The study was done by incorporating the Friedmann equations, dictating the dynamics of a universe governed by this theory of gravity, and the fluid equation, into a set of differential equations. The general behaviour of these dynamical systems was then studied using techniques from LST which uncovered the behaviour in the finite phase space of the systems without having to impose any initial conditions. Moreover, the behaviour in the infinite regime was studied using a change of variables which compactified the phase space. Using this method, behaviour which is hidden in the finite phase space, such as past/future singularities, could be uncovered.

This work was motivated by the discovery of the accelerating Universe and the growing tension between values of H_0 using early-time and late-time measurements, among other problems with the ΛCDM model. The aim of the work was to explain this acceleration via a modification of the theory of gravity itself, which dictates the evolution of the Universe. This is opposed to modifying the energy content of the Universe which is what is done in the ΛCDM model based on GR, in which a cosmological constant is used to represent dark energy.

All four $f(T, T_G)$ models that were analysed were found to describe an asymptotically de Sitter universe for specific values of the free parameters, i.e. the models can describe a universe with a cosmological-constant-like behaviour, without the need to introduce such a cosmological constant. The models investigated also show the potential to lead to cosmologies with a behaviour which varies significantly from that predicted by ΛCDM. Through the analysis at infinity, the models were observed to lead to past, future and intermediate singularities. However, the physical interpretation of past singularities was done with caution since the assumptions made are those appropriate to study the late-time behaviour of the Universe and not the early-time behaviour.

The analysis that was done in this work contributes to the ever-growing literature investigating the cosmological implications of TEGR and its modifications, with the hope that some cosmological tensions could be resolved using such theories. The $f(T, T_G)$ modification had not yet been studied in great detail so far, and the dynamical analysis of only one such model can be found in the literature. This work shows that similar dynamics as were observed in the previously published work can be produced using a different specific form of the function $f(T, T_G)$. This could indicate that certain dynamics, such as a de Sitter solution, are a general feature of the $f(T, T_G)$ modification. Nevertheless, the specific features of certain unique models, such as future singularities, show that the specific form of the function used as the Lagrangian can indeed affect other certain types of dynamics that can be achieved.

It was noted that only the variation of the first model, as seen in Sec. 4.1.4, alongside the model analysed in Kofinas et al. (2014), can result in a universe dominated by dark energy with values of q and ω_{DE} different from -1. The reason why the other models could not lead to these different cosmological solutions was because of the introduction of H as a dynamical variable. This forces the value of H at the fixed points to be constant and limits the different type of behaviour that can be uncovered. It is important to emphasize that this does not reflect an intrinsic limitation of the models themselves and if different dynamical variables were chosen, more dynamics might have been uncovered. This is why any future work should focus on choosing different dynamical variables to analyse the models.

From this initial dynamical systems approach, no new behaviour of the $f(T, T_G)$ modification was uncovered. This does not mean that models which produce similar solutions are redundant. On the contrary, a good selection of models which are all viable at this early stage is preferred so as to improve the chances of finding a model which fits the constraints imposed on it from cosmological data in the work that would follow.

Although using simple, fundamental aspects from dynamical systems theory, the method used gave a clear overall picture of the dynamics of these models. However, the method was not without its limitations. One of the main drawbacks of the method was the inability to obtain the stability conditions of the fixed points for general values of the free parameters α_i and P_i (alongside β_3 for the third model). This then forced the choice of such free parameters to be made using a method of trial and error, potentially missing some interesting cosmological scenarios. Ideally, this choice would have been made based on knowledge of the stability using analytical techniques. If a similar further work is done investigating the dynamical behaviour of these models using different dynamical variables, this should be something that is kept in mind.

Another limitation that was observed deals with the analysis of the behaviour at infinity. Although the coordinate transformation used allowed for the identification of the fixed points at infinity, the method for analytically studying the stability of these fixed points was inconclusive in most cases. This forced the stability of such fixed points to be inferred qualitatively from the phase portraits, however, due to numerical instability, these plots were not always generated very precisely, making the study of stability quite hard. Whilst this method made it possible to identify points which could represent past or future singularities, it was seen that in some cases the values of q, ω_{DE} and H were not consistent with each other. Thus, the type of singularity that these fixed points could represent could not be inferred with certainty. Different methods might need to be used to understand the behaviour in this infinite regime better in future works.

As was previously mentioned, one way to further this study is to use different dynamical variables on the same models so as to expose different dynamics. The analysis with the specific dynamical variables considered in this work can also be developed further. For example, the free parameters of the models can be tuned so as to obtain a more realistic value of H at the fixed points. This is something which was not done in this work so as to facilitate the exposition of the different dynamics that each model can lead to, but is an important next step to ensure that the models can indeed describe our physical universe. Once the dynamical analysis of the models has been exhausted, the next step would then be to constrain the models using cosmological data. One way to do this is to obtain a relationship between the free parameters of the models, as was done in Eq. (3.53), and study the dynamical behaviour under this constraint.

Another way to further the study is to apply the same dynamical systems techniques to more $f(T, T_G)$ models. Rather than adapting functions from other modifications to the $f(T, T_G)$ case, some form of reconstruction techniques could be used. In particular, a general function would first be considered, and then constrained through certain demands of either the theory or observations. The method used for analysing the dynamics of these models could also be generalised. For example, the dynamical variables are defined as functions of f and the analysis is done in a general way until it is necessary to define the specific form of the function. This would speed up this initial analysis so that viable functions can be identified quickly.

In order to generalise the analysis further, the modification can be considered in the context of the theory of cosmological perturbations (Malik and Wands, 2009). In this case, perturbations of the flat FLRW metric are considered. These perturbations have shown promise in explaining CMB fluctuations and the formation of large-scale structure while also, in the limit, achieving the homogeneity and isotropy of the Universe. Thus it would be interesting to see how the $f(T, T_G)$ modification would perform in such a setting.

It would also be worth comparing the $f(T, T_G)$ modification to the $f(T)$ one. Specifically, to check whether the $f(T, T_G)$ theory has any significant advantages over $f(T)$ which is of a lower order. This comparison should also be done with respect to other modified teleparallel gravity theories to place $f(T, T_G)$ in context with modifications that have been studied in more detail.

In summary, through this preliminary study, it was seen that the $f(T, T_G)$ modification of TEGR has the potential of being the correct theory of gravity which explains the late-time behaviour of the Universe. More generally, it also shows that the standard cosmological model could, in the future, be replaced with another model that explains the acceleration of the Universe in a more elegant way, while in the meantime eliminating the tensions that are growing within this model.

References

Abbott, B. P., Abbott, R., Abbott, T., Abernathy, M., Acernese, F., Ackley, K., Adams, C., Adams, T., Addesso, P., Adhikari, R. X., Adya, V., Affeldt, C., Agathos, M., Agatsuma, K., Aggarwal, N., Aguiar, O., Aiello, L., Ain, A., Ajith, P., and Zweizig, J. Observation of gravitational waves from a binary black hole merger. *Physical Review Letters*, 116, 02 2016. doi: 10.1103/PhysRevLett.116.061102.

Abbott, B. P., Abbott, R., Abbott, T. D., et al. A gravitational-wave standard siren measurement of the Hubble constant. *Nature*, 551(7678):85–88, November 2017. doi: 10.1038/nature24471.

Ade, P. A. R., Aghanim, N., Armitage-Caplan, C., Arnaud, M., Ashdown, M., Atrio-Barandela, F., Aumont, J., Baccigalupi, C., Banday, A. J., and et al. Planck2013 results. xvi. cosmological parameters. *Astronomy & Astrophysics*, 571: A16, Oct 2014. ISSN 1432-0746. doi: 10.1051/0004-6361/201321591.

Ade, P. A. R., Aghanim, N., Arnaud, M., Ashdown, M., Aumont, J., Baccigalupi, C., Banday, A. J., Barreiro, R. B., Bartlett, J. G., and et al. Planck2015 results. *Astronomy & Astrophysics*, 594:A13, Sep 2016. ISSN 1432-0746. doi: 10.1051/0004-6361/201525830.

Aghanim, N., Akrami, Y., Ashdown, M., Aumont, J., Baccigalupi, C., Ballardini, M., Banday, A. J., Barreiro, R. B., Bartolo, N., and et al. Planck 2018 results. *Astronomy & Astrophysics*, 641:A6, Sep 2020. ISSN 1432-0746. doi: 10.1051/0004-6361/201833910.

Akiyama, K., Alberdi, A., Alef, W., Asada, K., Azulay, R., Baczko, A.-K., Ball, D., Balokovic, M., Barrett, J., Bintley, D., Blackburn, L., Boland, W., Bouman, K., Bower, G., Bremer, M., Brinkerink, C., Brissenden, R., Britzen, S., Broderick, A., and Ziurys, L. First M87 event horizon telescope results. i. the shadow of the supermassive black hole. *The Astrophysical Journal Letters*, 875, 04 2019.

Alpher, R. A., Bethe, H., and Gamow, G. The origin of chemical elements. *Phys. Rev.*, 73:803–804, Apr 1948. doi: 10.1103/PhysRev.73.803.

Amendola, L., Gannouji, R., Polarski, D., and Tsujikawa, S. Conditions for the cosmological viability of $f(R)$ dark energy models. *Physical Review D*, 75(8), Apr 2007. ISSN 1550-2368. doi: 10.1103/physrevd.75.083504.

Arkani-Hamed, N., Finkbeiner, D. P., Slatyer, T. R., and Weiner, N. A theory of dark matter. *Phys. Rev. D*, 79:015014, Jan 2009. doi: 10.1103/PhysRevD.79.015014.

Arun, K., Gudennavar, S., and Sivaram, C. Dark matter, dark energy, and alternate models: A review. *Advances in Space Research*, 60(1):166–186, 2017. ISSN 0273-1177. doi: https://doi.org/10.1016/j.asr.2017.03.043.

Bahamonde, S., Böhmer, C. G., Carloni, S., Copeland, E. J., Fang, W., and Tamanini, N. Dynamical systems applied to cosmology: Dark energy and modified gravity. *Physics Reports*, 775-777:1–122, Nov 2018. ISSN 0370-1573. doi: 10.1016/j.physrep.2018.09.001.

Bahamonde, S., Dialektopoulos, K. F., Escamilla-Rivera, C., Farrugia, G., Gakis, V., Hendry, M., Hohmann, M., Said, J. L., Mifsud, J., and Valentino, E. D. Teleparallel gravity: From theory to cosmology, 2021.

Bamba, K., Geng, C.-Q., Lee, C.-C., and Luo, L.-W. Equation of state for dark energy in $f(T)$ gravity. *Journal of Cosmology and Astroparticle Physics*, 2011(01):021–021, Jan 2011. ISSN 1475-7516. doi: 10.1088/1475-7516/2011/01/021.

Bean, R. and Melchiorri, A. Current constraints on the dark energy equation of state. *Phys. Rev. D*, 65:041302, Jan 2002. doi: 10.1103/PhysRevD.65.041302.

Bengochea, G. R. and Ferraro, R. Dark torsion as the cosmic speed-up. *Phys. Rev. D*, 79:124019, Jun 2009. doi: 10.1103/PhysRevD.79.124019.

Bernal, J. L., Verde, L., and Riess, A. G. The trouble with H_0. *Journal of Cosmology and Astroparticle Physics*, 2016(10):019–019, oct 2016. doi: 10.1088/1475-7516/2016/10/019.

Bernardeau, F., Colombi, S., Gaztañaga, E., and Scoccimarro, R. Large-scale structure of the universe and cosmological perturbation theory. *Physics Reports*, 367(1-3):1–248, sep 2002. doi: 10.1016/s0370-1573(02)00135-7.

Blagojević, M. *Gravitation and Gauge Symmetries*. Series in high energy physics, cosmology, and gravitation. Institute of Physics Pub., 2002. ISBN 9780585485850.

Blake, C., Kazin, E. A., Beutler, F., Davis, T. M., Parkinson, D., Brough, S., Colless, M., Contreras, C., Couch, W., Croom, S., and et al. The WiggleZ Dark Energy Survey: mapping the distance-redshift relation with baryon acoustic oscillations. *Monthly Notices of the Royal Astronomical Society*, 418(3):1707–1724, Oct 2011. ISSN 0035-8711. doi: 10.1111/j.1365-2966.2011.19592.x.

Blanton, M. R., Bershady, M. A., Abolfathi, B., et al. Sloan Digital Sky Survey IV: Mapping the Milky Way, Nearby Galaxies, and the Distant Universe. *The Astronomical Journal*, 154(1):28, July 2017. doi: 10.3847/1538-3881/aa7567.

Bondi, H. and Gold, T. The Steady-State Theory of the Expanding Universe. *Monthly Notices of the Royal Astronomical Society*, 108(3):252–270, 06 1948. ISSN 0035-8711. doi: 10.1093/mnras/108.3.252.

Branch, D. and Tammann, G. A. Type Ia supernovae as standard candles. *Annual Review of Astronomy and Astrophysics*, 30(1):359–389, 1992. doi: 10.1146/annurev.aa.30.090192.002043.

Briffa, R., Escamilla-Rivera, C., Said, J. L., and Pullicino, J. M. N. L. Impact of H_0 priors on $f(T)$ late time cosmology, 2021. URL `https://arxiv.org/abs/2108.03853`.

Böhmer, C. G. and Chan, N. Dynamical systems in cosmology. *Dynamical and Complex Systems*, page 121–156, Dec 2016. doi: 10.1142/9781786341044_0004.

Cai, Y.-F., Capozziello, S., Laurentis, M. D., and Saridakis, E. N. $f(T)$ teleparallel gravity and cosmology. *Reports on Progress in Physics*, 79(10):106901, sep 2016. doi: 10.1088/0034-4885/79/10/106901.

Caldwell, R. R., Dave, R., and Steinhardt, P. J. Cosmological imprint of an energy component with general equation of state. *Phys. Rev. Lett.*, 80:1582–1585, Feb 1998. doi: 10.1103/PhysRevLett.80.1582.

Caldwell, R. R., Kamionkowski, M., and Weinberg, N. N. Phantom energy: Dark energy with $w < -1$ causes a cosmic doomsday. *Physical Review Letters*, 91(7), Aug 2003. ISSN 1079-7114. doi: 10.1103/physrevlett.91.071301.

Camilleri, C. J. *Tensor Analysis with applications to Geometry and Continuum Mechanics*. Malta University Press, 1999.

Capozziello, S., Lazkoz, R., and Salzano, V. Comprehensive cosmographic analysis by markov chain method. *Physical Review D*, 84(12), Dec 2011. ISSN 1550-2368. doi: 10.1103/physrevd.84.124061.

Carroll, S. *Spacetime and Geometry: An Introduction to General Relativity*. Benjamin Cummings, San Francisco, 2004. ISBN 0805387323.

Carroll, S. M., Hoffman, M., and Trodden, M. Can the dark energy equation-of-state parameter w be less than -1? *Physical Review D*, 68(2), Jul 2003. ISSN 1089-4918. doi: 10.1103/physrevd.68.023509.

Caruana, M., Farrugia, G., and Levi Said, J. Cosmological bouncing solutions in $f(T,B)$ gravity. *The European Physical Journal C*, 80(7), Jul 2020. ISSN 1434-6052. doi: 10.1140/epjc/s10052-020-8204-3.

Clifton, T., Ferreira, P. G., Padilla, A., and Skordis, C. Modified gravity and cosmology. *Physics Reports*, 513(1-3):1–189, mar 2012. doi: 10.1016/j.physrep.2012.01.001.

Coley, A. *Dynamical Systems and Cosmology*. Astrophysics and Space Science Library. Springer Netherlands, 2003. ISBN 9781402014031.

Combi, L. and Romero, G. E. Is teleparallel gravity really equivalent to general relativity? *Annalen der Physik*, 530(1): 1700175, 2018. doi: https://doi.org/10.1002/andp.201700175.

Cyburt, R. H., Fields, B. D., Olive, K. A., and Yeh, T.-H. Big bang nucleosynthesis: Present status. *Reviews of Modern Physics*, 88(1), feb 2016. doi: 10.1103/revmodphys.88.015004.

De Felice, A. and Tsujikawa, S. $f(R)$ theories. *Living Reviews in Relativity*, 13(1), Jun 2010. ISSN 1433-8351. doi: 10.12942/lrr-2010-3.

de la Cruz-Dombriz, A. and Dobado, A. $f(R)$ gravity without a cosmological constant. *Phys. Rev. D*, 74:087501, Oct 2006. doi: 10.1103/PhysRevD.74.087501.

de la Cruz-Dombriz, Á. and Sáez-Gómez, D. On the stability of the cosmological solutions in $f(R,G)$ gravity. *Classical and Quantum Gravity*, 29(24):245014, nov 2012. doi: 10.1088/0264-9381/29/24/245014.

de Sitter, W. On the relativity of inertia. Remarks concerning Einstein's latest hypothesis. *Koninklijke Nederlandse Akademie van Wetenschappen Proceedings Series B Physical Sciences*, 19:1217–1225, March 1917.

de Souza, J. C. C. and Faraoni, V. The phase-space view of $f(R)$ gravity. *Classical and Quantum Gravity*, 24(14):3637–3648, jul 2007. doi: 10.1088/0264-9381/24/14/006.

Debono, I. and Smoot, G. General relativity and cosmology: Unsolved questions and future directions. *Universe*, 2(4): 23, Sep 2016. ISSN 2218-1997. doi: 10.3390/universe2040023.

Di Valentino, E., Mena, O., Pan, S., Visinelli, L., Yang, W., Melchiorri, A., Mota, D. F., Riess, A. G., and Silk, J. In the realm of the Hubble tension—a review of solutions *. *Classical and Quantum Gravity*, 38(15):153001, Jul 2021. ISSN 1361-6382. doi: 10.1088/1361-6382/ac086d.

Dodelson, S. *Modern cosmology*. Academic Press, San Diego, CA, 2003.

Einstein, A. The Field Equations of Gravitation. *Sitzungsber. Preuss. Akad. Wiss. Berlin (Math. Phys.)*, 1915:844–847, 1915.

Einstein, A. *Zum kosmologischen Problem der allgemeinen Relativitätstheorie*, volume 96, pages 361 – 364. 1931. ISBN 9783527608959. doi: 10.1002/3527608958.ch43.

Escamilla-Rivera, C. and Said, J. L. Cosmological viable models in $f(T,B)$ theory as solutions to the H_0 tension. *Classical and Quantum Gravity*, 37(16):165002, Jul 2020. ISSN 1361-6382. doi: 10.1088/1361-6382/ab939c.

Ezquiaga, J. M. and Zumalacarregui, M. Dark energy in light of multi-messenger gravitational-wave astronomy. *Frontiers in Astronomy and Space Sciences*, 5, 12 2018. doi: 10.3389/fspas.2018.00044.

Feng, J. L. Dark matter candidates from particle physics and methods of detection. *Annual Review of Astronomy and Astrophysics*, 48(1):495–545, 2010. doi: 10.1146/annurev-astro-082708-101659.

Ferraro, R. and Fiorini, F. Modified teleparallel gravity: Inflation without an inflaton. *Phys. Rev. D*, 75:084031, Apr 2007. doi: 10.1103/PhysRevD.75.084031.

Fixsen, D. J. The temperature of the cosmic microwave background. *The Astrophysical Journal*, 707(2):916–920, nov 2009. doi: 10.1088/0004-637x/707/2/916.

Friedmann, A. Über die Krümmung des Raumes. *Zeitschrift fur Physik*, 10:377–386, January 1922. doi: 10.1007/BF01332580.

Frieman, J. A., Turner, M. S., and Huterer, D. Dark energy and the accelerating universe. *Annual Review of Astronomy and Astrophysics*, 46(1):385–432, Sep 2008. ISSN 1545-4282. doi: 10.1146/annurev.astro.46.060407.145243.

Gentile, G., Salucci, P., Klein, U., Vergani, D., and Kalberla, P. The cored distribution of dark matter in spiral galaxies. *Monthly Notices of the Royal Astronomical Society*, 351(3):903–922, jul 2004. doi: 10.1111/j.1365-2966.2004.07836.x.

Golovnev, A., Koivisto, T., and Sandstad, M. On the covariance of teleparallel gravity theories. *Classical and Quantum Gravity*, 34(14):145013, Jun 2017. ISSN 1361-6382. doi: 10.1088/1361-6382/aa7830.

Goobar, A. and Perlmutter, S. Feasibility of measuring the cosmological constant lambda and mass density omega using type IA supernovae. *The Astrophysical Journal*, 450:14, Sep 1995. ISSN 1538-4357. doi: 10.1086/176113.

Guth, A. H. Inflationary universe: A possible solution to the horizon and flatness problems. *Phys. Rev. D*, 23:347–356, Jan 1981. doi: 10.1103/PhysRevD.23.347.

Guth, A. H. and Pi, S.-Y. Quantum mechanics of the scalar field in the new inflationary universe. *Phys. Rev. D*, 32: 1899–1920, Oct 1985. doi: 10.1103/PhysRevD.32.1899.

Hilbert, D. V. Die grundlagen der physik . (erste mitteilung.). 1915.

Hirsch, M., Smale, S., and Devaney, R. *Differential Equations, Dynamical Systems, and an Introduction to Chaos*. Elsevier Inc., 2013. ISBN 9780123820105.

Holz, D. E. and Hughes, S. A. Using gravitational-wave standard sirens. *The Astrophysical Journal*, 629(1):15–22, aug 2005. doi: 10.1086/431341.

Hu, W. Structure formation with generalized dark matter. *The Astrophysical Journal*, 506(2):485–494, oct 1998. doi: 10.1086/306274.

Hubble, E. A relation between distance and radial velocity among extra-galactic nebulae. *Proceedings of the National Academy of Sciences*, 15(3):168–173, 1929. ISSN 0027-8424. doi: 10.1073/pnas.15.3.168.

Jackson, N. The Hubble constant. *Living Reviews in Relativity*, 10(1), sep 2007. doi: 10.12942/lrr-2007-4.

Jimenez, J., Heisenberg, L., and Koivisto, T. The geometrical trinity of gravity. *Universe*, 5:173, 07 2019. doi: 10.3390/universe5070173.

John, M. V. Cosmography, decelerating past, and cosmological models: Learning the bayesian way. *The Astrophysical Journal*, 630(2):667–674, Sep 2005. ISSN 1538-4357. doi: 10.1086/432111.

Jones, A. and Lasenby, A. The cosmic microwave background. *Living Reviews in Relativity*, 1, 12 1998. doi: 10.12942/lrr-1998-11.

Kaiser, N. and Squires, G. Mapping the Dark Matter with Weak Gravitational Lensing. *Astrophysical Journal*, 404:441, February 1993. doi: 10.1086/172297.

Klypin, A., Kravtsov, A. V., Valenzuela, O., and Prada, F. Where are the missing galactic satellites? *The Astrophysical Journal*, 522(1):82–92, sep 1999. doi: 10.1086/307643.

Kofinas, G. and Saridakis, E. N. Teleparallel equivalent of gauss-bonnet gravity and its modifications. *Physical Review D*, 90(8), Oct 2014. ISSN 1550-2368. doi: 10.1103/physrevd.90.084044.

Kofinas, G., Leon, G., and Saridakis, E. N. Dynamical behavior in $f(T, T_G)$ cosmology. *Classical and Quantum Gravity*, 31 (17):175011, Aug 2014. ISSN 1361-6382. doi: 10.1088/0264-9381/31/17/175011.

Krššák, M., van den Hoogen, R. J., Pereira, J. G., Böhmer, C. G., and Coley, A. A. Teleparallel theories of gravity: illuminating a fully invariant approach. *Classical and Quantum Gravity*, 36(18):183001, Aug 2019. ISSN 1361-6382. doi: 10.1088/1361-6382/ab2e1f.

Lahav, O. and Liddle, A. R. The cosmological parameters (2019), 2019. URL `https://arxiv.org/abs/1912.03687`.

Lemaitre, G. A Homogeneous Universe of Constant Mass and Growing Radius Accounting for the Radial Velocity of Extragalactic Nebulae. *Annales Soc. Sci. Bruxelles A*, 47:49–59, 1927. doi: 10.1007/s10714-013-1548-3.

Liddle, A. *An introduction to modern cosmology; 2nd ed.* Wiley, Chichester, 2003.

Linder, E. V. Einstein's other gravity and the acceleration of the universe. *Phys. Rev. D*, 81:127301, Jun 2010. doi: 10.1103/PhysRevD.81.127301.

Lovelock, D. The four-dimensionality of space and the einstein tensor. *Journal of Mathematical Physics*, 13(6):874–876, 1972. doi: 10.1063/1.1666069.

Lynch, S. *Dynamical Systems with Applications Using Mathematica®*. Springer International Publishing, 2017. ISBN 9783319614854.

Malik, K. A. and Wands, D. Cosmological perturbations. *Physics Reports*, 475(1-4):1–51, may 2009. doi: 10.1016/j.physrep.2009.03.001.

Mamon, A. A. and Bamba, K. Observational constraints on the jerk parameter with the data of the Hubble parameter, 2018.

Mattson, B. 100 years of general relativity, Nov 2015. URL `https://asd.gsfc.nasa.gov/blueshift/index.php/2015/11/25/100-years-of-general-relativity/`.

Melchiorri, A., Mersini, L., Ödman, C. J., and Trodden, M. The state of the dark energy equation of state. *Phys. Rev. D*, 68:043509, Aug 2003. doi: 10.1103/PhysRevD.68.043509.

Misner, C. W., Thorne, K. S., and Wheeler, J. A. *Gravitation*. W. H. Freeman San Francisco, 1973. ISBN 0716703343 0716703440.

Myrzakulov, R. Accelerating universe from $F(T)$ gravity. *The European Physical Journal C*, 71(9), Sep 2011. ISSN 1434-6052. doi: 10.1140/epjc/s10052-011-1752-9.

Ohanian, H. C. and Ruffini, R. *Gravitation and Spacetime*. Cambridge University Press, 3rd edition, 2013. doi: 10.1017/CBO9781139003391.

O'Raifeartaigh, C. and McCann, B. Einstein's cosmic model of 1931 revisited: an analysis and translation of a forgotten model of the universe. *The European Physical Journal H*, 39(1):63–85, feb 2014. doi: 10.1140/epjh/e2013-40038-x.

Ostriker, J. P. and Steinhardt, P. J. The observational case for a low-density Universe with a non-zero cosmological constant. *Nature*, 377(6550):600–602, October 1995. doi: 10.1038/377600a0.

O'Raifeartaigh, C. Investigating the legend of Einstein's "biggest blunder". `https://physicstoday.scitation.org/do/10.1063/PT.6.3.20181030a/full/`, 2018. Accessed: 12-04-2022.

Page, L., Nolta, M., Barnes, C., Bennett, C., Halpern, M., Hinshaw, G., Jarosik, N., Kogut, A., Limon, M., Meyer, S., Peiris, H., Spergel, D., Tucker, G., Wollack, E., and Wright, E. First year Wilkinson Microwave Anisotropy Probe (WMAP) observations: Interpretation of the tt and te angular power spectrum peaks. *Astrophysical Journal Supplement Series - ASTROPHYS J SUPPL SER*, 148, 02 2003. doi: 10.1086/377224.

Paliathanasis, A. and Leon, G. Cosmological evolution in $f(T, B)$ gravity. *Eur. Phys. J. Plus*, 136(10):1092, 2021. doi: 10.1140/epjp/s13360-021-02071-x.

Penrose, R. Difficulties with inflationary cosmologya. *Annals of the New York Academy of Sciences*, 571(1):249–264, 1989. doi: https://doi.org/10.1111/j.1749-6632.1989.tb50513.x.

Penzias, A. A. and Wilson, R. W. A Measurement of Excess Antenna Temperature at 4080 Mc/s. *Astrophysical Journal*, 142:419–421, July 1965. doi: 10.1086/148307.

Percival, W. J., Reid, B. A., Eisenstein, D. J., Bahcall, N. A., Budavari, T., Frieman, J. A., Fukugita, M., Gunn, J. E., Ivezić, Z., Knapp, G. R., and et al. Baryon acoustic oscillations in the sloan digital sky survey data release 7 galaxy sample.

Monthly Notices of the Royal Astronomical Society, 401(4):2148–2168, Feb 2010. ISSN 1365-2966. doi: 10.1111/j.1365-2966.2009.15812.x.

Perivolaropoulos, L. and Skara, F. Challenges for ΛCDM: An update, 2021. URL `https://arxiv.org/abs/2105.05208`.

Perlmutter, S., Aldering, G., Goldhaber, G., Knop, R. A., Nugent, P., Castro, P. G., Deustua, S., Fabbro, S., Goobar, A., Groom, D. E., and et al. Measurements of Ω and Λ from 42 high-redshift supernovae. *The Astrophysical Journal*, 517 (2):565–586, Jun 1999. ISSN 1538-4357. doi: 10.1086/307221.

Planck Collaboration, Adam, R., Ade, P. A. R., et al. Planck 2015 results. IX. Diffuse component separation: CMB maps. *Astronomy & Astrophysics*, 594:A9, September 2016. doi: 10.1051/0004-6361/201525936.

Poulin, V., Smith, T. L., Karwal, T., and Kamionkowski, M. Early dark energy can resolve the Hubble Tension. *Phys. Rev. Lett.*, 122:221301, Jun 2019. doi: 10.1103/PhysRevLett.122.221301.

Quiros, I. Avoiding the cosmological constant issue in a class of phenomenologically viable $F(R, \mathcal{G})$ theories. *arXiv e-prints*, art. arXiv:2101.03998, January 2021.

Rasia, E., Tormen, G., and Moscardini, L. A dynamical model for the distribution of dark matter and gas in galaxy clusters. *Monthly Notices of the Royal Astronomical Society*, 351(1):237–252, 06 2004. ISSN 0035-8711. doi: 10.1111/j.1365-2966.2004.07775.x.

Ratra, B. and Peebles, P. J. E. Cosmological consequences of a rolling homogeneous scalar field. *Phys. Rev. D*, 37:3406–3427, Jun 1988. doi: 10.1103/PhysRevD.37.3406.

Readhead, A. C. S. and Lawrence, C. R. Observations of the isotropy of the cosmic microwave background radiation. *Annual Review of Astronomy and Astrophysics*, 30(1):653–703, 1992. doi: 10.1146/annurev.aa.30.090192.003253.

Riess, A., Casertano, S., Yuan, W., Macri, L., Bucciarelli, B., Lattanzi, M., MacKenty, J., Bowers, J., Zheng, W., Filippenko, A., Huang, C., and Anderson, R. Milky way cepheid standards for measuring cosmic distances and application to gaia dr2: Implications for the Hubble constant. *The Astrophysical Journal*, 861:126, 07 2018. doi: 10.3847/1538-4357/aac82e.

Riess, A. G., Filippenko, A. V., Challis, P., Clocchiatti, A., Diercks, A., Garnavich, P. M., Gilliland, R. L., Hogan, C. J., Jha, S., Kirshner, R. P., and et al. Observational evidence from supernovae for an accelerating universe and a cosmological constant. *The Astronomical Journal*, 116(3):1009–1038, Sep 1998. ISSN 0004-6256. doi: 10.1086/300499.

Riess, A. G., Macri, L. M., Hoffmann, S. L., Scolnic, D., Casertano, S., Filippenko, A. V., Tucker, B. E., Reid, M. J., Jones, D. O., Silverman, J. M., and et al. A 2.5% determination of the local value of the Hubble constant. *The Astrophysical Journal*, 826(1):56, Jul 2016. ISSN 1538-4357. doi: 10.3847/0004-637x/826/1/56.

Riess, A. G., Yuan, W., Macri, L. M., Scolnic, D., Brout, D., Casertano, S., Jones, D. O., Murakami, Y., Breuval, L., Brink, T. G., Filippenko, A. V., Hoffmann, S., Jha, S. W., Kenworthy, W. D., Mackenty, J., Stahl, B. E., and Zheng, W. A comprehensive measurement of the local value of the Hubble constant with 1 km/s/mpc uncertainty from the Hubble Space Telescope and the SH0ES team, 2021.

Riess, A. The case for an accelerating universe from supernovae. *Publications of the Astronomical Society of the Pacific*, 112 (776):1284–1299, Oct 2000. ISSN 1538-3873. doi: 10.1086/316624.

Rubin, V. C. The rotation of spiral galaxies. *Science*, 220(4604):1339–1344, 1983. doi: 10.1126/science.220.4604.1339.

Schmidt, B. P., Suntzeff, N. B., Phillips, M. M., Schommer, R. A., Clocchiatti, A., Kirshner, R. P., Garnavich, P., Challis, P., Leibundgut, B., Spyromilio, J., Riess, A. G., Filippenko, A. V., Hamuy, M., Smith, R. C., Hogan, C., Stubbs, C., Diercks, A., Reiss, D., Gilliland, R., Tonry, J., Maza, J., Dressler, A., Walsh, J., and Ciardullo, R. The High-Z Supernova Search: Measuring Cosmic Deceleration and Global Curvature of the Universe Using Type IA Supernovae. *The Astrophysical Journal*, 507(1):46–63, November 1998. doi: 10.1086/306308.

Schutz, B. *A First Course in General Relativity*. Cambridge University Press, 2nd edition, 2009. doi: 10.1017/CBO9780511984181.

Tanabashi, M., Hagiwara, K., Hikasa, K., et al. Review of particle physics. *Phys. Rev. D*, 98:030001, Aug 2018. doi: 10.1103/PhysRevD.98.030001.

Turyshev, S. G. Experimental tests of general relativity. *Annual Review of Nuclear and Particle Science*, 58(1):207–248, 2008. doi: 10.1146/annurev.nucl.58.020807.111839.

Velten, H. E. S., vom Marttens, R. F., and Zimdahl, W. Aspects of the cosmological "coincidence problem". *The European Physical Journal C*, 74(11), Nov 2014. ISSN 1434-6052. doi: 10.1140/epjc/s10052-014-3160-4.

Wainwright, J. and Ellis, G. *Dynamical Systems in Cosmology*. Cambridge University Press, 1997. ISBN 9780521554572.

Wald, R. M. *General relativity*. Chicago Univ. Press, Chicago, IL, 1984.

Weinberg, D. H., Bullock, J. S., Governato, F., Kuzio de Naray, R., and Peter, A. H. G. Cold dark matter: Controversies on small scales. *Proceedings of the National Academy of Sciences*, 112(40):12249–12255, 2015. ISSN 0027-8424. doi: 10.1073/pnas.1308716112.

Weinberg, S. The cosmological constant problem. *Rev. Mod. Phys.*, 61:1–23, Jan 1989. doi: 10.1103/RevModPhys.61.1.

White, M., Scott, D., and Silk, J. Anisotropies in the cosmic microwave background. *Annual Review of Astronomy and Astrophysics*, 32(1):319–370, 1994. doi: 10.1146/annurev.aa.32.090194.001535.

Wiggins, S. *Introduction To Applied Nonlinear Dynamical Systems And Chaos*. Springer, New York, 2nd edition, 01 2003. ISBN 0-387-00177-8. doi: 10.1007/b97481.

Wolfram Research. FindRoot. `https://reference.wolfram.com/language/ref/FindRoot.html`, 2003. [Accessed: 28-February-2022].

Wolfram Research, Inc. Mathematica, Version 13.0.0. URL `https://www.wolfram.com/mathematica`. Champaign, IL, 2021.

Xu, C., Saridakis, E. N., and Leon, G. Phase-space analysis of teleparallel dark energy. *Journal of Cosmology and Astroparticle Physics*, 2012(07):005–005, Jul 2012. ISSN 1475-7516. doi: 10.1088/1475-7516/2012/07/005.

Zwicky, F. Die Rotverschiebung von extragalaktischen Nebeln. *Helvetica Physica Acta*, 6:110–127, January 1933.